Ground Target Classification for Airborne Bistatic Radar

Amit Kumar Mishra

A thesis submitted for the degree of Doctor of Philosophy.
The University of Edinburgh.
August 2006

Abstract

The present thesis documents the results and insights gathered in the project, dealing with the development of algorithms to classify ground targets using synthetic aperture radar (SAR) images formed by bistatic airborne radars.

Recently there has been an intensive upsurge in the interest of the radar community in bistatic and multistatic radar systems. The reason for this is twofold. First of all, bistatic radar systems are the superset of monostatic radar systems. Hence, bistatic systems might give certain advantages over the monostatic systems in the current usages of monostatic radar systems. Secondly, bistatic technology, if implemented successfully, can give rise to a wide spectrum of novel and innovative usages, which would have been impossible using the simpler monostatic system. Automatic target classification and recognition for monostatic radars, has been an area of active research. This is also one of the major usages of an airborne radar system. Hence, it is pertinent at the current stage to look at different aspects of automatic target recognition (ATR), using the synthetic aperture radar (SAR) images, as collected by a bistatic radar system. This, as applied to classification of ground targets, has been the aim of the present project. The contributions from the present work could be grouped under three major heads.

Simulating a database of bistatic SAR images of ground targets using a generic electromagnetic (EM) computational tool, is the first contribution of the present project. Major challenges in this approach consisted of selecting a usable and available [1] EM simulator, modelling a selection of ground targets, developing a simple and efficient image formation algorithm for bistatic SAR image generation, and managing the database to be used efficiently in a classification task. All of these challenges have been successfully tackled in the present project and form the dimensions of novelty from this part of the project.

The second contribution is the analysis of different aspects of bistatic SAR ATR. This consists of developing an efficient and fast ATR algorithm, studying the effect of clutter noise, bistatic angle, polarisation, k space support on bistatic ATR, comparison of monostatic and bistatic ATR, and suggestion of ways to improve bistatic ATR performance. In this it has been shown that contrary to the popular reservations, bistatic ATR is not much worse than monostatic ATR. Given a proper ATR algorithm, the bistatic ATR performance could be made as good as, but

[1] availability was a major issue, as most of the established EM simulators to simulate radar returns, are not available for academic research

Ground Target Classification for Airborne Bistatic Radar

Amit Kumar Mishra

A thesis submitted for the degree of Doctor of Philosophy.
The University of Edinburgh.
October 2006

Abstract

The present thesis documents the results and insights gathered in the project, dealing with the development of algorithms to classify ground targets using synthetic aperture radar (SAR) images formed by bistatic airborne radars.

Recently there has been an intensive upsurge in the interest of the radar community in bistatic and multistatic radar systems. The reason for this is twofold. First of all, bistatic radar systems are the superset of monostatic radar systems. Hence, bistatic systems might give certain advantages over the monostatic systems in the current usages of monostatic radar systems. Secondly, bistatic technology, if implemented successfully, can give rise to a wide spectrum of novel and innovative usages, which would have been impossible using the simpler monostatic system. Automatic target classification and recognition for monostatic radars, has been an area of active research. This is also one of the major usages of an airborne radar system. Hence, it is pertinent at the current stage to look at different aspects of automatic target recognition (ATR), using the synthetic aperture radar (SAR) images, as collected by a bistatic radar system. This, as applied to classification of ground targets, has been the aim of the present project. The contributions from the present work could be grouped under three major heads.

Simulating a database of bistatic SAR images of ground targets using a generic electromagnetic (EM) computational tool, is the first contribution of the present project. Major challenges in this approach consisted of selecting a usable and available [1] EM simulator, modelling a selection of ground targets, developing a simple and efficient image formation algorithm for bistatic SAR image generation, and managing the database to be used efficiently in a classification task. All of these challenges have been successfully tackled in the present project and form the dimensions of novelty from this part of the project.

The second contribution is the analysis of different aspects of bistatic SAR ATR. This consists of developing an efficient and fast ATR algorithm, studying the effect of clutter noise, bistatic angle, polarisation, k space support on bistatic ATR, comparison of monostatic and bistatic ATR, and suggestion of ways to improve bistatic ATR performance. In this it has been shown that contrary to the popular reservations, bistatic ATR is not much worse than monostatic ATR. Given a proper ATR algorithm, the bistatic ATR performance could be made as good as, but

[1] availability was a major issue, as most of the established EM simulators to simulate radar returns, are not available for academic research

not better than, the monostatic ATR performance. Lastly, the loss of ATR performance in the bistatic domain is more due to the loss of image resolution, than due to any loss of image information.

The last contribution of the project is the study of the use of multipolar data in an ATR exercise. There have been studies on the use of multipolar data in SAR image classification, for spaceborne radar systems. However, such approaches for airborne radar systems have been very few and preliminary. In this part of the project, a group of different algorithms were developed to use the multipolar information, for a better ATR performance. It was shown that using multipolar data significantly improves the ATR performance. For some of the multipolar ATR algorithms, the ATR performance was shown to be more stable than the single-polarisation ATR. A new algorithm was proposed to use multipolar data so that the ATR performance becomes independent of the polarisation of the radar antenna in the test phase. It was also shown that bistatic multipolar data does hold information about the targets which could easily be exploited, as contrary to reservations held by experts in the past.

Declaration of originality

I hereby declare that the research recorded in this thesis and the thesis itself was composed and originated entirely by myself in the Department of Electronics and Electrical Engineering at The University of Edinburgh.
The list of exceptions are as follows:

- Figures 2.3 and 2.4 are from the tutorial [1].

Acknowledgements

First and foremost I would like to acknowledge my grandfather for the example he has set in front of me of finishing any endeavour one takes.

Academically I am thankful to Prof. Bernard Mulgrew, my thesis supervisor for his timely guidance and measured feedback. In addition I thank Prof. Dave Laurenson my second supervisor, for his helpful comments.

I acknowledge the electromagnetic remote sensing defence technology centre (EMRSDTC), for funding this project and the royal academy of engineers (RAE), for the equipment grant. Sincere thanks to the members of the DTC board, Mr.Tony Kinghorn (Selex), and Dr.Iain Anderson (DSTL) for their invaluable comments on the work and for fine-tuning the work all through the three years. The timely feedback and sharing of ideas from Mr.Gordon Vigurs (Sula Systems), Prof Mike Cherniakov (University of Birmingham), Dr.Robert Miller (Selex), Dr.Ian Scott (Selex), and Dr.Iain McColl (Selex), are much appreciated. I also thank Dr.Daniel Andre and Dr.David Blacknell of QinetiQ for the interesting discussions and the continued help.

I thank all my friends in the lab, Chin Heng, Gavin, and David for making the lab a perfect place to work, in a relaxed and jovial manner. Thanks to Agnes, the claening lady, for all the football talks (which I hardly could understand!). Thanks to Vimal for his continued friendship, help and guidance, and to Somu and others for making my stay in Edinburgh so lively and enjoyable. Thanks to Sharad for all the generous coffees! Thanks to my friends Debasis, Deba, and Moti, whose e-contact has never let me feel that I am too far from home! Thanks to Shreyan for all those hours of talk over the phone, and to Ashutosh for his invaluable support (during the thesis-writing period). Special thanks to Prasad, my friend, philosopher and guide.

I thank the university science communication team, the Scottish Homelink, and SETNET-Scotland, for giving me the scope to broaden my experience and vision, by volunteering in a breadth of different fields.

Lastly, I would also like to sincerely thank my parents for all, that is mine today, though thanking them is underestimating their greatness. Thanks to my young brother Nepuli, who has always given me the security that someone is there back home. And thanks to all my relatives, who have always stood with my family, and given me such grand welcome, all the times I have gone home.

Contents

List of figures

List of tables

Acronyms and abbreviations

1D	One dimensional
2D	Two dimensional
3D	Three dimensional
APC	Armoured personnel carrier
ATR	Automatic target recognition
BW	Band width
CAD	Computer aided design
CFAR	Constant false alarm rate
CGBC	Conditional Gaussian model based Bayesian classifier
CW	Continuous wave
DFT	Discrete Fourier transform
ECCM	Electronic counter counter measures
EM	Electro-magnetic
EMC	Electromagnetic compatibility
FEKO	*FEldberechnungbei Korpern mit beleibeiger Oberflache*
FFT	Fast Fourier transform
FOPEN	FOliage PENetration
GB	Giga byte
GHz	Giga hertz
GMTI	Ground moving target indication
GO	Geometrical optics
GTD	Geometrical theory of diffraction
H	Horizontal
HMM	Hidden Markov model
HRR	High range resolution
HRRP	High range resolution profile
ICA	Independent component analysis
IMINT	IMage INTelligence
kNN	k nearest neighbours

MHz	Mega hertz
MBT	Main battle tank
ML	Maximum likelihood
MLE	Maximum likelihood estimator
MTI	Moving target indication
MoM	Method of moments
MSE	Mean square estimation
MSL	Missile launcher
MSTAR	Moving and stationary target acquisition recognition
NN	Nearest neighbour
PCA	Principal component analysis
PCA-NN	Principal component analysis based nearest neighbour
PO	Physical optics
PRESS	PREdictive Sum of Squares
Radar	Radio detection and ranging
RCS	Radar cross-section
RP	Range profile
RF	Radio frequency
ROC	Receiver operating characteristics
ROI	Region of interest
SAR	Synthetic aperture radar
SAIC	Science application international corporation
SBR	Shooting and bouncing ray
SC	Scattering centre
SIGINT	SIGnal INTelligence
SNR	Signal to noise ratio
STR	Stringer launcher
SVD	Singular value decomposition
TATA	Train all test any
UTD	Unified theory of diffraction
V	Vertical

Nomenclature

$(\cdot)^*$	complex conjugate operator
$(\cdot)^H$	Hermitian operator (complex conjugate transpose)
$(\cdot)^T$	transpose operator
$(\cdot)^{-1}$	inverse operator
$\|\cdot\|^2$	modulus operator
$\|\cdot\|$	magnitude operator
σ	Standard deviation
λ	Wavelength of an EM wave
k	Wavenumber of an EM wave
c	Speed of EM wave in the propagation medium
σ^0	Radar cross section (RCS)
$Det(\cdot)$	Determinant operation
$g(E)$	Stoke's vector of the electrical field vector of an EM wave
E^t	Transmitted electric field in an EM wave propagation
E^i	Incident electric field in an EM wave propagation
E^s	Scattered electric field in an EM wave propagation
E^r	Electric field at the receiver in an EM wave propagation
K	Kennaugh's matrix
P_{cc}	Probability of correct classification
P_{fa}	Probability of false alarm
S	Scattering or Sinclair matrix
T_p	Pulse width of the transmitted wave from a radar system
i	Square-root of -1
t	Time variable
f_0	Central frequency of the transmitted bandwidth of an EM signal
s_t	Transmitted waveform
s_r	Received waveform
β	Bistatic angle

Chapter 1
Introduction

With the development in the hardware domain keeping abreast with Moore's law, and major advances in the signal processing domain, radar researchers are hoping to implement more and more sophisticated radar systems in the near future. One such futuristic radar system is the bistatic radar system. Given the strategic importance of some of the usages of a bistatic system, it is expected to be implemented in the near future. Hence, at this juncture, a study of automatic target recognition using a bistatic radar system, was deemed timely and pertinent. The present thesis documents the project undertaken to study different aspects of bistatic automatic target recognition.

This chapter begins with a section on the inspiration behind the present work. The next section deals with the major contributions from the project. The chapter ends with a section on the layout of the rest of the thesis.

1.1 Motivation for the work

Radar systems in which the transmitter and the receiver are co-located, are termed as *monostatic* radar systems, while those where the transmitter and the receiver are in different platforms, are termed as *bistatic* radar systems. Bistatic radar system is the more generic configuration of the monostatic configuration (in the sense that monostatic system can be defined as the bistatic system with the bistatic angle equal to zero degree). This makes it logical to expect more utilities from a bistatic configuration than from the monostatic configuration. This includes, the likely improvement in performance in the existing usages of monostatic systems and would also include a spectrum of novel innovative applications. The amount of unique and strategic applications of a bistatic configuration, have given a boost to the recent researches undertaken involving bistatic systems. There are three major fronts of such research interest. First of all, there is the research on the hardware front to over come the transmitter-receiver synchronisation problem, which is a major bottle-neck for an implementable bistatic system. Secondly, there is research into the signal processing aspects of bistatic configuration which could be utilised

in the various applications, using the system. Thirdly, there is the research into solving some typical problems rising from the bistatic geometry. For example, the problem of *beam scan-on-scan*. This is the problem of inefficient use of radar energy in bistatic configuration (where only the amount of energy from the intersection of the transmitter and receiver beams is usable). One of the innovative solution to this problem, is the implementation of *pulse chasing* by using an electronically steering receiver beam.

Signal-intelligence (SIGINT) is one of the major applications of any military instrument. Target recognition is an advanced form of SIGINT, and is a field of active research. Given that a radar is one of the major instruments of an airborne military vehicle, a dependable radar based automatic target recognition (ATR) system is a major value addition. While research in the field of ATR in general and radar-based ATR in particular, has been going on for almost two decades, present technology is still far from a dependable automatic target recognition system, which could work without the *person in the loop* element [2, 3]. Still, the progress in the field of monostatic radar based ATR has been fairly extensive.

Given the present active research into bistatic radar systems, it was deemed pertinent to look into the possibility of ATR using bistatic radar systems. There are many important questions, answering which, was the major motivation behind the present piece of research. Some of the questions which have been dealt with in this work, are as follows:

How feasible is an ATR ability using a bistatic system? The answer to this question will serve two purposes. First of all, if the answer is positive, this gives another support in favour of developing bistatic systems. Secondly, if the answer is positive, this will add a major application, for which the futuristic bistatic radar system could be used.

How much does the ATR performance in a bistatic system, depend on the bistatic angle of operation? The answer to this question would be a major addition to the knowledge available, which in turn would help designing an implementable bistatic radar system.

Is there any way to improve the ATR performance, while using a bistatic system? Suggestions of such kind, if any, would again be invaluable for the bistatic-radar designers.

What is the effect of using multiple polarisation data (instead of single polarisation data), on bistatic ATR performance? Use of multipolar data for ATR performance enhancement, is not widespread even for monostatic configuration. Hence the answer to this question and an analysis based on this, would be invaluable for the design of futuristic radar systems, which are expected to be have multipolar abilities [4, 5].

1.2 Thesis contribution

The present project was carried out, inspired by the questions discussed in the last section. Major contributions from the project will now be discussed briefly.

The study of an automatic target recognition algorithm, needs a well defined database of sample images. This was a major bottleneck for the present project. Airborne bistatic radar systems are still in a developmental phase. Hence, a database of SAR images of ground targets collected by airborne bistatic radar system, is either non existent or is highly classified and not available in the public domain. The alternative was to simulate a database of bistatic SAR images of ground targets using certain electro magnetic (EM) computational methods. This is the first contribution of the present project. Currently, there are a few EM computational tools, which have been reported to have been used in generating SAR images of targets. However, such tools are mostly restricted, and hence not available for academic research. Hence, the first step was the search for a generic EM computational tool, which could be used to generate SAR images of modelled ground targets. Next was the development of a detailed procedure to model ground targets, and to generate bistatic SAR images of the targets using the EM computational tool. Generating bistatic SAR images synthetically, in itself is an activity, never reported in any open literature. Other novelties of this step includes modelling an acceptable ground clutter generation algorithm, extracting the bistatic shadow information using the EM-tool and including that in the SAR image generated, and developing the complete flow to maintain the database of SAR images, so that it could be used efficiently in the ATR experiments to be carried out further in the project.

The second contribution of the project consists of the study of the different aspects of bistatic SAR ATR. This consists of four major achievements. The first achievement is the development of an efficient and fast ATR algorithm, which was proved to be an excellent match for the challenges posed by the bistatic SAR ATR problem. The next achievement is the study of different aspects of bistatic SAR ATR. This consisted of studying the effects of clutter noise, the bistatic angle of imaging, the polarisation of the SAR data, and the k space support of imaging, on the bistatic SAR ATR performance. The third achievement is the comparison of SAR ATR performance using monostatic and bistatic databases. It was shown that contrary to popular expectations, bistatic ATR is not significantly worse than monostatic ATR. The final achievement is the suggestion of methods to achieve better ATR performance using a bistatic radar system. It was shown that the loss of ATR performance in bistatic domain, is more due to the loss of image resolution. Hence, by transmitting a higher bandwidth signal with increasing bistatic

angle, the ATR performance degradation with increasing bistatic angle, could be compensated for.

The final contribution of the project is the study of the use of multiple polarisation data in ATR exercise. This part of the project consists of three major achievements. First of all, a group of different algorithms were developed in the project, to exploit the multiple polarisation data, to achieve better SAR ATR performance. In this it was shown that by using multiple polarisation data, the ATR performance increases and also becomes more stable. Second achievement consists of the *train all test any* algorithm, where the multiple polarisation data were used in the training phase, and single polarisation data are used in the test phase. It was shown that this makes the SAR ATR performance robust to the radar antenna polarisation. Finally, it was shown that contrary to reservations held by some experts [6], bistatic multi-polar data do contain information about the target, which in turn could be exploited for better ATR performance.

1.3 Thesis organisation

The rest of the thesis is organised as follows:

Chapter 2 discusses the background studies for the present work. Background knowledge and contemporary works are discussed from three major fields. First of all, some basics are discussed from the fields of radar image formation and SAR image simulation for synthetic scenes. The next section discusses contemporary work on classification of ground targets using radar images. Lastly, the basics of radar polarimetry are discussed.

Chapter 3 deals with the synthetic data generation part of the project. After a short discussion of the problem at hand, the electromagnetic (EM) simulator based approach is introduced. Certain basic experiments on the EM simulator used for this project, are discussed, along with their results. After this, the theories behind the present method of database generation, are expounded, followed by a detailed presentation of the algorithm. Some representative images are presented along with the detailed analysis of the features in one of the images. The chapter ends with a section detailing the steps towards the simulation of a monostatic SAR image database.

Chapter 4 explains the classification algorithm developed in this project and the results from using it in the bistatic and the monostatic target recognition exercises. The chapter starts with a note on principal component analysis (PCA) and its correspondence to scattering centres in radar images. Next, the PCA based nearest neighbour algorithm for ATR is explained. ATR performance of this algorithm is compared with the conditional Gaussian model based Bayesian

classifier (one of the best from the open literature). The comparisons are done both in the monostatic and bistatic domains. Various aspects of bistatic ATR are discussed in this chapter. These include the effect of clutter noise, increasing bistatic angle, and normalised k space on the bistatic ATR. Lastly, a comparison of ATR performance in monostatic and bistatic domains is done.

Chapter 5 deals with the use of fully polarimetric data for target recognition in the bistatic domain. A number of algorithms have been proposed to fuse the information from different polarisation datasets, so as to increase the classification performance. The results have been compared and remarks have been made regarding the best algorithm for multi-polar ATR. Along with this, a novel algorithm has been proposed using fully polarimetric data in the training and single polarisation data in the test phase of an ATR system. This type of ATR was shown to offer many advantages over the conventional single-polarisation ATR. Lastly, by analysing in detail the effect of using a multi-polar dataset for bistatic-ATR, it was shown that multipolar data in the bistatic domain does have information about the target being imaged.

Chapter 6 summarises the results with a note on the limitations of the present work. It also hints at the possible directions of future research in the present field.

Chapter 2
Literature review

The present chapter is devoted towards discussing briefly some of the basic principles required for the current project, and a review of the work done by the research community in the field of radar target classification and bistatic radar configuration. First of all, this provides the reader with a brief background for the future chapters. Moreover, the discussion of previous research in the field, puts the current work in context.

The first section of the chapter discusses basic background of radar signal generation and processing, including synthetic aperture radar (SAR) imaging fundamentals. It also discusses the fundamentals of a bistatic radar system, and the advantages of using a bistatic radar system. This in turn puts into context and justifies the present work on bistatic automatic target recognition (ATR). The next section discusses approaches in the open literature, on electromagnetic signal simulation, and on generation of simulated radar signal. The section after this, discusses some of the major SAR ATR and SAR-classification [1] algorithms from the open literature. The last section discusses the basics of radar polarimetry.

2.1 Basic background

In this section, some of the basic principles are discussed, which are core, complimentary or supplementary to the research work undertaken for the current project.

2.1.1 Electro-magnetic (EM) wave interaction and scattering principles

Radio detection and ranging (radar) as an instrument, has been used for civilian and military uses since the first world war. The major advantages of a radar based electromagnetic sensor, as compared to other sensors (like optical sensors, infra-red sensors, laser-based-sensors and acoustic-sensors) are [2, 7]:

[1] as applied in the remote sensing applications

- EM wave of lower frequency is able to penetrate foliage, which may be cloud or rain or vegetation canopy (in military applications). This follows from the fact that if the dimension of the object with which the EM wave interacts is smaller than the wavelength of the EM wave, the EM can penetrate past such an object.
- Radar can be used for all weather day-and-night surveillance.
- Radar has the ability to scan larger areas.
- Radar based sensors can achieve larger atmospheric range than most other sensors.

Basic characteristics of EM wave propagation and of its interaction with materials, are determined by the famous set of Maxwell equations. When an EM wave interacts with an object or surface, a range of phenomena can take place. All these wide spectrum of phenomena rising from the interaction of EM energy and matter, can be termed as *scattering phenomena*. Broadly speaking, it can consist of one or more of the following types of interactions.

- *Extinction* is the phenomenon of complete absorption of part of the EM energy by the object.
- *Change of direction of travel* is the phenomenon, where the original direction of propagation of the EM wave suffers a change. This consists of reflection, refraction and diffraction.
- *Depolarisation* is the phenomenon where the polarisation of the incident EM wave is changed. This phenomenon would be discussed in more detail in section 2.4.

Scattering involves the EM wave and the object. Hence it will depend on the properties of both.

- Properties of the EM wave consist of frequency, polarisation and the angle of arrival of the incident wave.
- Properties of the matter or object consist of size, shape, material of the object and its environment (medium of transmission).

Scattering, depending upon the area of return can be of two types:

- *Surface scattering* consists of the energy scattered at the boundary surface between the two media.

- When the EM energy penetrates a material, it interacts with all the electrons in it. Hence, some scattered energy comes from the inside of the material. This is the *volume scattering* phenomena. Mostly, the contribution from this phenomenon is negligible. However, depending upon the wavelength of radiation and the properties of the media, this can sometimes be significant enough and it also helps in foliage penetration capabilities of EM sensors.

One important term in the study of scattering phenomena, is the radar cross section (RCS) or the scattering coefficient. It is defined as [7]:

$$\sigma^0 = \lim_{R \to \infty} \frac{4\pi R_r^2 |E^r|^2}{|E^i|^2} \tag{2.1}$$

E^i and E^r are the incident electric field and the electric field received at the receiver. R_r is the radial distance from the scattering surface to the receiver, and $|$ is the magnitude operator.
Scattering depends to a large extent, upon the surface EM-parameters, surface structure and the wavelength and polarisation of the incident radiation.
Depending upon the *relative roughness* of the surface in comparison to the wavelength of the incident ray, the scattering can be of two types.

Specular: In specular scattering, the maximum amount of the scattered energy is in the same direction. This occurs when the surface roughness is very less in terms of the wavelength of the incident EM waves.

Diffused: In diffused scattering, the surface is rough in terms of the wavelength and the scattered energy is concentrated in no single direction.

If the standard deviation of the surface height is σ_h, then the Rayleigh criterion [7] for the surface to be considered smooth, is given by:

$$\sigma_h < \frac{\lambda}{8\cos(\theta)} \tag{2.2}$$

Here, λ is the wavelength of the EM wave and θ is the angle of incidence.

2.1.2 Synthetic aperture radar (SAR) and its working principle

Radar systems, as a sensor to map the ground, have been used since the forties. A radar works on the fundamental principle of echo detection on a scaled time base. This gives the range of a scatterer from the radar. As in any instrumentation system, resolution is an important parameter in radar systems. In the simplest echo-return radar, the best range resolution achievable, is determined by the pulse width of the transmitted EM wave, and is given by [8]

$$\rho_r \geq \frac{cT_p}{2} \approx \frac{c}{2BW} \tag{2.3}$$

Here, ρ_r is the range resolution, c is the speed of EM wave in the medium of propagation, and T_p is the pulse width. BW is the band width of the radar system, and is given by $BW = 1/Tp$ for the CW radar system.

To improve this resolution, as is evident, the band width should be increased. This can be achieved effectively by using a chirp (frequency modulated burst of EM energy), a method well-known as the *pulse compression* technique, [7–11].

In a pulse compression technique, the expression for the radar range resolution remains the same. However, the advantage here is that, the BW no longer depends on the duration of the pulse transmitted. Hence, the duration of the pulse can be increased to transmit more power, so that the signal to noise ratio (SNR) of the returned echo can be made higher. With higher SNR, the instrument can be used to measure longer range. The processing of the returned pulse can be done by either of the two methods:

Matched Filtering: In the linear FM chirp case, the input can be expressed as

$$s_t(t) = \exp[2\pi i(f_0 t + \alpha t^2)], \tag{2.4}$$

within the time bounds of time t, varying from $-T_p/2$ to $T_p/2$. Here α is the rate of change of frequency in the chirp, and f_0 is the central frequency of the chirp. Then the received echo is given by

$$s_r(t) = \exp(2\pi i[f_0^d(t - \tau_D) + \alpha(t - \tau_D)^2]), \tag{2.5}$$

where τ_D is the total time delay of the return-signal from the transmitter to the scatterer and back to the receiver antenna, and f_0^d accounts for any Doppler component. If the

received echo is matched filtered with $h(\tau) = exp(2\pi i(f_0\tau + \alpha\tau^2))$, then the output is given by [9]:

$$g_F(t) = \text{sinc}(\alpha T_p(t - \tau_D)) \times \exp(-i2\pi f_0\tau_D), \tag{2.6}$$

if the quadratic phase terms are neglected [9]. As is clear from the expression, the width of the sinc function is

$$\Delta\tau_D = 1/\alpha T_p = 1/BW. \tag{2.7}$$

Hence the corresponding range resolution is

$$\rho_r = c\Delta\tau_D/2 = c/2BW. \tag{2.8}$$

Deramp Processing: This consists of demodulating the return signal to filter out the central frequency. This is done, mostly by multiplying the return signal by the in-phase and the quadrature components of the original transmitted signal(delayed by appropriate round trip delay to the scene centre) and adding the product terms [10]. Then the signal is filtered using a low pass filter, and the result is frequency transformed(FFT). The transmitted signal has a time varying frequency. Hence the received signal also has a time stamp in its frequency variation. This method tries to retrieve this time stamp in the frequency domain and hence determines the range in the frequency domain. The range resolution in this method [10], is also given by

$$\rho_r = \frac{c}{2BW}. \tag{2.9}$$

In addition to the range resolution (which is one dimensional), two dimensional imaging also needs appropriate resolution in the cross-range dimension. However, for general radar systems, the cross-range resolution is controlled by the beam width, and is given by

$$\rho_{cr} = \frac{R\lambda}{D}, \tag{2.10}$$

where λ is the wavelength, D is the physical dimension of the reflector of the radar transmitter, and R is the radial distance from the transmitter to the scene-centre. Hence for better resolution, a bigger antenna is required and practical resolution demands impractical antenna size. The alternative to a bigger aperture-antenna, is to synthetically simulate a bigger antenna-aperture, using signal processing. For this, the antenna is moved and the received echo at every point

in the trajectory, is combined *coherently* to give the similar effect as that of having a bigger antenna.

Depending on the operation and the mode of scanning the scene, SAR operation can be

Strip-map SAR , in which the antenna is fixed in one direction. Hence with the motion of the antenna bearing platform, the beam traces a strip and only that strip from the ground is imaged [7, 8, 11].

Spot light SAR , in which a particular area is illuminated by the antenna beam, by steering the antenna in that particular direction through out the motion of the platform. This mode gives much higher resolution than the strip map mode, for the same amount of illumination-energy [10].

Scan SAR , in which the antenna is steered to illuminate a broader strip of land. This is best suited for surveillance purpose [8].

There are many different ways of looking at this process and analysing the operation of this synthetic aperture radar(SAR). Some of these are [7]:

- Synthesised antenna approach.
- Doppler beam sharpening.
- Correlation with reference point-target response.
- Matched filter for received point-target signal.
- De-chirping of Doppler frequency shift.
- Optical-focusing equivalent.

As shown in various monographs [7–11], the optimal resolution obtained following any of these view points, for strip-map SAR, is the same and is given by:

$$\rho_{cr} = D/2. \tag{2.11}$$

This is the resolution achievable, if the synthesised aperture is of the optimal length given by $R\lambda/D$. And in this case, the resolution is independent of the distance of the imaging platform

from the scene [7–11].

2.1.3 Bistatic radar, advantages and issues

Bistatic radar is defined as a radar that uses antennas at different locations for transmission and reception [12]. Figure 2.1 shows the generic configuration of a typical bistatic radar system. Figure 2.2 gives a few of the important parameters in a bistatic configuration. Of these, the most used parameter is the bistatic angle (β). It should be noted that, when $\beta = 0$, the transmitter and receiver are co-located, and the bistatic configuration behaves as a monostatic system. Hence the monostatic configuration is a special case of the bistatic configuration.

Most of the early radar systems were bistatic in a strict sense, as they were using different antenna for transmission and reception. With technical advances, the same antenna was used for both transmission and reception. This is the monostatic configuration. Till now, most of the conventional radars are monostatic.

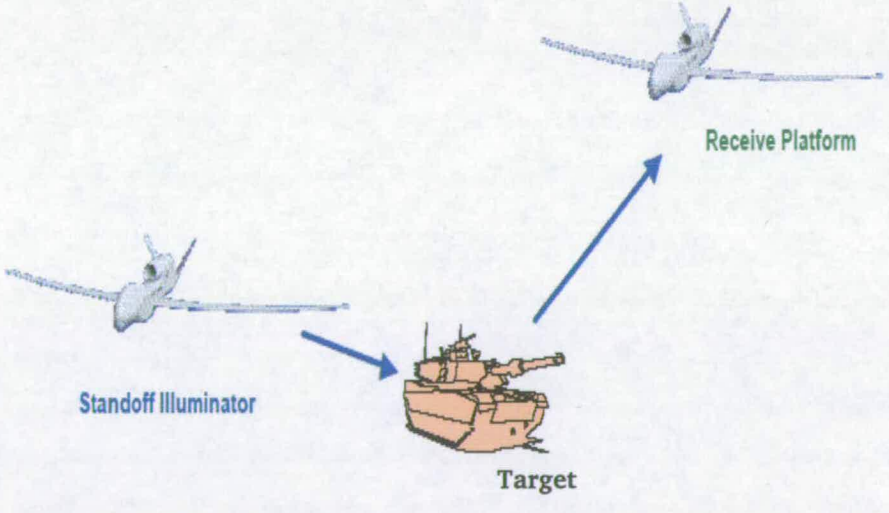

Figure 2.1: *Generic bistatic configuration*

Of late, there has been a revival of interest in the bistatic radars. This is because of the fact that the bistatic radar system is the superset of the monostatic radar system. Hence, many innovative

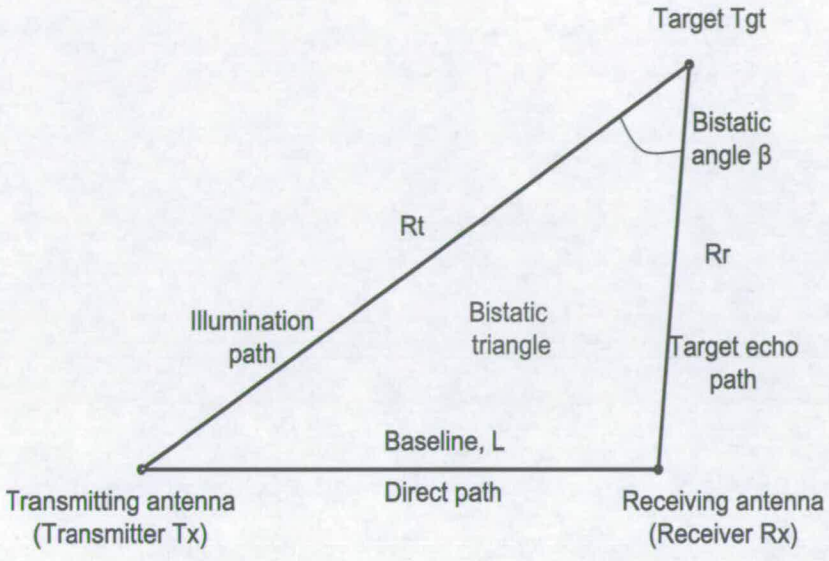

Figure 2.2: *Some conventions in a bistatic configuration*

applications which could not be achieved using a monostatic system, could be implemented using a bistatic system. Some such applications are [13]:

Semi-active homing missiles: This is a guided missile system, with the transmitter in the control platform, and the receiver in the missile. The feasibility of a radar guided missile depends much upon the design of a light transmitter unit (which is extremely challenging) or the use of a receiver-only unit in the missile, which uses a standby transmitter in the control platform. The second option is a bistatic radar system.

Hitchhikers: A bistatic hitchhiker or opportunistic bistatic radar [14], uses transmitted power from a station, which is not a part of it. Hence the transmitter can be friendly (for example EM radiation from satellites, or some other radar system, which has been designed as a monostatic radar), or hostile (in which case the transmitter may be some enemy radar system). This area is an attractive and active area of research world-wide [15].

Counter measures: Mostly, ground based air surveillance systems reveal themselves. Because they have the transmitter *in situ*. The system could be made safer, if the transmitter can be moved to a friendly location, while keeping the receiver (which is passive) in the enemy area. This again needs the implementation of a bistatic configuration.

Counter-retrodirective jammers: Present day jammers mostly exploit the angle of arrival(AOA) configuration and hence are highly effective against monostatic systems. Bistatic configuration based radars would be mostly immune to such jammers.

Counter stealth: Most of the stealth techniques employed currently, are designed in decreasing the monostatic RCS. However, stealth against bistatic radars is highly challenging. This is because the bistatic angle can be of any value and with a different bistatic angle, the bistatic RCS changes. And the bistatic angle of operation is not known during the design-phase.

ECCM: Prototype bistatic radars have also been shown to be effective in detecting stealth targets which are not detectable by monostatic radars [16].

FOPEN: Certain studies have also shown the effectiveness of a bistatic radar as compared to a monostatic radar, in its foliage penetration (FOPEN) abilities [17].

Clutter tuning: When both transmitter and receiver platforms are in motion, the velocity of the two can be controlled so as to get minimum amount of clutter Doppler shift and clutter Doppler spread. This also makes it possible to have the moving target indication(MTI) facility possible, in the direction broadside to the transmitter's motion.

Remote Sensing: In remote sensing, having a second satellite moving as a receiver-station-only can give many advantages [18, 19]. By this, two views of the ground can be generated by a low cost receive-only satellite. Moreover, as RCS varies with the change from monostatic to bistatic operation, more information could be obtained of the land as compared to simple monostatic information.

Pulse Chasing: This is one of the innovative use of the bistatic configuration, mainly used for battle time surveillance. This needs that the transmitter and the receiver are properly synchronised, and that the orientation of the transmitter beam and the exact timing of the EM energy or pulse leaving the transmitter, are known by the receiver. Then using an electronically steerable receiver beam, the receiver beam could be synchronised to the transmitted pulse (hence the name *pulse chasing*). This results in an extremely quick surveillance speed.

Possibilities Open: Lastly, as has been mentioned, the monostatic system is a subset of the bistatic system. Hence by intuition, limitations in monostatic geometry should get alleviated in the bistatic case [20].

There are a few major issues that hinder the popularity and implementability of the bistatic system. First of all, bistatic radars are extremely challenging to design. This is mostly due to the transmitter-receiver clock synchronisation issue. This issue becomes more crucial, if SAR operation is desired, as the basic principle behind SAR imaging is the *coherent* combination of the return signal. Hence synchronisation and phase noise are some of the biggest challenges in Bistatic implementation.

Secondly, the performance of the bistatic radar system is mostly measured, in the scale of the monostatic system performance. However, the applications where the monostatic radars have proved themselves, are mostly not handled any better by the bistatic radar systems. For example, the bistatic spatial coverage is always smaller than that in monostatic case, other parameters remaining the same [13]. This often raises the question of, why to go for bistatic, if it can not give better performance. This in turn stops the end users from getting sufficiently interested in the bistatic configuration.

Lastly, due to limited field trials, the availability of the analysis of bistatic systems in modern capabilities, is highly limited. Hence, unless a certain specific highly demanding purpose is fulfilled, large scale bistatic implementation as of now is not practical. However, futuristic trends do seem to be supporting bistatic trends. With the ongoing interest in bistatic operation, technical problems and hence cost barriers against bistatic radar seem to be fast receding. Futuristic systems are expected to integrate both bistatic and monostatic operations in the same platform to some extent [4, 21].

2.1.4 Speckle and clutter

SAR image is formed by coherent combination of the electromagnetic energy scattered from the whole scene illuminated. However, all the scatterers in a particular resolution cell are not homogeneous, and their geolocations in relation to the radar are mostly random (or could be modelled as random in most of the practical cases). This introduces a noise, which is typical of any image formed using highly coherent EM-waves, and is termed as *speckle noise*. Formally, speckle can be defined as [12]

> A mottled effect in coherent radar images, such as those from synthetic aperture radar(SAR) and laser radars caused by random additive and subtractive interference of signals from the individual scatterers within each resolution cell.

Speckle has been shown to be best modelled as a multiplicative noise [22, 23]. Depending on the level of statistical modelling, SAR-speckles can be modelled by three main models [22]:

Multiplicative speckle model: In this model, the intensity of each pixel is modelled as the product of signal intensity and the speckle noise intensity.

$$I(i,j) = S(i,j)N_{sp}(i,j), \tag{2.12}$$

where $S(i,j)$ is the signal intensity, $I(i,j)$ is the image intensity and $N_{sp}(i,j)$ is the speckle noise intensity for the pixel in a SAR image, of indices i and j. The speckle noise can be modelled by some statistical distribution, like the $K - Distribution$, the $Gamma - Distribution$,the $Weibull - Distribution$ or the $Log - normal - Distribution$ [24].

Product Model: This can also be called a doubly stochastic model, in which the parameters of the speckle noise distribution are modelled as non-stationary. However, the variation of the parameters is assumed to be ergodic.

Multiple Stochastic Model: In this model, deeper levels of statistics are assumed. However at some arbitrary deepest level of statistics, parameters are assumed to be ergodic.

Even though the *product model* has proved fairly satisfactory for SAR images, for more sensitive images like medical imaging, the *multiply stochastic model* is used for better performance. Another characteristic feature of radar returns, mostly from sea and land is the radar clutter. Clutter is defined as *unwanted echos, typically from the ground, sea, rain or other precipitation, chaff, birds, insects, meteors, and aurora* [12]. Study of clutter and modelling of clutter, have been major areas of focus for the radar researchers [25,26]. This is mainly because, clutter modelling helps in proper clutter filtering. Secondly, clutter characterisation can also help in land form classification.

2.1.5 Approaches in bistatic SAR signal processing

Bistatic radars have been slowly gaining their popularity due to the reasons discussed in section 2.1.3. However, there still exists very few open literature on bistatic radar signal processing in general and bistatic SAR processing in particular.

In their works, Lowe *et al.* [27] and Horne *et al.* [20] have discussed signal processing methods

for bistatic SAR processing with some preliminary results. In a limited study of practical images from some exemplar simple bodies, Gupta *et al.* [16, 28] have studied some of the differences between monostatic and bistatic images. Their results show important differences between the monostatic and the bistatic images, with which they have concluded that for higher order diffraction, the bistatic images vary markedly from the monostatic images. In another recent study, Fung *et al.* [29] have proposed scattering models for bistatic multiple scattering phenomena. There also have been studies for the calibration of bistatic polarimetric radars [30]. This has been done with an eye on satellite imaging radars. Because, bistatic radars have gained a good reputation in satellite imaging [18], with space borne bistatic radar mounted satellites, from both USA and Europe. Germond *et al.* [31, 32] have given studies and closed formula for calculating polarimetric variables for bistatic radars.

Recently, there has been some reports in the open literature on bistatic SAR imaging [33–35]. Of interest is the work by Rigling *et al.* [35], where they have given complete analytical analysis for the bistatic SAR image formation, using the polar-to-rectangular reformatting algorithm. Even though the simple matched filter based image formation would give the best quality image, it could not be accepted for most of the practical cases, due to its heavy computational demand. Polar-to-rectangular reformatting algorithm for forming SAR image, not only gives a good compromise between image quality and computational speed, it also gives the advantage of looking at the whole process from the k space perspective (which is geometrical and hence more intuitive).

However there has appeared no report in open literature about bistatic radar imaging applied for ATR purpose. Some initial studies by Ulaby *et al.* [17], where they have tried to measure the bistatic RCS of a target in clutter using a Ka band VV polarised radar, show that bistatic radars are more effective in detecting targets in clutters, the bistatic target classification problem has not been studied in any report before.

2.2 EM signal modelling and simulation

2.2.1 SAR raw signal simulation

SAR raw signal simulation is important from two main perspectives:

- For the purpose of study of a SAR system, before it has become operational [36]. Design and development of a new SAR system is costly. Hence, the design of the actual signal

processing, is in many cases preceded by the analysis of simulated data [10].

- For the purpose of evaluating any algorithm for a system, the actual data from which are rare. The current project demands SAR simulation for this reason. Bistatic radar systems are still in a developmental phase. Hence, field collected bistatic SAR data are hard to find. Some organisations have run bistatic exercises to collect bistatic SAR images of ground targets. However, either the dataset is too limited (for example, of only a few targets and from a few bistatic configurations), taken just to demonstrate bistatic SAR imaging capabilities, or is classified. Hence, generating synthetic SAR target-signatures is the only viable option.

Depending on the level of abstraction assumed in the physics of the scattering phenomena, the SAR simulation can be developed based on a scattering centre model, or a facet-based model or a strictly EM-computational approach like the method of moment (MoM) model. Of these, though the MoM approach is the most correct one, it is extremely time consuming and complex in nature. This is specially so, when the wavelength of the illuminating wave is an order larger than the dimension of the target or objects of interest in the scene. Depending on the signal processing approach taken to simulate, SAR simulation can be performed using the space-time processing approach or using the frequency domain approach.

2.2.1.1 Facet approach

The facet approach assumes a specular-reflection model rather than a dispersed scattering model. [7]. In this approach the continuous surface is modelled as summation of planar facets, which should be smaller than the size of the resolution cell of the radar-system, and larger than the wavelength of the illuminating wave. For practical simulation purpose, 4×4 facets per resolution cell have been prescribed sufficient [36]. Facets have also been used for military target simulation [37], and the approach has proved promising.

2.2.1.2 Scattering centre approach

From the geometrical theory of diffraction (GTD) [38], if the wavelength of the illuminating wave is sufficiently smaller than the dimension of the target features, the scattering return from a target can be modelled as the sum of responses from distinct scattering centres. There are

five major canonical scattering mechanisms, depending upon the frequency-dependence of the scattered energy [39].

- Edge diffraction which is from a curved surface, and where the diffracted return varies inversely with the square-root of the frequency.
- Corner diffraction, where the frequency dependence is that of inverse proportionality.
- Reflection from sphere (doubly curved surface), in which case the scattered energy is frequency independent.
- Reflection from cylinder surface (singly curved), where the scattered power is proportional to the square-root of the frequency.
- Reflection from a flat plate, where scattered power is directly proportional to the frequency.

The validity and the practical appropriateness of scattering centre approximation has been shown, both from exact simulation [40] and using theoretical rigour [37]. Hence, if the target features are known accurately and the type of diffraction can be estimated properly, then the SAR image of the targets can easily be generated by this approach [41].

2.2.1.3 Space-time domain approach

In SAR image generation, one of the most popular ways, is to first model the scene to be imaged. This can be done either by a facet approach or a scattering centre approach or a combination of the two. Then in a simulated flight path, the total return from the scene is to be collected with appropriate delay and weighting (by the scattering coefficient) from all the scattering centres or facets. This is to be done from all the points on the simulated flight path. This forms the raw signal, and could be processed by the matched-filter approach or the deramping approach [7, 8, 10] to get the final SAR image.

2.2.1.4 Frequency domain approach

Another method of processing of SAR images, is to directly deal with the signal in the frequency domain. This can be done in two ways.

Scattering Centre Approach: The return from a group of scattering centres can be modelled as [42],

$$E_n^s(f,\phi) = A_n(j\frac{f}{f_c})^{\alpha_n}\text{sinc}(\frac{2\pi f}{c}L_n\sin(\phi-\phi_n))$$
$$.\exp(-2\pi f\gamma_n\sin\phi).\exp(j\frac{4\pi f}{c}(x_n\cos\phi+y_n\sin\phi)) \quad (2.13)$$

where E_n^s is return from the n^{th} scattering centre, whose frequency dependence is given by the parameter α_n, spatial position is x_n, y_n, and its length is given by L_n. The damped-exponential factor of the scattering centre is given by the parameter γ_n(for localised scattering centre), and its orientation angle given by the parameter ϕ_n. ϕ is the azimuth angle of the radar with respect to the scene centre. As can be seen, if the angular swath and the frequency-band over which the scene is to be imaged, are known, then the above model gives directly, the frequency response of the scene. This in turn is the phase information of the scene in k or frequency space or the polar map [10]. This data for a range of f and ϕ, can be polar-rectangular reformatted or directly taken for an IFFT to get the simulated SAR image in the spatial domain.

RCS generating tools: Some of the commercially available tools calculate the RCS of the target, using the method of moments or physical optics (PO) approximation (detailed treatment given in the next chapter). Hence, if we know the angular swath and the frequency band, over which the scene is to be imaged, the output from the tool can be reordered to represent the phase history of the scene or the target. The SAR image can then be obtained by taking the IFFT of the data (preferable after polar-to-rectangular reformatting).

2.2.1.5 Shadow regions and their implementation

Practical scenes and targets to be imaged, are all in three dimension and hence pose shadow. The shadow information is an important piece of information and has been used in the detection of moving objects [43]. However the formation and the effects of shadow in EM imaging are sometimes different from that of physical optics scenario. For grazing angle more than 10 to 20 degrees, the geometrical optics (GO) can be used with no drastic inaccuracy. For lower grazing angles, the inaccuracies in the vertically polarised component of the scattered field can be unacceptable, if modelled using geometrical optics approximation [44].

Shadows and their modelling is more important in a bistatic scenario. Because, in the bistatic

case the transmitter and the receiver being at different locations, will pose two different shadows of the same target. As the shadows depend upon both the shape of the target and the orientation of the transmitter or receiver, shadow information contains a lot of information about the target. In bistatic geometry, the two shadows give information of the target from two orientations. Hence, shadow in bistatic operation can play an important role in target recognition. The next chapter describes an innovative approach taken in the current project to generate approximate bistatic shadow.

2.2.2 SAR raw signal simulation approaches

SAR raw signal simulation needs proper and accurate modelling of both, the systems and the physical phenomena involved. The approaches in this regard can be studied under three headings consisting of the study of the EM simulation approaches in general, of simulation for remote sensing data generation, and of simulation for military scene data generation.

- Scattering returns of a wide range of natural materials have been studied, modelled and formulated into closed expressions in some recent monographs [26]. A similar exhaustive study has not been found for man-made materials and objects. For generic scattering phenomena, models have been tried and put into closed expressions by Fung *et al.* [7,45,46]. Their study covers mostly scattering from natural terrain, and have dealt with multiple scattering, depolarisation effects, and variation with angle of incidence. About man made targets, it has long been known that, if the wavelength is smaller than the physical dimension of the target being illuminated (more accurately, the standard deviation of the surface roughness), then a physical optics (PO) approximation can be used to generate the EM scattering from the body. In a detailed study on this matter, Soriano *et al.*, have shown that PO indeed does a practical approximation for most of the cases, except for man made objects on ocean [47].

- There have been significant contributions from Franceschetti *et al.*, in the field of simulation approaches for remote sensing SAR images. One of the major contributions from them, has been the use of frequency domain approach in generating the final SAR raw signal. Taking the frequency domain representation of the scene scattering parameters, and the radar system impulse response, they have approximated the whole procedure of image formation to simple 2-D deconvolution in the time domain, and hence 2-D FFT in

the frequency domain.

$$H(\eta,\xi) \approx \Gamma(\eta,\xi).G_0(\eta,\xi), \tag{2.14}$$

where $H(\eta,\xi)$, is the reconstructed SAR image in the frequency domain, $\Gamma(\eta,\xi)$ is the modified scene scattering coefficient matrix in the frequency domain, and $G_0(\eta,\xi)$ is the system transfer function. The above results have been mathematically derived and established for both strip-map SAR [36,48], and spot-light SAR systems [49].

In one of the works [36], they have suggested a SAR simulator named as SARAS, for generic SAR image simulation. Even though intended towards natural terrain SAR image simulation using a facet approach, the work does give a nice review and approach towards any SAR simulator. They have dealt specifically with the landscape simulation, in another work [50], and in a recent attempt they have handled the simulation of urban landscape [51]. Urban landscape differ markedly from natural terrain, in that it offers much more multi-path effects in the scattering phenomena.

The general SAR image simulation approach has been summarised in [52].

- SAR simulation for man made targets have mostly been achieved using geometrical theory of diffraction (GTD), physical theory of diffraction (PTD), or the method of moments (MoM) to calculate the target RCS, as the first step. The methods used for finding the RCS is [53], target modelling using simpler geometrical models, like planes, ducts, cones, wedges etc. Then comes the step of computing the total scattered field, taking into account various parameters like frequency, geometry of sensors, and polarisation. It has been shown [54] that for target RCS simulation using millimetre waves, UTD approximations give almost the same result as the more exhaustive MoM. There has also been the application of hybrid methods, using both UTD and MoM [55]. In such approaches, the target surfaces are grouped, so that simpler surfaces are modelled using UTD. More complex textured surfaces are modelled using MoM. A more detailed and exhaustive analysis of RCS modelling for aerial targets have been given by Shirman *et al.* [37].

  To generate the SAR image of a target, the RCS has to be calculated for the band of frequencies used by the radar system. This gives the frequency response of the target to that frequency band. The process is then repeated over the range of aspect angles through which the real SAR is to operate. This gives a two dimensional phase history of the target [47]. This phase history or k space data is in polar format. Hence for best result it has to be polar-to-rectangular resampled [10]. Then taking the 2D IFFT gives the SAR image of the target. Detailed steps on this procedure are presented in the next chapter.

2.2.3 Commercial SAR simulators available and the features thereof

As discussed in the previous section, SAR simulation of man-made targets invariably needs the calculation of RCS as the first step. For this, utilising some computational EM simulation tool is the best choice. Some of the available computational EM RCS-calculation tools are:

$SAIC - XPatch^{TM}$ **[56]:** XPatch is one of the most widely used RCS prediction tool developed by the department of defence(DoD) of the USA. Developed in 1997, XPatch uses the shooting and bouncing ray(SBR) technique [41], which is built upon the GTD approximation principles. It is capable of RCS prediction, 1D high range resolution(HRR) profile prediction, 2D SAR image prediction, and scattering centre(SC) prediction for a three dimensional target [57]. One of the drawbacks in XPatch has been shown to be the use of flat facets, due to which it needs a large number of facets in modelling doubly curved surfaces [58].

$SAIC - RCSSIG^{TM}$ **[59]:** This is a tool from Science Application International Corporation (SAIC). This product mainly aims at predicting RCS of 3D targets, based on physical optics and physical theory of diffraction approximations. This tool does not use MoM method, and hence is more suitable for very high frequency RCS prediction.

$Epsilon^{TM}$ **[60]:** Epsilon is a product from the joint effort of Roke Manor research and the UK defence evaluation research agency (DERA). It has been shown [61] to be useful in :

- bulk RCS prediction,
- range profile prediction,
- SAR and ISAR imaging, and
- pulse synthesis,

from the CAD model of the target.

$Lucernhammer^{TM}$ **[62]:** This is another popular tool from the USA, which uses PTD, PO approximations and SBR technique, like the XPatch. It is able to predict the RCS and ISAR Image.

$WIPL - D^{TM}$ **[63]:** WIPL-D has been a tool for EM modelling and simulation, mostly used for the analysis of scatterers, antennas and EMC (EM-computability). This tool is completely based on MoM calculation, and hence is highly demanding in terms of computing

resources. Even though not so suitable for SAR image calculation of real life size targets, it can be used for small scale modelling of targets and environments. One such endeavours have been the FOPEN experiments done by Simcoe *et al.* using WIPL-D [47].

$FEKO$ **[64]:** FEKO (*FEldberechnungbei Korpern mit beleibeiger Oberflache*, a German phrase meaning field computations involving bodies of arbitrary shape) is a relatively new tool for RCS simulation. It has also been designed mainly for the analysis of EMC, shielding, coupling, antenna design, antenna placement analysis, design of micro-strip antennas and circuits, and scattering analysis. Due to its ability of RCS prediction, it can also be used for SAR image calculation. FEKO can be set to use either MoM or PO approximation. It can also be programmed to use a hybrid approach [55], by setting a portion of the object to be modelled using MoM and rest of the object to be modelled using PO.

Out of the tools described above, $SAIC - XPatch^{TM}$, and $SAIC - RCSSIG^{TM}$ are export restricted, and hence not available to researchers out side the USA. $Epsilon^{TM}$ and $Lucernhammer^{TM}$ are not available for academic use. $WIPL - D^{TM}$ could not be used for calculating RCS of life-size targets for GHz range frequencies. Out of all these, $FEKO$ was found powerful enough and easily available. The next chapter will discuss at length, the use of $FEKO$ in the current project.

2.3 Approaches towards SAR image classification

2.3.1 SAR ATR and issues

Modern combat aircraft is becoming ever more complex and powerful in their abilities and performance. A major contribution towards the performance and power of any real-world system in general and of a defence system in particular, is the amount of information output. The modern combat plane systems do output a huge amount of data, about a wide spectrum of parameters to the operator. Hence, automated or semi-automated systems for defence applications are on an ever increasing demand. SAR automated target recognition(ATR) systems are a great value addition, if SAR mapping is already integrated in an airborne system. SAR ATR for ground based targets is also important in battle field surveillance using unmanned air vehicle based SAR systems. SAR imaging is one of the most convenient imaging for surveillance purpose, because [2]:

- of the all weather imaging ability of SAR system.
- with higher resolution, SAR images have come very close to optical images as far as clarity or resolution is concerned.
- SAR systems can use longer wavelength, and hence can often be used for foliage penetration (FOPEN) to detect hidden targets.
- SAR images are built from the raw EM scattered data, and so they contain information about the EM properties of the targets, and hence can sometimes prove more important than simple optical images in target recognition.

The whole process of ATR using SAR image can be divided into three major steps [65]:

Detection/Prescreening: Usually the SAR map is obtained of a fairly large area of the (battle) scene, and may be having a number of targets in the same image. Hence, the first step is to choose only those portions from the SAR image, which might contain a target. It has been found that the SAR images of man-made targets often consist of brighter pixels than the surrounding clutter. Hence, the prescreening is mostly done by comparing the local brightness of the image pixels and comparing them to some threshold value (chosen from proper consideration of the scene being imaged and the target parameters).

Discrimination: The prescreening stage gives the possible regions of interest (ROI). In the discrimination step, the ROI is further processed to reject possible false alarms that might have crept in through the prescreening stage. The output from this stage is a more certain ROI, and might also consist of some of the features of the target (like orientation, and target-area).

Classification: In this final step, the features generated in the last step are used to classify or recognise the target, using some classification or recognition algorithm. Even though classification literatures [66, 67] keep a distinction between the classification and the recognition algorithms, the SAR ATR literatures mostly use classification and recognition in the same sense [12].

The steps described above may not all be so distinct in all the ATR approaches. Especially the discrimination and the classification steps mostly are not so distinguishable.
Some of the major research on SAR classification, as reported in the open-literature, is discussed in the next few subsections.

2.3.1.1 Approaches by the MIT-Lincoln lab:

US-DARPA (Defence advanced research project agency) funded semi-automated IMINT processing (SAIP) project has been a fore-runner in research into SAR ATR. In this, the major role has been played by the Novak *et al.* team from the MIT-Lincoln laboratory. In all the approaches, due to the exhaustive amount of data available, a mean square estimation (MSE) algorithm has been used for the classification purpose. Some of the early works have been based on the SAR images collected through the Lincoln laboratory 35 GHz SAR sensor [68]. In 1995, DARPA and AFRL initiated a programme called the moving and stationary target acquisition recognition (MSTAR). Under this program, a huge amount of SAR image datasets were collected using X-band, HH-polarised SAR sensors. A large number of different military vehicles were imaged in spotlight mode over 360 degrees of aspect, with 0.3×0.3 m. resolution. The MSTAR database with some manipulation and reduction in original image resolution, has been released in public domain for the wider research community [69]. Hence the MSTAR data base has been one of the accepted and widely used source of database for testing and validating most of the ATR algorithms in the literature.

In one of their works [65], Novak *et al.* have reviewed the Lincoln lab approach towards dealing with fully polarimetric SAR data. The original results were published in the MIT-Lincoln lab journal in 1995 and have been made public in this paper. This is a feature based MSE classifier. The features used, have been carefully chosen and are markedly different from the features used in any typical optical target recognition task.

In another work [70], Novak *et al.* have reported the investigation on super resolution SAR ATR. In this, it is shown that, better performance of the ATR systems result with higher resolution SAR imaging.

In [71], Novak *et al.* have given a consolidated review of their approach towards SAR ATR. An MSE classifier was used in the work. The targets included in the classification exercise were of three types, armoured personnel carrier (APC), infantry fighting vehicle (IFV) and main battle tanks (MBT). The interesting part of this report is the analysis of the ATR performance with change of features of the same target class. For example, some of the features of an MBT that were changed are

- skirt of the MBT.
- barrel of the MBT.

- reactive armour of the MBT.

Other configurations considered were

- target in open;
- target in half revetments, and
- targets in full revetments.

The authors have speculated that, classification could be improved if templates could be made for various rotations of turret, in the training phase.
Reports from the MIT-Lincoln lab group is one of the standard sources of an exhaustive set of SAR ATR experiments, where the complete chain of the ATR process has been examined in a detailed manner. Based on real data, and done with interaction from the user community, this set of works could be taken as a reference in study towards ATR using any sensor.

2.3.1.2 Approaches using likelihood test algorithm

There has been a few approaches in using a likelihood test algorithm for monostatic SAR ATR (validated using the MSTAR data base) [72,73]. In the work by O'Sullivan *et al.*, three types of models have been assumed and applied to the MSTAR data base. The models considered are:

Conditionally Gaussian model: The SAR image pixels are modelled as conditional *Gaussian* random variables, conditioned on the target type and target orientation. Further, the noise is modelled as additive zero-mean Gaussian noise. For determining the parameters of the model for a particular target type and within a range of aspect angle, all the test image-clips are considered from the same target and within the given set of aspect angles. Due to the simplicity of the model, the estimated mean and variance are simply the mean and the variance of the pixel from all the test image-clips.

Log-magnitude model: In this model, the *complex valued* pixels of the SAR image, are assumed to be independent and follow a *log-normal* distribution. The parameters of the distribution are assumed dependent on the target-type and orientation of the target. In this case, the estimated parameters can be calculated by using the pixel values in dB scale from all the training image clips available for the given target and in the given range of aspect angles.

Quarter power model: The image pixels can also be modelled as random variables following a *gamma* distribution, with the parameters depending upon the target-type and the aspect angle. In this case, the estimated mean can be shown to be equal to the mean of the square-root of the magnitude of the corresponding pixel from all the training image clips.

The conditional Gaussian model was shown as the best choice among the three [73]. The SAR-ATR performance reported by this set of works, is one of the best in the open literature. Hence this approach has been used as the standard ATR algorithm in the present project to compare the results from any new ATR algorithm.

2.3.1.3 Approaches in exploiting fully polarimetric SAR data

Most of the major ATR approaches have used single polarisation SAR data. There have been very few studies on using multi polar SAR data for better ATR performance.
Novak *et al.*, have used the fully polarimetric data using the polarimetric whitening filter (PWF) processing, developed by their team [68], for filtering the speckle and getting better quality SAR images [65,68]. The different polarisation information has been used in a limited sense in the ERIM polarimetric feature determination to give information about odd or even bouncing of the scattered rays [65].
However the polarimetric SAR data in monostatic configuration have been proved to have much more particular information about the target physical features and aspects [6]. In another work [74], a way of decomposing the scattering matrix into three components, has been proposed. This has been done with the assumption that scattering from any surface can be approximated to that from a sphere or a diplane or a helix. Another important representation in analysis of the polarimetric characteristics of the SAR imaged objects is the *polarimetric signature* [2]. Polarimetric signature, with some modifications to it, has been shown [75] to contain rich information about the target EM-properties. Polarimetric return has also been shown theoretically to provide better information, which could be exploited for better classification of SAR images [76,77].
Chapter 6 of the current thesis will describe in detail, the algorithms developed in the current work, to exploit multiple polarisation SAR images, for enhanced SAR ATR performance.

[2]Polarimetric signature is a 3D surface, to represent the variation of the scattered energy return, with respect to the variation in the polar-tilt angle and the polar-ellipticity angle, which in turn define the polarisation state of an EM radiation.

2.3.1.4 Approaches in dealing with complex SAR data

Radar is a coherent illuminator. Hence SAR raw data have both amplitude and phase components. However, mostly, the image is formed using the magnitude-only data and the classification steps are taken after the image-formation procedure. Hence, the phase information is mostly neglected. There have been some ATR approaches [72, 73] using complex valued data. In one of the limited studies [78], it was shown that taking complex data *may* increase the classification performance by around 10 to 100 times, than by taking the amplitude-only data. This limited work, does show the scope for complex-valued data for classification purposes.

2.3.1.5 Approaches dealing with scattering centre model

As has been discussed, SAR images of man-made objects often can be approximated as coming from distinct scattering centres. There has been some research work, on using this model and extracting the scattering centres from the SAR image and using them in turn, for the recognition exercise. There are a few advantages of this approach of using scattering centres for ATR purpose.

- By considering the scattering centres, the computational load is reduced by several orders. Because, instead of dealing with all the pixels in the image, operations are performed with a much smaller number of scattering centres.
- Scattering centre model of SAR image is dependent on the scattering phenomena experienced by the radiated EM energy. Hence it depends on the physical features of the target, which information in turn may prove useful in the ATR operation.

The approach in using scattering centres for ATR can be consolidated under two major steps:

Extracting the scattering centres from the SAR image: Many approaches have been presented in the open literature for this step. For example, Rajan *et al.*, have proposed to use the CLEAN algorithm for extracting the position information of the scattering centres from the SAR image [41, 79, 80]. The algorithm is an iterative algorithm, which assumes the brightest available pixel in the SAR image to correspond to the position of a scattering centre. In each iteration, it determines the brightest pixel and tries to separate that pixel(scattering centre), and its effect from the whole image. It has also been claimed that the same algorithm should work for bistatic case [41].

Extracting information from the scattering centres: The return from a group of scattering centres can be modelled by the expression 2.13 [42]. According to this model, each scattering centre can be associated with a set of 7 parameters $(A_n, x_n, y_n, \alpha_n, \gamma_n, L_n, \phi_n)$. These parameters give important information about the physical and EM characteristics of the scatterers, and hence could be used as important features in the SAR image classification exercise.

In some of their works [81, 82], Moses *et al.* have used the scattering-centre model for SAR image classification. They have considered the more detailed model as put above and also two simpler approximate models [82], the *damped exponential model* and the *undamped exponential model*. They have used the least square estimator (LSE) for estimating the parameters of the scattering centres, and have reported encouraging results. In a later work [81], they have utilised the approach for SAR ATR using the MSTAR database. Results are comparable to those reported by Novak *et al.*.

2.3.1.6 ANN and SVM approaches:

There have been certain reports on SAR ATR using nonlinear classifier approaches like artificial neural network (ANN), support vector machines (SVM), radial basis functions network (RBFN) etc. In one of the correspondences, Gross *et al.* [83] describe an ANN based approach to detect moving targets using the high range resolution (HRR) profile data. In that, it has been claimed that if the HRR profile data is handled directly, before framing any image, then it can help in the detection of moving targets as well. Though results have not been very encouraging, still they claim that in real life flight it might be of use.

In another approach [84], Zhao *et al.* have used RBFN for recognising targets. In this approach, the HRR profiles have been used, both in training and in test phase. They have shown how to determine the decision boundary, RBFN is more effective than the traditional (Parzen window) kernel classifiers.

Principe *et al.* [85] have used SVM for SAR ATR. In this approach dealing with MSTAR data set, the SAR image has been directly used for the purpose (instead of generating the HRR profiles). SVM along with optimal hyperplane networks have been considered in the work. Though SVM has been concluded as the best among all the algorithms considered, no comparison has been made of the performance of SVM, with the performance using conventional linear ATR algorithms.

In a recent work by Yang *et al.* [86], they have compared the SAR ATR performance using

a number of feature extraction techniques (principal component analysis (PCA), independent component analysis (ICA), and Hu-moment) and a number of classification algorithms (k-NN, SVM, linear discriminant classifier, and quadratic discriminant classifier). It was shown that for the MSTAR database, PCA based k-NN algorithm works the best.

2.3.1.7 Sub-aperture and HMM approaches

In addition to the above methods, there have been some novel ways in the open literature, of solving the SAR ATR problem.

Kim *et al.* [87] have used a novel idea for SAR image segmentation and analysis. The SAR image formation step needs a particular aperture for a particular desired resolution. In their work, they have proposed to extract multiple images from the supplied SAR image, by taking smaller apertures, a process which they coin as sub-aperture analysis. As the speckle and scattering centre response change according to the aspect angle, the sub-aperture based images are claimed to give different features of the image. The authors also claim that this analysis can exploit the speckles in the SAR image, for better classification performance. The ATR performance has been compared (using the MSTAR database) with the results from wavelet and template-matching methods, showing the proposed method to be comparable and in some aspects better than the other two.

Runkle *et al.*, have tried to use the principle of hidden Markov model (HMM) in SAR ATR [88, 89]. The HRR profile for the same target varies with the aspect angle [87], but can be assumed to be almost stationary within a small variation of aspect angle. The authors have assumed Markov chain rule in relating the consecutive HRR profiles. As the target type and its pose are the factors determining the final observation and they in themselves are not known, the whole procedure is modelled by a hidden Markov model (HMM). MSTAR data base has been used in the classification exercise and the HRR profiles have been reverse-generated from the target SAR images. Though results reported are comparable to those from Novak *et al.*, the processing involved is too much demanding. The use of 120 states in the HMM (as done in the correspondence) in itself seems formidable.

2.3.2 Relevant classification approaches using remote-sensed SAR images

Classification exercises in remote sensed SAR images from space borne radars, are in many ways different from the SAR ATR approach. Because, remote sensed SAR image classifi-

cation is done to classify the terrain coverings. Secondly, processing for space borne radar SAR images, could be done off-line. Hence, the timing limitations are not as severe as in the case of the SAR ATR problem. Hence more complete approaches like fully-polarimetric SAR and multi-frequency SAR, and more complicated approaches like ANN are more common and more exploitable within present technological constraints, for remote sensed SAR classification problem. Some of the approaches which deal with the problem of ATR will be discussed in this section.

In an approach towards automatic image segmentation, Bhanu *et al.* [90] have used functional templates and have trained the templates using a genetic algorithm. Due to the availability of fully polarimetric data in this field, there has been many approaches using fully polarimetric data. Using the fully polarimetric complex-valued SAR data, a fuzzy based classifier [91], and a fuzzy-neural classifier [92] have successfully been implemented. Use of fully polarimetric data in filtering the speckle from the remote sensed SAR image, has also been tried successfully [93]. Certain other approaches [92, 94, 95] have used the principal component extraction and ANN for this task. One of the most powerful algorithm in utilising polarimetric information has been from a work by Ulaby *et al.* [96], where the effectiveness of using just one or two polarimetric features in classifying the terrain effectively, has been demonstrated.

Even though, not directly related to SAR ATR, a study of approaches in remote sensing SAR image classification is pertinent. This is mostly because, out of all classification problems, remote sensed SAR classification problem is the closest to SAR ATR problem, and hence can give both insight and novel ideas regarding how to solve the SAR ATR problem more efficiently.

2.4 Radar polarimetry

For uniform plane EM wave, the electric or the magnetic components of the field, can lie in any direction in the plane perpendicular to the direction of propagation, and perpendicular to each other. However, the direction of either the electric or the magnetic field might change from time to time. If the tip of the magnetic or electric field vector is projected on a plane perpendicular to the direction of propagation, it traces a generic ellipse (figure 2.3).

Unless there is any obstruction in the path of the EM wave, the ellipse traced by the tip of a field vector is fixed. This defines a characteristic property of an EM wave, called polarisation. The electric and the magnetic fields are perpendicular to each other and determining the direction of one, fixes that for the other. Hence either the electric field vector or the magnetic field vector

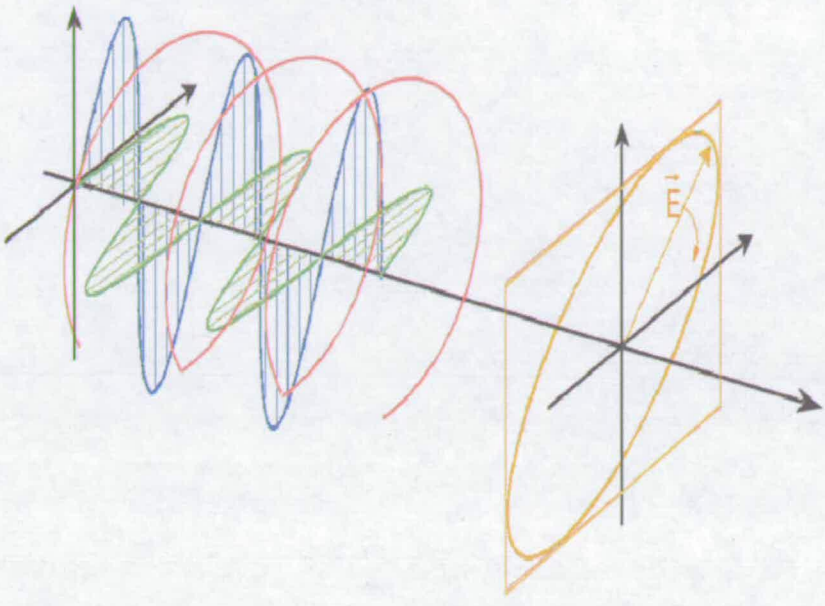

Figure 2.3: *Projection of the tip of a field vector on a plane perpendicular to the direction of propagation would trace a generic ellipse (courtesy [1])*

could be taken to define the polarisation of an EM wave. By convention, the electric field is used to define the polarisation of an EM wave.

If the length of the minor axis of the ellipse defining the polarisation of an EM wave becomes zero, the electrical vector traces a straight line with time, and this type of polarisation is termed as *linear polarisation*. If the minor and the major axes of the ellipse are equal, it becomes a circle and this type of polarisation is termed as *circular polarisation*. If the tip of the electric field vector traces an ellipse, its called *elliptical polarisation*. If the wave is a mixture of various polarised waves with little or no correlation among themselves, it is called unpolarised wave [97]. Two of the major electro-optical phenomena that can affect the polarisation state of the wave, are scattering and reflection [1]. The study of the change in polarisation state of an EM wave during scattering, would give certain properties of the scatterer. This makes the study of polarimetry and polarimetric properties of radar return, important exercises, to be exploited for better ATR performance. There are many established monographs [97, 98] and review papers [99–101] on radar and SAR polarimetry, which give excellent background in this field. In this section, only very basic introduction is given to the field in a more qualitative way.

Reviewing the fundamentals of the scattering matrix [99, 101], let it be assumed that the trans-

mitted wave is represented in some polarisation basis as:

$$[E^t] = \begin{bmatrix} E_1^t \\ E_2^t \end{bmatrix} \tag{2.15}$$

Here E_1^t and E_2^t represent the complex magnitude of the transmitted wave in two mutually orthogonal polarisation bases. Similarly the scattered wave can be represented in the same polarisation bases as:

$$[E^s] = \begin{bmatrix} E_1^s \\ E_2^s \end{bmatrix} \tag{2.16}$$

The incident and scattered wave are related as follows:

$$[E^s] = \begin{bmatrix} E_1^s \\ E_2^s \end{bmatrix} = \begin{bmatrix} S_{11} & S_{12} \\ S_{21} & S_{22} \end{bmatrix} \begin{bmatrix} E_1^t \\ E_2^t \end{bmatrix} = [S][E^t] \tag{2.17}$$

Here, the matrix S, called the scattering or Sinclair matrix is the ratio between the scattered and incident wave for a pair of polarisation bases. More formally it's elements are defined as:

$$S_{11} = \left.\frac{E_1^s}{E_1^t}\right|_{E_2^t=0} \tag{2.18}$$

$$S_{12} = \left.\frac{E_1^s}{E_2^t}\right|_{E_1^t=0} \tag{2.19}$$

$$S_{21} = \left.\frac{E_2^s}{E_1^t}\right|_{E_2^t=0} \tag{2.20}$$

$$S_{22} = \left.\frac{E_2^s}{E_2^t}\right|_{E_1^t=0} \tag{2.21}$$

A complete polarimetric characteristic of the scatterer can be obtained by using a proper combination of antennas, so as to obtain all the parameters of the matrix.

Another representation of the polarimetric information from a scattering phenomena is the Stoke's vector representation. This is given by:

$$g(E_{HV}) = \begin{bmatrix} g_0 \\ g_1 \\ g_2 \\ g_3 \end{bmatrix} = \begin{bmatrix} |E_H|^2 + |E_V|^2 \\ |E_H|^2 - |E_V|^2 \\ 2\Re(E_H^* E_V) \\ 2\Im(E_H^* E_V) \end{bmatrix} = \begin{bmatrix} g_0 \\ g_0 \cos(2\psi)\cos(2\chi) \\ g_0 \sin(2\psi)\cos(2\chi) \\ g_0 \sin(2\chi) \end{bmatrix} \tag{2.22}$$

Here E_{HV} represents the field in terms of linear bases of horizontal and vertical polarisation. Function $\Re(\cdot)$ represents the real part of the argument, and $\Im(\cdot)$ represents the imaginary part of the argument. In some applications this form of representation is more convenient. Because all its elements are real valued (as compared to complex valued elements of Sinclair matrix). Secondly, this representation is more helpful for representing partially polarised waves (where $g_0^2 \neq g_1^2 + g_2^2 + g_3^2$). Lastly, this helps in generating a geometrical representation of the polarisation state as shown in figure 2.4. This is termed as the Poincare sphere, and is useful in polarimetric analysis, as this represents the polarisation state geometrically.

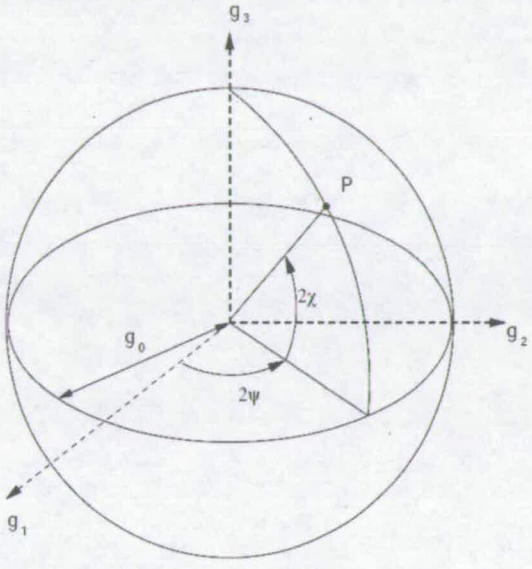

Figure 2.4: *Poincare sphere representation of the polarisation state, using the elements from the Stoke's vector (courtesy [1])*

Using *Poincare's Sphere* notation, the scattering matrix can be visualised geometrically, as a point inside an imaginary sphere [6].

In monostatic scenario, following the reciprocity theorem [99, 100], the S_{hv} and S_{vh} terms are equal. Hence much of the calculation and complexity reduces. However, for bistatic scenario, all the elements of the Jone's Matrix have information, and hence the processing becomes more complicated. The closed form expressions for the value of the elements of the Stoke's Matrix have been found [31, 32] for bistatic case. However the sort of correspondence established between physical features and the elements of various scattering matrices, as has been done for

the monostatic case [6], has not yet been done for the bistatic case. It has also been suggested by some experts that bistatic polarimetry might not hold any information at all [6].

2.5 Summary

This chapter was devoted to the analysis of the current knowledge database regarding the different aspects of the present problem of bistatic SAR ATR. This gives a background to the present work, and also establishes the novelty of the current work. Later chapters will discuss the technical aspects of the present work, and hence will mostly depend on the present chapter for the background studies.

Chapter 3
SAR target signature simulation

3.1 Introduction

There have been some reports in the open literature [40,41,47,57,61,79,80,102,103], on the usage of specific electro magnetic (EM) simulation computational tools, for generating synthetic aperture radar (SAR) images, of modelled targets. The major need for such an approach [3,104] is to generate a database of radar signatures, when field-trials are not economical or impractical. One example is the database needed for developing automatic target recognition algorithms for ground target classification. In this chapter, the work dealing with generation of such a signature database using an EM-simulation tool, is presented.

Lack of data and field trials, is a major bottleneck for research in futuristic radar systems. Limited theoretical analysis has been the traditional solution in such cases. For example in the 1970s and 1980s, implementable polarimetric radars were not available to the wider research community. Hence, a lot of the theoretical and mathematical analysis was done in these periods, on the polarimetric features and decompositions. However, with the increase in the computing power available, computer aided electro-magnetic simulation has been proving itself as another alternative, in the recent years. Although computer aided simulations can not replace theoretical analysis, it can certainly complement purely mathematical analysis. In certain usages, like the problem in the present project, computer aided simulations have the potential to supplement pure-theoretical analysis.

Recently, bistatic radar systems have drawn considerable interest and research efforts. Implementable bistatic systems have been integrated in satellites. However, the use of bistatic systems in airborne systems, is still a field of active research. In the present project, it is the aim to study target classification for airborne bistatic radar systems. For such a futuristic project, the availability of field collected data is almost non-existent. The study of the intricacies of bistatic imaging and the usages of bistatic images, need bistatic synthetic aperture radar (SAR) images collected in a controlled environment. In the case of the unavailability of real data, the options left are, a strictly mathematical-model based approach or a computer aided electromagnetic (EM) simulation based approach. For a task like analysing bistatic SAR image features

or bistatic SAR automatic target recognition (ATR), the latter is a more practical choice.

There are certain computer aided EM simulators, which have been reported to be efficient at the task of SAR image simulation. However, most such tools are restricted and not available for a wider research community. This left us with the choice of trying a generic EM simulator FEKO, and to examine, if it can be used for the task of generating SAR images of life-size land vehicles.

The present chapter discusses the steps and procedures undertaken in testing this generic EM simulator, for simulating the bistatic radar signatures of ground targets, theoretical analysis on how a generic EM simulator could be used to generate SAR images, and steps on modelling the targets and generating the SAR images. This is the first effort of its kind in the open literature. Hence to verify the results, a detailed analysis of a sample SAR image, is also presented.

The next section describes some of the basic experiments done on the generic EM simulator FEKO, to test its suitability for the present application. This is followed by a description of the ground target CAD model generation steps, and then a section on theoretical analysis of SAR image formation using an EM simulator. This is followed by a section describing the simulation of ground clutter in the SAR images. The next section analyses a sample SAR image, and is followed by a section on managing the database generated. Next to it, the work dealing with the generation of a limited monostatic SAR image database, is discussed. The chapter ends with a summary of the work and with some notes on any possible future improvements.

3.2 Experiments on FEKO for analysing forward scattering and shadow effects

The generic EM simulator that has been used for the current work is FEKO [64]. The simulation of radar signatures of ground vehicles, has never before been reported as an application of FEKO. Hence, in this section, a few key experiments will be described, which gave the confidence that FEKO could be used for the purpose of the present work.

In simulating the signatures of ground vehicles, the ground itself plays an important role. Hence, the capabilities of an EM simulator in dealing with ground reflection, forward scattering and in generating a shadow region on the ground, are of importance. In this section the forward scattering and shadow generation capabilities of FEKO will be demonstrated. The ground reflection capabilities will be more evident in section 3.6, where a typical SAR image will be analysed in detail.

In an experiment to examine the forward scattering capability, the CAD model of a long rectangular perfectly electrical conducting (PEC) prism was modelled (figure 3.2). The size of the rectangular cylinder was $1m \times 1m \times 10m$. The frequency of the wave transmitted, was fixed at 1GHz. The transmitter was fixed at 0^o elevation and 45^o azimuth, and the bistatic radar cross section (RCS) was measured round the target at 0^o elevation (figure 3.1). The model and the bistatic RCS observed are shown in figure 3.2 and figure 3.3.

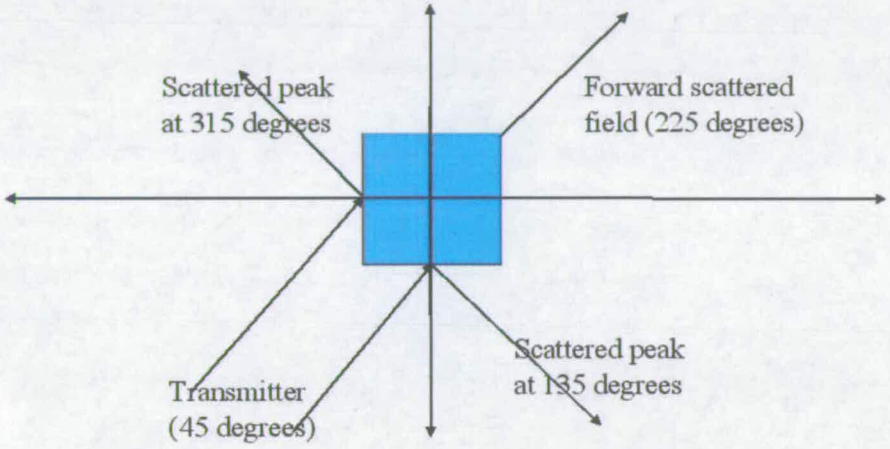

Figure 3.1: *Cross section of the rectangular PEC prism, and explaining the peaks found in the bistatic RCS plot*

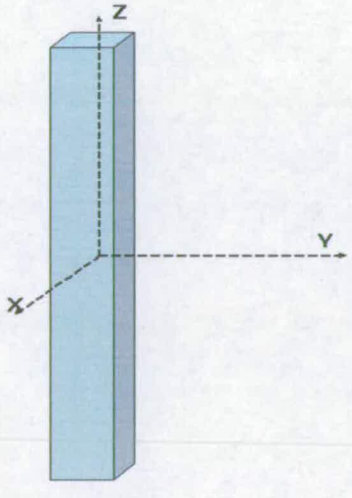

Figure 3.2: *Model of the PEC rectangular prism*

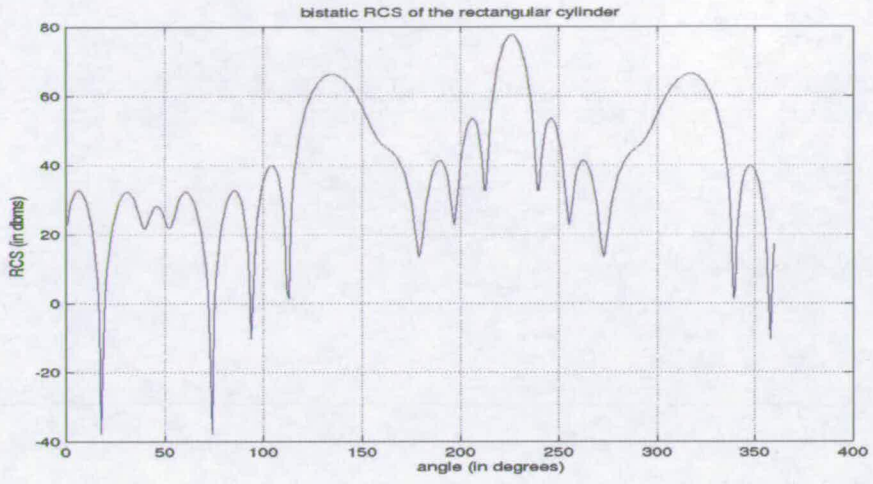

Figure 3.3: *Bistatic RCS (in dbsm) versus azimuth angle in degrees*

As can be seen from figure 3.3, there are three peaks in the RCS plot, the first and the third corresponding to the specular-reflection, and the second peak corresponding to the forward scattering returns (figure 3.1). This demonstrates FEKO's ability in simulating forward scattering.

In testing the shadow region simulation abilities, a simple experimental set-up was designed. The CAD model is shown in figure 3.4. In this setup, a wall like structure was modelled on the ground. The transmitter was fixed on one side of the structure, and the surface current intensity on the ground was mapped (figure 3.4).

As can be observed, the surface current distribution clearly shows a shadow region behind (w.r.t. the transmitter) the structure. Fringes of surface current, due to interference, can also be seen on the current-map.

These experiments established FEKO's ability to simulate forward scattering and shadow regions.

3.3 CAD modelling for EM simulation

Military ground vehicles have highly involved and complex surfaces and features. Hence, to model even a fairly approximate ground target, it needs considerable expertise from the modeller and a highly efficient CAD tool. This was a major bottleneck in this phase of the project.

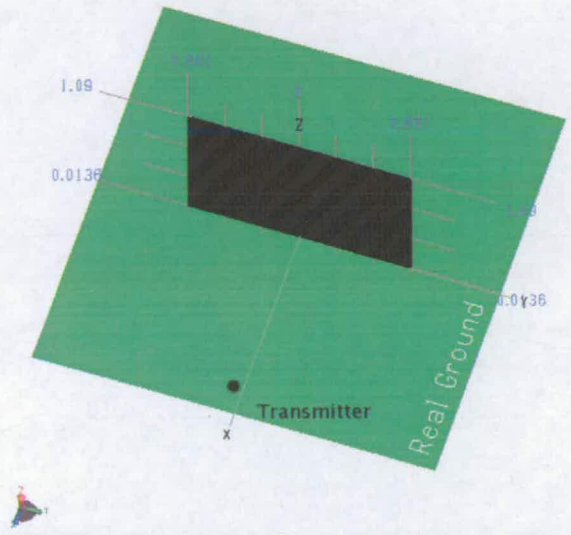

Model setup

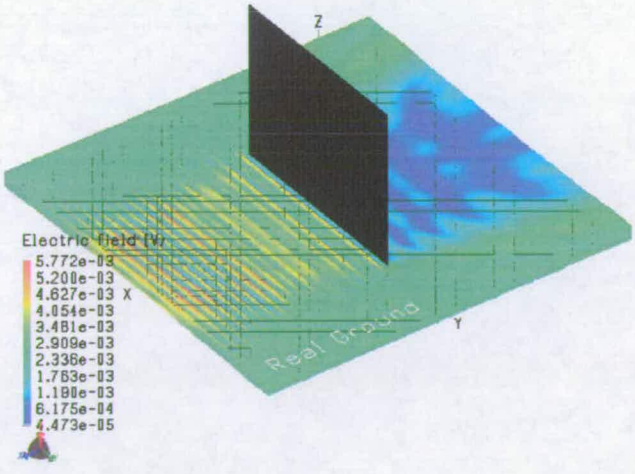

Surface current

Figure 3.4: *FEKO model of the setup and the surface current on the ground (red represents highest density of current and violet the least)*

Another problem was the issue of surface alignment. Like most other EM simulation tools, FEKO replaces the surfaces with small triangular facets. The dimension of these facets should be an order less than the central frequency wavelength. For two mutually touching triangular facet surfaces, the respective sides of the triangles should exactly match each other. This strict condition is often extremely difficult to satisfy for complex structures. However in the present work, the final objective was to generate a data base of SAR images, to study bistatic SAR ATR. Hence, instead of modelling the finer details of a target, the more prominent features of the target were modelled. Such features are termed as the *classifiable features*[1]. For example, the turret and the canon of a main battle tank, or the guidance antenna of a land-to-air missile launcher.

Figure 3.5 shows the CAD models of the four ground targets, modelled in the current project. Dimensions of the targets have been kept close to that of real-life targets. As can be observed, the targets are quite distinct from each other, and represent four of the major classes of vehicles which could commonly be found in ground combat environments. Each target has been associated with the main features of the class, which it represents.

1. The *classifiable features* modelled for the armoured personal carrier (APC), are the typical body shape, and a communication antenna in the front.
2. The *classifiable features* modelled for the main battle tank (MBT), are the turret, group of wheels, canon, and the communication antenna.
3. The *classifiable features* modelled for the stinger launcher (STR), are the battery of four stinger missiles, phased-array type guidance antenna, turret and a communication antenna.
4. The *classifiable features* modelled for the land missile launcher (MSL), are the truck-type body, a communication antenna and the attached big missile.

[1]These are the classifiable features, as evident from the optical image of the models

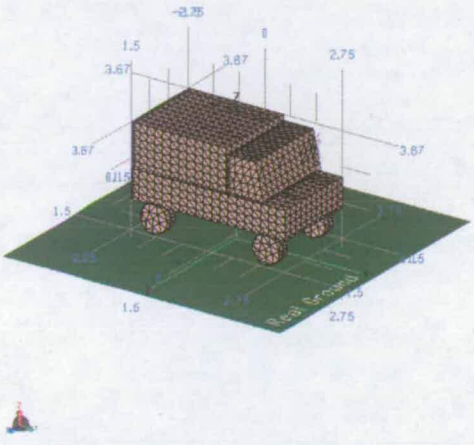

Armoured personal carrier (APC)

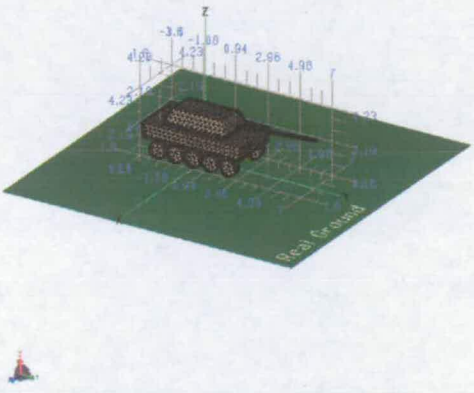

Main battle tank (MBT)

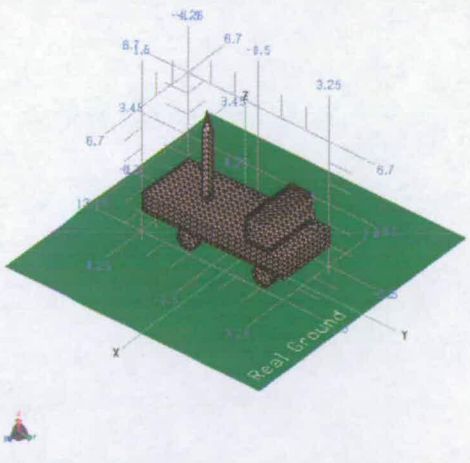

Missile launcher (MSL)

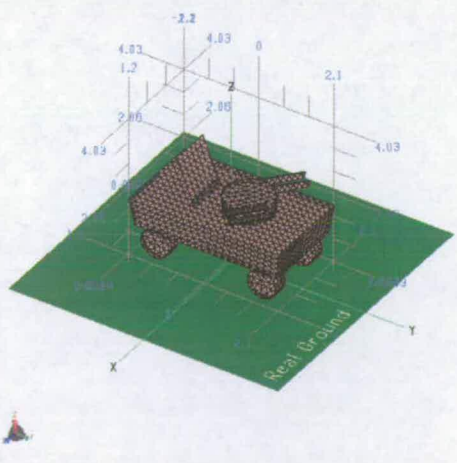

Stinger (STR)

Figure 3.5: *The CAD models of the four targets simulated in the present project (dimensions in meters)*

3.4 SAR image formation steps

In this section, the idea of bistatic k-space [105, 106], and the use of it in bistatic SAR image formation [7, 107, 108], will be discussed. This is crucial from the perspective of the present work, because the samples collected by FEKO can be shown to form points in the k space domain of the scene being imaged. Hence the post-processing of the output from FEKO is based on the bistatic k space analysis.

Figure 3.6 shows the generic geometry of a scene to be imaged with an arbitrary scatterer. As shown, the reference point or the scene centre in the scene is **O**. $\overline{r}$ is the position vector of a point scatterer in the scene. $\overline{R}_t$ is the position vector of the transmitter with respect to the scene centre, and $\overline{r}_t$ is the position vector of the transmitter with respect to the point scatterer. Similar notations are applicable with the receiver, with the subscript replaced by r. Let $s_t(t)$ be the transmitted signal, and $S_t(f)$ the Fourier transform of the transmitted signal. Let $s_r(t)$ be the received signal at the receiver, and $S_r(f)$ the Fourier transform of the received signal at the receiver. Let $\gamma(\overline{r})$ be the electromagnetic reflectivity coefficient of the point scatterer (including the phase factor). In most of the practical cases, we can take a narrow band assumption, where

$$\Delta F \ll f_c \tag{3.1}$$

ΔF is the bandwidth and f_c is the central frequency of the transmitted signal. With narrow band assumption, $\gamma(\overline{r})$ can be assumed constant over the transmitted bandwidth. Then the received signal can be expressed as:

$$s_r(t) = \oint_V \gamma(\overline{r}) s_t(t - \frac{|\overline{r}_t| + |\overline{r}_r|}{c}) d\overline{r} \tag{3.2}$$

In the above equation, c is the speed of EM waves in the medium of transmission, $||$ is the magnitude operation to represent the magnitude of a vector, and $\oint_V$ is the volume integral which considers all the points in the targeted area. Taking the frequency transform of equation 3.2,

$$\begin{aligned} S_r(f) &= \int s_r(t) \exp(-j2\pi f t) dt & (3.3)\\ &= \int (\oint_V \gamma(\overline{r}) s_t(t - \frac{\overline{r}_t + \overline{r}_r}{c}) d\overline{r}) \exp(-j2\pi t f) dt & (3.4)\\ &= \oint_V \gamma(\overline{r}) S_t(f) \exp(-j2\pi f \frac{\overline{r}_t + \overline{r}_r}{c}) d\overline{r} & (3.5) \end{aligned}$$

With far field approximation ($r \ll R_t$), it can safely be assumed that (figure 3.7):

$$r_t = |\overline{R}_t - \overline{r}| \approx R_t - \overline{r} \cdot u(\overline{R}_t). \tag{3.6}$$

In equation 3.7, $u()$ is the unit vector operation. and $\cdot$ is the inner product operation. Similarly,

$$r_r = |\overline{R}_r - \overline{r}| \approx R_r - \overline{r} \cdot u(\overline{R}_r). \tag{3.7}$$

Equations 3.6 and 3.7, when applied to the expression 3.5 gives:

$$S_r(f) = \oint_V \gamma(\overline{r}) S_t(f) \exp(-j2\pi f \frac{R_t + R_r}{c}) \exp(j\frac{2\pi f}{c}\overline{r} \cdot (u(\overline{R}_t) + u(\overline{R}_r)))d\overline{r} \tag{3.8}$$

$$= S_t(f) \exp(-j2\pi f \frac{R_t + R_r}{c}) \oint_V \gamma(\overline{r}) \exp(j\frac{2\pi f}{c}\overline{r} \cdot (u(\overline{R}_t) + u(\overline{R}_r)))d\overline{r} \tag{3.9}$$

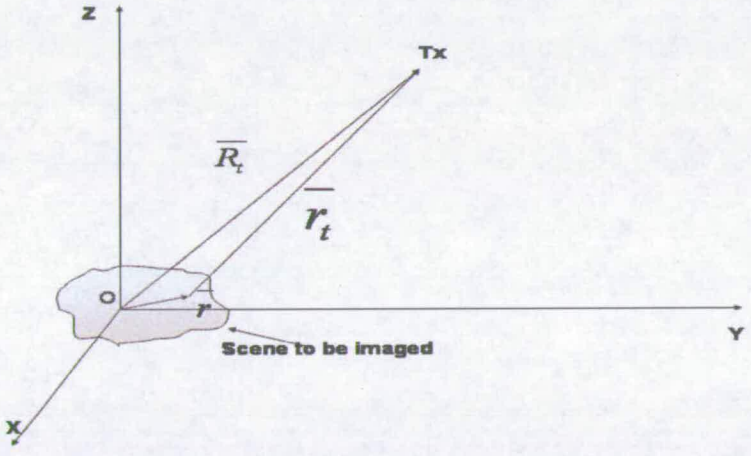

Figure 3.6: *Geometry of the scene to be imaged, and the transmitter*

In the next phase, the following substitutions are made.

$$\overline{r}_b = \frac{1}{2}(u(\overline{R}_t) + u(\overline{R}_r))) \tag{3.10}$$

$$\overline{f} = \frac{2f}{c}\overline{r}_b \tag{3.11}$$

In the substitution equation 3.10, a new directional vector is introduced, which can be termed

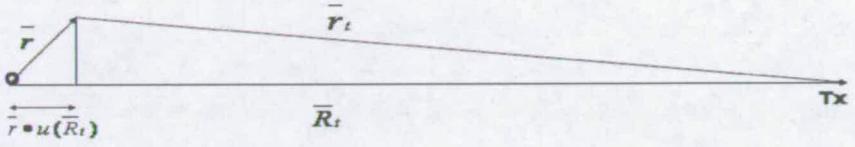

Figure 3.7: *Far field approximation*

as the bistatic directional vector. It should be remarked here that, this directional vector is no longer of unit length. In the substitution equation 3.11, the scalar frequency variable f is replaced by its vectorial form $\overline{f}$, with the directional component given by the bistatic directional vector $\overline{r}_b$. It should be remarked here that from wave physics, $\frac{2\pi f}{c}$ is the wave number k. Associated with a directional vector, this is sometimes termed as the k vector. Similar to the expression 3.11, bistatic k vector can be defined as $\overline{k} = \frac{2\pi f}{c}\overline{r}_b$. SAR imaging literatures prefer to handle the frequency space in terms of k and term it as the k space [105, 106, 109, 110]. For the present analysis, the frequency space and the k space would be used interchangeably and in the same sense. However, it could be noted that $\overline{f}$ and $\overline{k}$ vectors are almost synonymous and from SAR imaging point of view, k space and f or frequency space represents almost the same information.

With these substitutions, expression 3.9 becomes:

$$S_r(f) = S_t(f)\exp(-j2\pi f\frac{R_t + R_r}{c})\oint_V \gamma(\overline{r})\exp(j2\pi\overline{r}\cdot\overline{f})d\overline{r} \tag{3.12}$$

The exponential term $\exp(-j2\pi f\frac{R_t+R_r}{c})$, is due to the time delay with respect to the scene centre, and could be ignored for far field analysis, where its the scene which is of importance. Then it can safely be assumed that $R_t + R_r$ remain almost constant for all the points in the scene to be observed. This assumption is a limitation of the current imaging algorithm, and could be overcome by using certain range-migration algorithms [34]. For the present analysis,

this assumption can be taken to be valid. Now the expression 3.12 reduces to:

$$S_r(f) = S_t(f) \oint_V \gamma(\overline{r}) \exp(j2\pi\overline{r} \cdot \overline{f}) d\overline{r} \tag{3.13}$$

This shows that the return from each transmitted pulse, produces a polar line segment in the three dimensional vector Fourier transform of the scene scattering coefficients $\gamma(\overline{r})$ (with a support in the frequency space, as given by the vectorial frequency mapping of 3.11). The integral $\oint_V d\overline{r}$ is the frequency response measured by the radar system for a particular position of the transmitter and the receiver. As shown, it is also a polar line segment through the 3D Fourier transform of the reflectivity coefficient of the scatterer distribution $\gamma(\overline{r})$. Thus, what is measured by the radar or the EM-simulator, is the Fourier transform of the image of the scene. The simulated output from FEKO (the position of the transmitter and the receiver, and the effective direction of the $\overline{k}$ vector, are elucidated in figure ??), is thus the values of $H(\overline{f})$, with frequency or k space support given by the actual frequency band and transmitter-receiver geometry, transformed by the mapping of 3.11.

$$\Delta\overline{f}_b = \frac{2\Delta f}{c}\overline{r}_b = \frac{2\Delta f}{c}\frac{1}{2}(u(\overline{R}_t) + u(\overline{R}_r)) \tag{3.14}$$

As shown in the figure 3.9 , this is reduced to (β is the bistatic angle, the angle between the lines joining the scene centre to the transmitter and the receiver):

$$\Delta\overline{f}_b = \frac{2\Delta f}{c}\frac{1}{2}(2\cos(\beta/2)u(\overline{r}_b)) = \frac{2\Delta f}{c}\cos(\beta/2)u(\overline{r}_b) \tag{3.15}$$

Equation 3.15 is quite important in the sense that, it determines the frequency or k space span of the data collected from the EM simulator, for a bistatic simulation. Two important observations in it are:

1. The real frequency band is scaled by the factor of $\cos(\beta/2)$.
2. The direction of this polar line segment in k space, is in the direction of the bistatic angle bisector $u(\overline{r}_b)$ as shown in the figure 3.9 .

Looking at this geometry of the bistatic scene k space, this is given by the locus of the point whose polar coordinate is $(\cos(\beta/2), \beta/2)$, which is a circle with the centre at $(0.5, 0)$, and of radius of 0.5 (as shown in the figure 3.15).

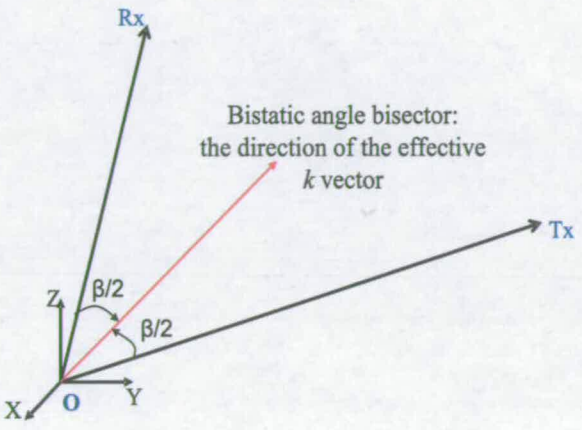

Figure 3.8: *The position of the transmitter and the receiver, and the effective direction of the* $\overline{k}$ *vector*

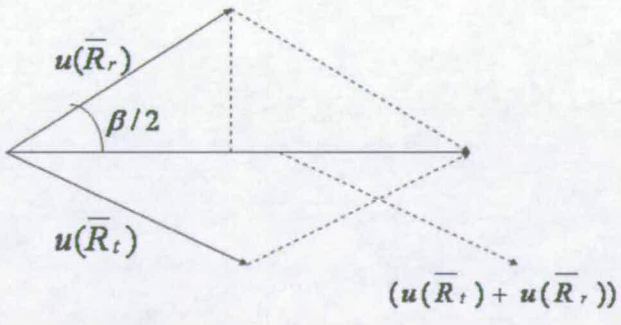

Figure 3.9: *Finding the bistatic directional coefficient*

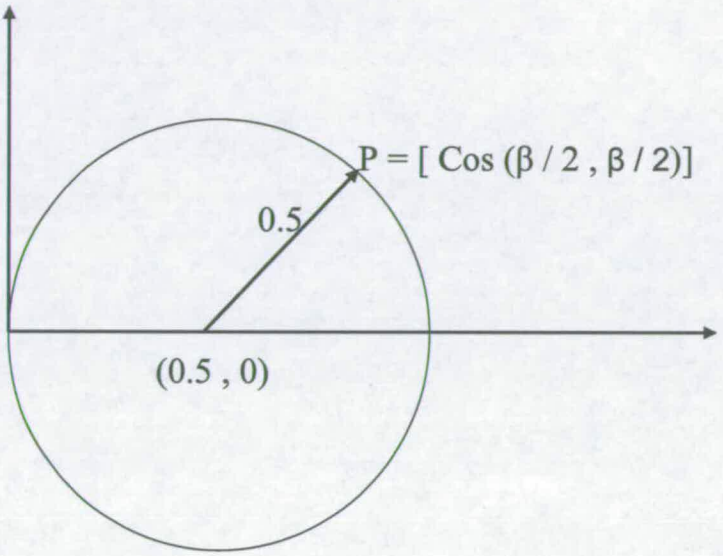

Figure 3.10: *Locus of the bistatic directional coefficients*

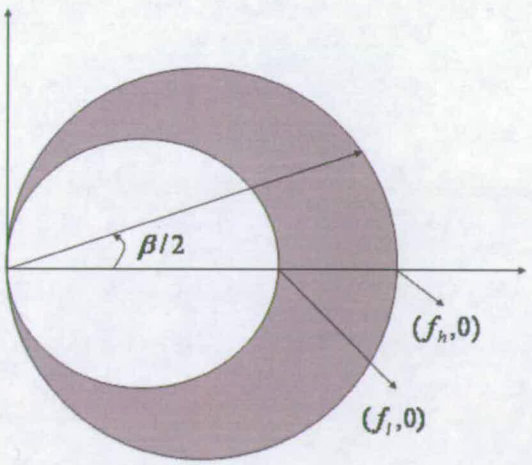

Figure 3.11: *Frequency or k-space support in the bistatic simulation done in the present project*

In the present simulation, for the ease of setting the simulation environment, in place of a moving transmitter and receiver, the transmitter is kept fixed. The simulation is done with a fixed transmitter, and the receiver revolving round the scene-to-be-imaged at a fixed elevation angle and with the azimuth angle varying from 0^o to 360^o. The projection of the k space data sampled by this combination is as given by the shaded area in figure 3.11 .

To form an image of the scene, small sub-regions are to be taken from this sampled k space. This is done by using the samples collected for a range of consecutive receiver azimuth positions. This k space data has a polar support, and hence the next step is to reformat the support into a rectangular-one by proper extrapolation of the sampled data points.

The algorithm followed in the present work is that of keystone resampling [10]. After the polar-to-rectangular resampling, an inverse Fourier transform of the data grid gives the bistatic SAR image of the scene.

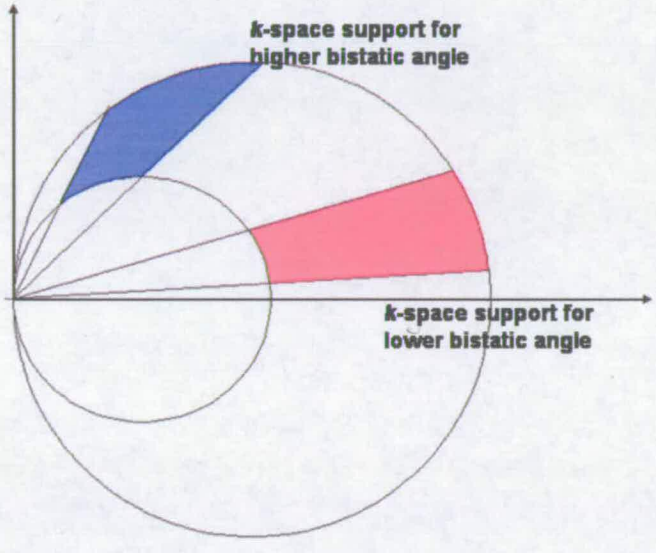

Figure 3.12: *k space support is larger for lower bistatic angle*

A few points worth mentioning here are:

- The resolution and hence the image quality of the generated bistatic SAR image, would depend on the k space support of the data, which in turn depends on the bistatic angle. Hence, the image resolution and the quality, depend on the bistatic angle of data

collection.

- For very high bistatic angles (as $\beta/2$ tends to 90^o), as can be seen from figure 3.12 , the k space support nullifies, and the image quality is not acceptable.

The image formation steps can be summarised as follows:

- The input parameters for the simulation are:
  - Angle and frequency step;
  - Bandwidth (BW) for which the EM simulator need to be run;
  - CAD models of the targets.
- With the above input parameters and files fed to the FEKO simulator, the transmitter was fixed at a certain azimuth and elevation, and the target was illuminated from the transmitter for the range of frequencies. This is done in frequency steps (as determined by the input parameters), covering the BW.
- For a given transmitter position, and given frequency and polarisation of transmission, the EM simulator is used to generate the surface current on the CAD model. This surface current file is stored.
- Once the surface current file is known, the far field could be calculated for any given receiver azimuth and elevation. Hence the next step was to collect the scattered power from the target CAD model, for the range of frequencies, and with receiver position varying over a fixed elevation angle and a varying azimuth angle through 0^o to 360^o. This in turn is done at a few predetermined azimuth angular steps.
- This gives the scattered field in both H and V polarisations of the receiver, for the range of frequencies and for the range of receiver azimuth angles. This forms an annular space in the k space as shown in the figure 3.11 , and is termed as data collected in *one run*.
- The process was repeated for different positions of the transmitter and the receiver, and for different transmitter polarisations.
- A total of four targets have been modelled. For each target, data $runs$ were collected for all the four polarisation combinations, for the following configurations of transmitter:

Transmitter Elevation (in degrees)	Transmitter Azimuth (in degrees)
10	0, 60, 120, 180, 240, 300
15	0, 60, 120, 180, 240, 300

Table 3.1: *Transmitter positions for which the bistatic EM simulations were performed*

- For each transmitter position, scattered signals were collected for 360^o of receiver azimuth round the target (one run) for two elevations: 10^o and 15^o. Hence, a total of 48 $runs$ of data were collected for each polarisation, for each target model.

- Each run, as has been mentioned, gives the k space data for an annular ring as shown in figure 3.11 . From this, data are collected for a certain range of receiver angles for the BW of frequencies. This patch of k space data is polar-to-rectangular reformatted, as shown in the figure 3.13 to make the k space support rectangular. Next the IFFT was taken to form the image of the target model. This image of the target model will display the target in the centre of the image, and represents the SAR image of the target as obtained in real-SAR systems after discrimination phase [65]. This forms a **target clip**[2].

- With some overlapping of receiver azimuth angles for consecutive target clips, each run of data was used in the current project to generate around 25-50 image clips.

The following guiding equations were used in determining the parameters used in the EM simulation and imaging exercises of this project. The resolution expressions below are for monostatic cases. For bistatic case, the resolution is diluted by the $\cos(\beta/2)$ factor, where β is the bistatic angle of imaging [111, 112]. However, as the bistatic angle varies from clip to clip, not all the image clips will have the same resolution. Hence, the monostatic expressions are used as guidelines in deciding the approximate resolution and hence the parameters of simulation.

Determining the frequency range and the frequency steps: These parameters are decided

[2]a target clip is the SAR image of the target, with the image of the target at the centre of the image. In an automatic target recognition exercise, after the detection stage, a particular part of the original SAR image of the scene is taken for further processing. This part of the SAR image, with the target at its centre, is termed as the target-clip. In the present project, only the classification problem is handled. Hence, the input taken are the target image clips. Though no clipping operation is done, for convention, the word *target clip* is used through out the present report.

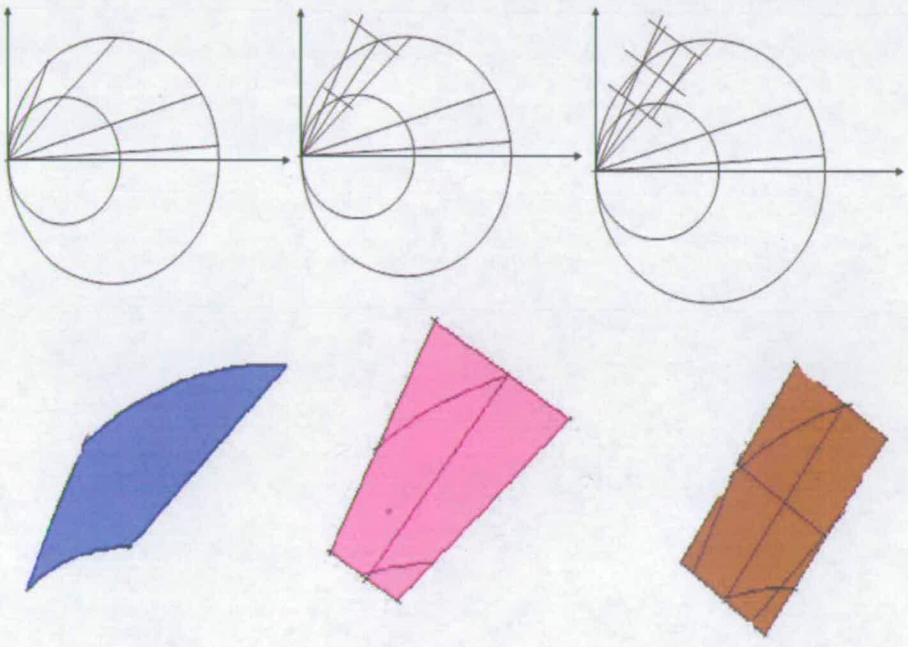

Figure 3.13: *Key-stone approach of polar-to-rectangular reformatting of data collected*

by the desired spatial resolution and maximum spatial distance in the range direction:

$$\delta x = \frac{c}{2\Delta F}; \delta f = \frac{c}{2\Delta X} \tag{3.16}$$

where δf is the frequency step, ΔF is the band width, δx is the range resolution and ΔX is the maximum range to be imaged [10].

Determining the angular range and step in angular dimension: These parameters are determined by the spatial resolution and maximum spatial distance in the cross-range direction:

$$\delta\theta = \frac{\lambda}{2\Delta Y}; \delta y = \frac{\lambda}{2\Delta\Theta} \tag{3.17}$$

where λ is the central frequency wavelength, $\delta\theta$ is the step in angle, $\Delta\Theta$ is the total angular swath, δy is the cross range resolution and ΔY is the maximum cross range to be imaged [10].

The central frequency was kept at 1GHz. This decision was mainly controlled by the simulation constraints. In most of the EM-simulators, the model body is approximated as the summation of a triangular or rectangular mesh. The dimension of the triangles in the meshing must be an order smaller than the central frequency wavelength. Hence higher the central frequency, the smaller is the central frequency wavelength, and hence smaller the size of the triangles in the meshing. This results in a higher number of triangles required for the same model as compared to that required for a lower frequency. This heavily slows down the simulation speed. A centre frequency of 1GHz was found to be a compromise between our desired image resolution and a reasonable simulation speed. The spatial resolution was kept at around 0.2m in both range and cross-range dimensions. For this requirement, the bandwidth was chosen to be 750MHz and angular swath for each image formation was chosen to be 36^o. All the target models were less than 8m in dimension. Hence the maximum scene to be imaged was limited to around 10m in both dimensions. This parameter was used to decide on the frequency step (15MHz) and the angular step (0.72^o) [3].

[3]The choice of bandwidth and central frequency makes the setup a wide-band simulation. Hence most of the derivations done earlier would not hold. However, in actual simulation, the complete bandwidth is discretised. For each simulation the bandwidth under consideration is just 15MHz. Hence, the narrow band assumption still holds true for each simulation.

3.5 Ground clutter modelling

One of the important features of the SAR image of a ground target as compared to an air-target, is the presence of ground clutter and shadow. Hence, in any SAR image database for ground targets, a well acceptable ground clutter is a must, which not only makes the database more acceptable, but also aids in testing the performance of ATR algorithms with different levels of clutter.

The obvious choice to generate ground clutter, is to model an acceptable ground in the scene of the target. The present EM simulator could only model a plane dielectric ground (which is easy to simulate and does not heavily load the simulation procedure). A plane dielectric ground can not give any ground clutter. Hence a better option would be to model a random height ground plane in the scene. However the problems with this approach are:

- In most of the EM simulators and also in FEKO, the features are to be modelled with detailed coordinates of the points. In modelling the ground, the randomness of the ground features should be an order smaller than the central frequency wavelength (so that the speckle is properly simulated). Hence, effectively it is a problem of modelling a huge number of triangular patches.

- To account for the interaction of the EM waves reflected from the ground, with the target, the ground plane should be large enough not to miss any of the reflected energy from the target. This needs the ground plane to be around two to three times as large as the target size, which is a huge area to be modelled.

- The ground plane has to be dielectric, and the methods available with most of the general purpose EM simulator for simulating dielectric surfaces, are the method of moments (MoM) or the physical optics (PO) methodologies, which need the calculation of the surface currents on the ground, and hence are extremely time and memory consuming. In most cases the simulation of a ground for a life size target for a gigahertz range frequency, is almost impossible using a 32 bit computer.

The above facts make the whole problem impossible to be handled by a 32 bit processor (which can address only 4GB of memory).

Some of the other possible approaches which were studied, consisted of different combinations of symmetric and translation features of modelling tools to get over the problem. However,

finally an EM simulation approach to modelling ground clutter had to be abandoned.

The innovative method adopted in the present project, uses the present generic EM simulator FEKO, and Matlab for the ground clutter simulation! It is well established that, if there are not too many scattering centres in the area representing one pixel of the final SAR image, then the combined interferences from the scattering centres in the pixel-area, result in a non-Gaussian distributed image intensity. This explains the non-Gaussian characteristics of clutter noise [22, 23, 113]. If the scattering centres are put at random heights, this results in a random clutter return. Following this logic, a scene was modelled in Matlab with scattering centres all round the scene. The number of scattering centres was fixed so as to allow around 4 to 6 scattering centres to be contained in the area represented by one pixel in the final image. The height of the scattering centres was made random Gaussian. Each scattering centre was associated with a complex scene-reflectivity coefficient γ, whose real and imaginary parts are Gaussian random variables. Using Matlab, the SAR image of this scene was generated using the same parameters (central frequency, bandwidth, aperture span, and angular step) as the main FEKO simulation. The process was repeated with 20 different realisation of the ground and hence finally 20 clutter images were generated.

The clutter image thus generated, was to be added to the SAR image of a target, to generate the final image. As an example, figure 3.14 shows the surface current maps on the ground plane for the target MBT, from the point of view of the transmitter (at 0 azimuth and 10 elevation) and receiver (at 60 azimuth and 10 elevation). From these shadow maps, the bit-map files were generated. These bit-map files are finally rotated to account for the look direction of the particular scene. In figure 3.14 the final bit map files are also shown. The transmitter and receiver bit-map shadow files and the clutter file are added, so that the clutter is preserved at the pixels where the shadow maps are both 1 and is made zero where either shadow map is 0. Essentially, this is the process of multiplying the three files (point-to-point multiplication). The final shadow-clutter image is added with the image file of the target. The complete procedure is illustrated by the figures in figure 3.14, which show the interim output images at different phases. (The transmitter and receiver configuration during the FEKO simulations is given in figure **??**) As can be observed from the figures, the final image has both ground clutter and the information due to bistatic shadow.

The final image is quite encouraging, despite the simplicity of the algorithm used. The algorithm does not takes into account the higher order diffractions and EM-interactions between the

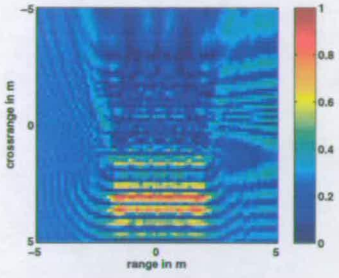

Shadow from Tx view-point

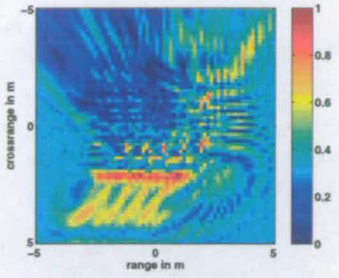

Shadow from Rx view-point

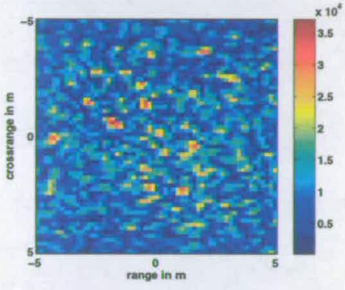

Clutter-only from Matlab simulation

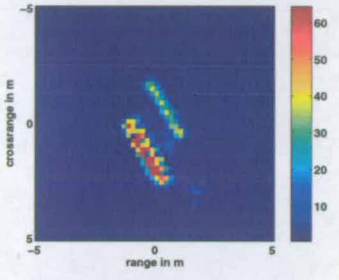

Target-only image

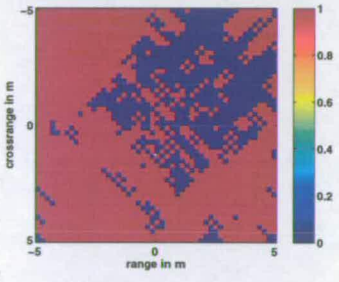

Bit-map file for Tx-shadow
(after rotation)

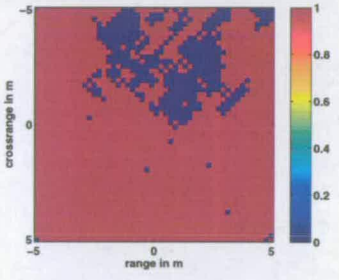

Bit-map file for Rx-shadow
(after rotation)

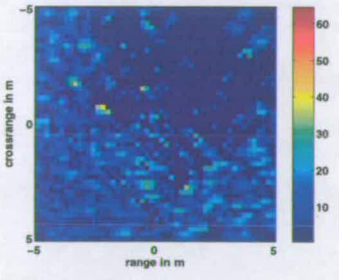

Clutter and shadow
information from both Tx and Rx

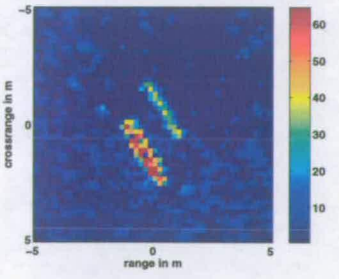

Final image clip
with bistatic shadow and ground clutter

Figure 3.14: *Steps in forming the target image clip with bistatic shadow and ground clutter*

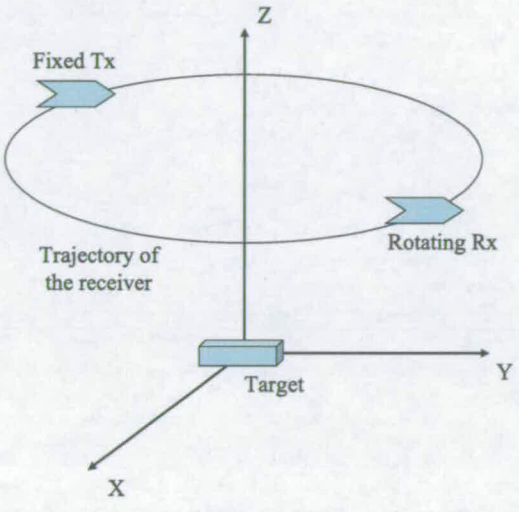

Figure 3.15: *Transmitter and receiver configuration during the FEKO simulations*

target and the ground plane. The major advantages of this algorithm are:

1. The algorithm is simple and easy to implement.
2. Results are qualitatively similar to the image clips from the MSTAR monostatic images. In other words visually, they look similar with similar (visually) ground clutter and shadow areas.
3. Since the clutter is added offline, the clutter energy is controllable. This is an important feature while testing the performance of an ATR-algorithm with increasing clutter energy.

3.6 Analysis of a sample image

For a more detailed study of the SAR images generated in this project, this section analyses one of the images, in a more systematic way, to see how features in the image correspond to the physical features in the CAD model. Sometimes features are quite conspicuous, and sometimes difficult to identify. The aim of this analysis is twofold. First of all, it will be shown that all the features in the image have some link to the CAD model. This gives confidence in the images

generated. Secondly, this also suggests that FEKO may be a competent tool for the task.
For the current analysis, the bistatic SAR image of the model, *missile launcher* is chosen. The imaging parameters are, transmitter at 0^o azimuth and 15^o elevation, and receiver tracing an aperture of around 30^o of azimuth starting from 0^o to 30^o, at a fixed elevation of 15^o.

- Figure 3.16 gives the optical and the bistatic SAR images of the target. The target in the scene, is a generic land to land missile launcher. The dimensions of the base of the vehicle are 6.5m in length, 3m in width and 1m in height. The missile is 4m in length and 0.5m in diameter. A number of artifacts can be observed in the image, which may not be easily be linked to the physical features. To analyse the image and the correspondence of the image domain features to the physical features, features of the target were added one by one and the corresponding changes in image domain were observed.

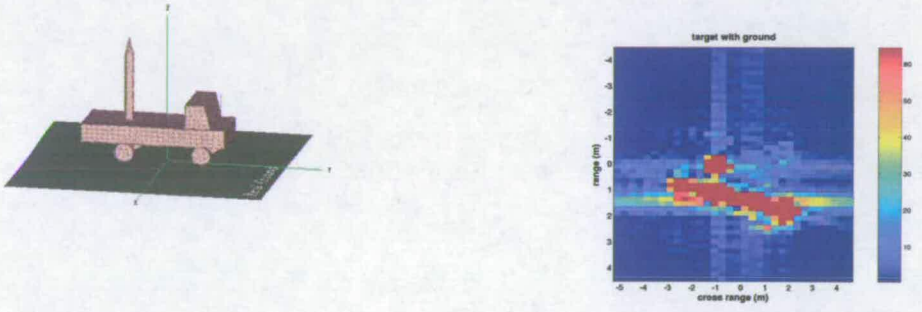

Optical Image Bistatic SAR Image

Figure 3.16: *Optical and bistatic SAR images of the target on ground plane*

- First of all, the simplest feature, a perfectly electrical conducting (PEC) plate, was imaged (figure 3.17). As can be observed from the figure, the PEC plate behaves like four scattering centres, physically near the corners of the plate. Even though the exact position of these scattering centres could not be calculated, the SAR image in the figure is fairly accurate. Because of very low elevation angle, the scattering centres give very low return (as can be observed from the low amplitude spots in the image).

- Next, the complete body and the head of the vehicle were added (figure 3.18). Now, the return from the side plate of the body, which is perpendicular to the incident wave, is

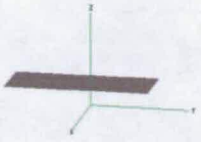

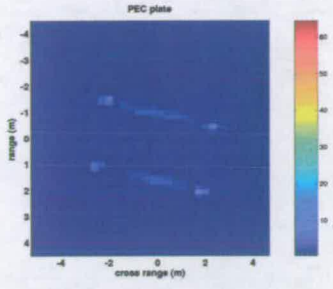

Optical Image

Bistatic SAR Image

Figure 3.17: *Optical and bistatic SAR images of the PEC flat plane*

much stronger than the return from any other part.

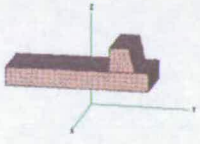

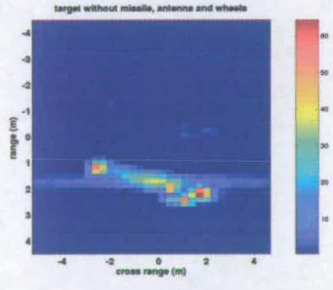

Optical Image

Bistatic SAR Image

Figure 3.18: *Optical and bistatic SAR images of the target with no wheels, no missile, no antenna and no ground plane*

This accounts for the brightest patch in the image.

- In figure 3.19, the wheels are added, and the changes in the SAR-image domain can be observed. Since the elevation angle is very low, the returns from all the wheels are visible to the receiver and hence form four bright spots in the image. Two of these spots lie close to the side plate and hence are not so conspicuous. The other two wheels to the rear,

show up as significant bright spots.

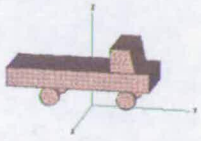

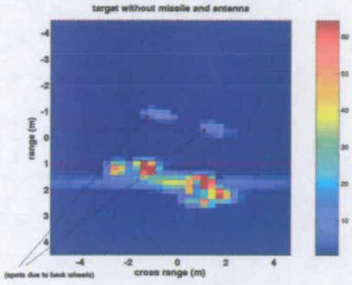

Optical Image

Bistatic SAR Image

Figure 3.19: *Optical and bistatic SAR images of the target with no missile, no antenna and no ground plane*

- Next, in figure 3.20, the antenna element was added to one corner of the cabin (approximate position (1m range and 2m cross range)). A bright spot appears in almost the same position in the SAR image.

- In figure 3.21, the missile was added to the trolley of the vehicle. The corresponding appearance of a feature in SAR image can be observed clearly. The new feature in the image is nearer to the front edge than to the back edge. This can be explained with geometry in figure 3.22, where $d1$ is the distance between the missile head range bin and the front edge range bin. $d2$ is the distance between the missile range bin and the back edge range bin. It can be observed that, $d1 < d2$. Hence the missile head appears closer to the front edge. Analytically, the missile is 4m in length and hence in the image domain, it would appear to be $4\sin(15^o) = 1.035m$ long. Breadth of the vehicle is 3m and would appear in the image domain as approximately $3\cos(15^o) = 2.89m$. Hence the missile head would appear approximately $(2.89/2 - 1.035) = 0.41m$ from front edge.

- Finally, comparing figure 3.21 with figure 3.16, the later has a ground plane added. This makes the return more strong and hence the overall image appears brighter and some faint artifacts are also observed in the image due to interaction with the ground plane.

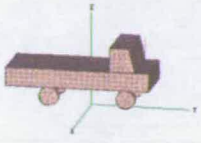

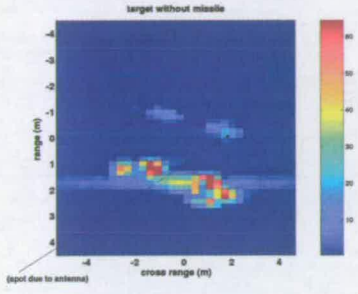

Optical Image

Bistatic SAR Image

Figure 3.20: *Optical and bistatic SAR images of the target with no missile, and no ground plane*

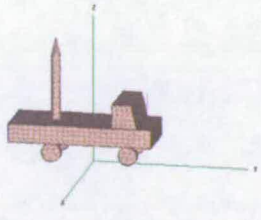

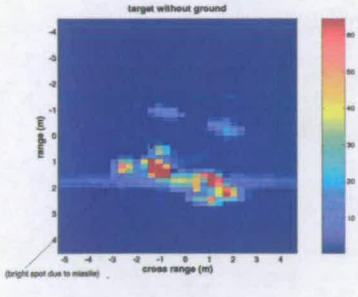

Optical Image

Bistatic SAR Image

Figure 3.21: *Optical and bistatic SAR images of the target with no ground plane*

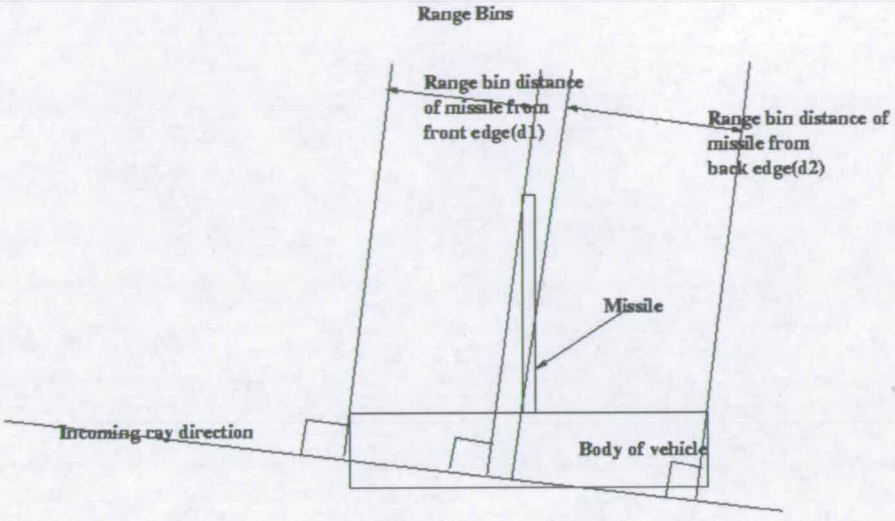

Figure 3.22: *Ray diagram to show the reason for the proximity of the missile head to the front edge in SAR image*

SAR imaging in a bistatic configuration is a complex procedure in itself, involving phenomena of different degrees of complexity. Using the simple physical optics (PO) method, features in the SAR image domain may not always appear so crisp and conspicuous when compared with the optical image. The above exercise was helpful in giving a fair insight into the SAR images and the correspondence of image domain features to the physical features.
The typical bistatic SAR images of all the target models, (for one particular transmitter-receiver combination) are shown in figure 3.23.

3.7 Managing the dataset

Once the main job of simulation using the EM-simulator is completed, the next task is to properly sort and archive the database, so that it could effectively be used for the task of validating classification algorithms. The complete setup is as shown in figure 3.24.
The whole system is used, anytime a new classification exercise is run. So that the data is not exactly the same, even for different runs of the same algorithm. There are three databases used:

1. The EM-simulator output file, containing scattered signal from the targets for different orientations of transmitter and receiver.

2. The bank of clutter image files, generated by Matlab simulation.

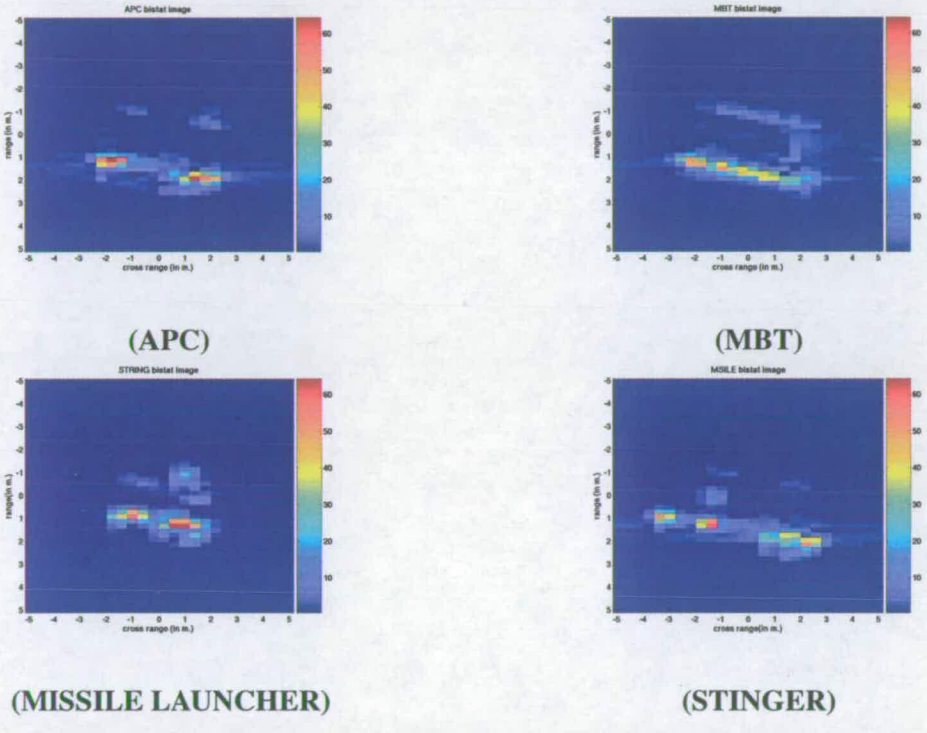

Figure 3.23: *Representative bistatic SAR images of the four targets modelled (HH polarised images)*

3. The bank of shadow files. These are basically the surface current map files as simulated by FEKO for different positions of the illuminating source.

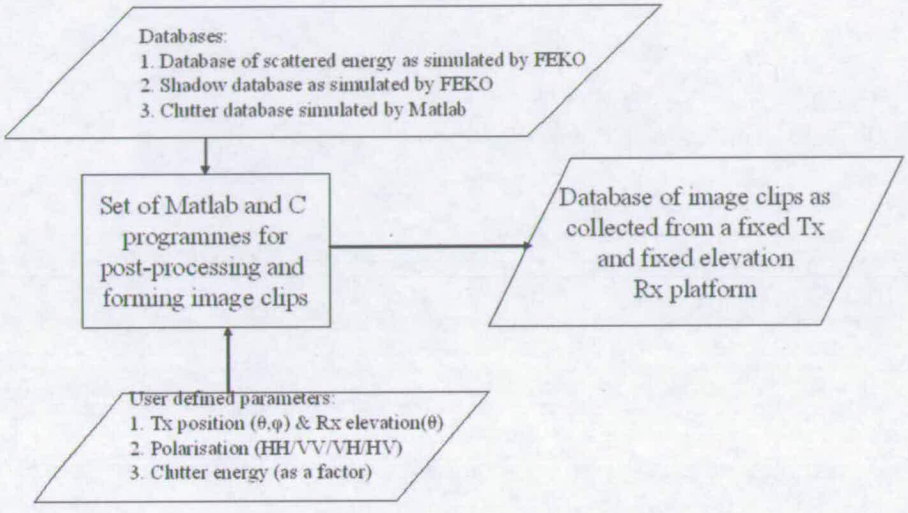

Figure 3.24: *Database management steps*

The EM-simulator (FEKO) output files are in a special format. Hence a group of C-programmes were coded to extract the data from such files and to write them in Matlab readable files. Each dataset actually traces an annular section in k-space. The final aim is to slice desirable pieces (depending on desired resolution), and form the image. Three parameters that the user can define for any run, are:

1. The position of the transmitter and the elevation of the receiver. Depending on these, the particular FEKO-output file is chosen for post processing.
2. The desired polarisation of data.
3. The amount of clutter energy to be added in the final image.

Depending on these parameters, the group of programmes, perform the slicing of the k-space data, resampling and the polar-to-rectangular reformatting. Finally a two dimensional IFFT is taken and the desired shadow and clutter files are added. This process is repeated for all images, to finally give a group of target SAR image clips from the chosen FEKO-output file.

3.8 Monostatic dataset generation

One of the major expectations from this project was the comparative study of ATR in monostatic and bistatic domain. As discussed in this chapter, due to the unavailability of a practical dataset, the bistatic database was generated by simulation using an electro-magnetic simulator. For a monostatic configuration, a real database is available. However, for a fair comparison of the ATR performances in bistatic and monostatic configurations, the only difference between the two datasets should be the configuration (i.e. in one case monostatic and in the other case bistatic). Hence, a detailed set of simulations were performed to generate a dataset of monostatic SAR image clips of the same modelled targets, as those modelled for bistatic simulation. The collection of radar return was done as would have been done in a field trial. The model was kept static and the simulated radar platform was made to move in a circular orbit round the target, while keeping the elevation constant. To simulate a pseudo bistatic scenario, the simulated transmitter was kept fixed at a point and the receiver was rotated round the target at a fixed elevation, at the same time not exceeding a certain particular maximum value of bistatic angle. Radar returns were collected from each target, and for a given position of transmitter and receiver, a range of frequencies were transmitted, the response to which forms the range resolution profile of the target at the given positions of the transmitter and receiver. Collection of the range profiles for a range of positions of the transmitter and the receiver, forms a collection from the k-space. Patches from the k-space were taken to form the SAR image clips of the target.

For forming the monostatic image-clip database, the simulated radar platform (with both the transmitter and the receiver) was moved round the target at a fixed elevation angle, collecting the radar returns from the target for the range of frequencies. This gave a patch in the k-space for the given target. Sub-patches were taken from this to form image clips of the target at different orientations. Figure 3.25 gives a rough schematic of the processes followed.

The advantage in bistatic simulation was that for a given transmitter position, the radar return was collected from a range of receiver positions. For a given transmitter position, the surface currents were calculated for a given target, and this would be used to calculate the radar return for any receiver position. The major time consuming job in any EM simulation is the calculation of surface currents. Hence, in bistatic simulation, a huge amount of data could be simulated in a relatively short time period (as compared to the time taken for similar amount of simulation to be done in monostatic configuration). However, in monostatic simulation, for each position of

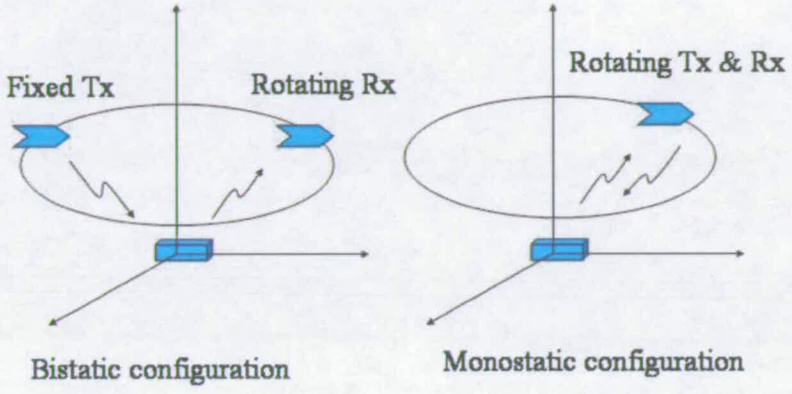

Figure 3.25: *Generic configuration for monostatic and bistatic simulation setup*

the radar, the surface currents have to be calculated. Hence, the monostatic simulation activity was several orders of magnitude more time consuming than the bistatic simulation. So the monostatic simulation was kept limited in certain respects.

- In bistatic simulation, data has been collected for two elevation angles of the radar platform, 10^o and 15^o. In the monostatic simulations, simulation was done for one elevation angle of the platform, 15^o.
- In bistatic simulation, all four combinations of linear polarisation scattered data have been collected, viz. HH, HV, VH and VV. In the monostatic case, simulation was done for one polarisation of the transmitter (horizontal), and hence data collected were for HH and VH polarisation.

For a given target, the monostatic simulation gives an annular patch of data in the frequency or k-space.

The next activity was to collect subsets from the collected bistatic data to form SAR image clips. However, the k-space data collected in the bistatic scenario, is different in geometry, than the simple annular type k-space data collected in the monostatic scenario. The higher the

bistatic angle, the more is the difference between the bistatic and monostatic collected k-space. Hence in bistatic data collection, there are two needs to be met:

1. The bistatic angle should be limited to a certain small angle.
2. To make the data similar to the monostatic data, image-clips of the target from all aspect angles are required.

For a given transmitter position, to meet condition 1, the k-space data was taken with bistatic angle below a certain angle. To meet condition 2, this was repeated with transmitter at various positions. The final result is a synthesised approximate annular ring of k-space data, obtained by joining subsets of k-space data from different bistatic simulations.
In one set of data collected, the receiver azimuth angle was kept below an angle of 60^o. This makes the bistatic angle for the collection less than 60^o. Another set of bistatic data was collected keeping the bistatic angle less than 30^o. Patches of k-space data were collected keeping the receiver azimuth less than 30^o. This was repeated for six transmitter positions, so that the combined k-space data forms an approximate annular space as collected in the monostatic case. This makes the collected data for monostatic and bistatic scenarios, as close as possible, to make the final comparison as fair as possible.
To form the images, k-space data was taken from the annular ring, keeping the full support in temporal frequency dimension, and for a range of azimuth angles. The temporal and angular frequency support taken for forming any given image-clip were 750MHz and 36^o of azimuth. Keeping the temporal frequency support fixed, overlapping blocks were taken in azimuth dimension to form a set of image clips for a given target. From a given annular data, a total of 225 image clips were generated out of which 114 randomly picked images were used as a training dataset and all the image clips were used as a test dataset. In the monostatic case, this procedure is straight forward. In the bistatic case, for example in the less-than-60^o case, there are three subsets of k-space. Hence approximately one third of the total of 225 images, were collected from each subset.
To compare the images in the bistatic and monostatic domain, figure 3.26 to figure 3.29 give the SAR images at a particular configuration for both monostatic and bistatic configuration. Certain conspicuous observations are:

- The bistatic image resolution is less than its monostatic counterpart. It may be noted that the images shown in the figures are formed with the least bistatic angle (less than 15^o).

Still a loss in resolution could be observed clearly.

- Both the image-sets do show certain different features. For example, for the MBT, in the monostatic image the turret is clearer than it is in the bistatic image. The cannon end is more clear in the bistatic image than it is in the monostatic image.
- Another subtle difference not obvious from the images, is the image intensity. The monostatic images are of several order higher intensity than their bistatic counterparts. The images shown in the figure, have been normalised before being plotted. If the figures had been drawn to the same scale, the bistatic images would have been completely invisible.

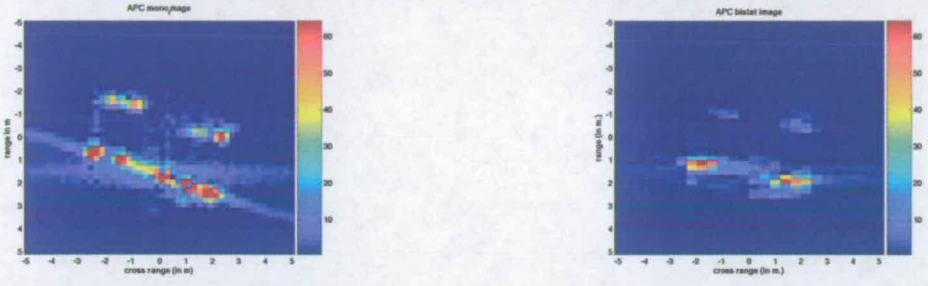

Monostatic Bistatic

Figure 3.26: *Monostatic and bistatic SAR images of the target APC*

Monostatic Bistatic

Figure 3.27: *Monostatic and bistatic SAR images of the target MBT*

3.9 Summary

The present work has been done almost from scratch, with almost no previous guidelines. Even though EM simulation packages like Epsilon and XPatch do give solutions to the problem of

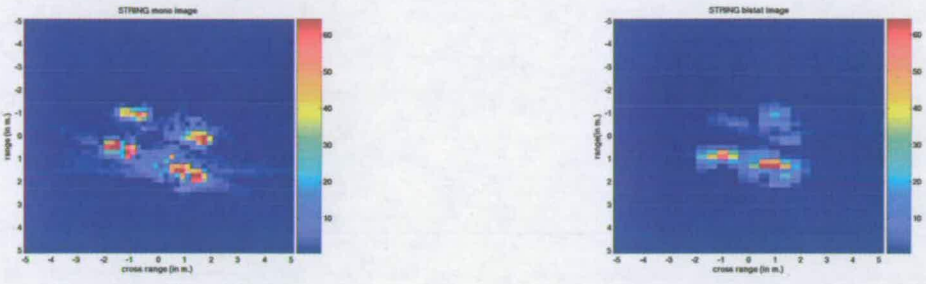

Monostatic Bistatic

Figure 3.28: *Monostatic and bistatic SAR images of the target stinger launcher (STR)*

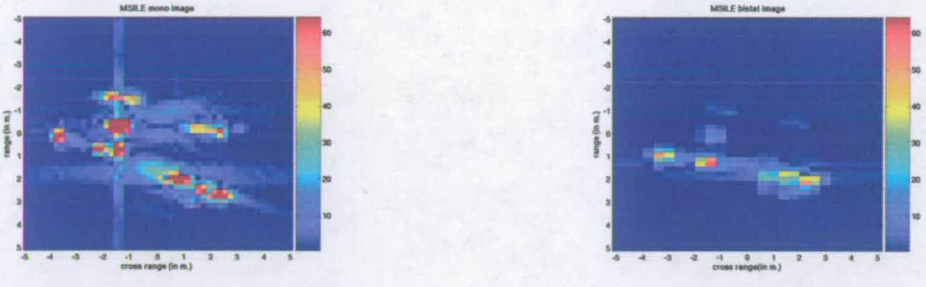

Monostatic Bistatic

Figure 3.29: *Monostatic and bistatic SAR images of the target Land-missile launcher (MSL)*

generating radar images of life sized vehicles, they are of restricted access. The present work is based on work done with the EM simulator FEKO. However it should be noted that FEKO is a general purpose EM modelling tool, mostly used for antenna design and EMC analysis. Secondly, no particular FEKO based feature has been used. All the features of FEKO used in the present work, can be found in any other general purpose EM simulator (for example WIPL-D). Hence, the present work is almost tool independent, and hence available to a much wider research group.

One of the drawbacks of the present work is the lack of any standard validation. The novelty of the work put us in a situation where there were neither any standard results to compare our results against, nor were there any standard procedures to test such results. Hence, a lot of efforts have been put in understanding the results and validating them in whatever methods were found suitable. The other limitation of the work is in the ground clutter modelling. The model adopted in the present work, is elegant and easy to implement. However, it is not the best model that could have been adopted. It certainly is one of the best compromises between *accuracy* versus *simplicity and computing-resources needed.* The final results are quite acceptable for the main project of testing ATR algorithms in a bistatic scenario. In the present work, only the prominent features of the targets were modelled. For such simple target models, unified theory of diffraction (UTD) gives fairly accurate solution in very less time and computing-power consumption. The reason why UTD could not be used for the present project is its unavailability in FEKO. However, as an extension to the present work, if some theoretical models could be developed using UTD, then simple targets could be simulated and their far field could then be calculated much easily. This would result in a much more exhaustive database at a much higher frequency [4]. However the accuracy of UTD for higher frequencies of operation, has not yet been established.

[4]the operating frequency in the present work is 1GHz and practical systems are fast surpassing this operating frequency.

Chapter 4
ATR in bistatic scenario

4.1 Introduction

There has been a steady increase in the use of artificial sensors for battle field surveillance. This is primarily because human intelligence (HUMINT) is not always feasible due to safety and accessibility issues. Secondly, use of sensors increases utilised signal bandwidth (by using different bandwidths than those used by human sensors), and hence highly enriches the available information. Given the information from a sensor collected from a battle scene, the first step would be to look for any object of interest in the scene. This constitutes the *detection* phase. *Detection* might be done by human, by an automated algorithm or by the hybrid of both. An object of interest is termed as a *target*. After the *detection* stage, the next step is to get more information about the target and try to recognise it as belonging to a certain class of targets. This is the step of *target recognition* or *target classification*. Target recognition, if performed by an automated algorithm, is termed as automatic target recognition or ATR. In some specific cases, the target could be identified as belonging to a certain brand or make, and this step is the *target identification* step. In a battle field scenario, target *detection*, *classification* and *identification* are the three broad usages of any instrument system.

Bistatic radars have got certain operational and strategic advantages over their monostatic counter parts. The bistatic geometry could be exploited in many innovative ways of deploying and using a radar system [13]. However, unless the end usages of the system are studied, it does not make a case for the development of a bistatic radar system. For radar based instruments, detection and classification are the two major usages in combative environment. Study of both these usages, using a bistatic radar system, is a must in the developmental phase of the system. The present project in general deals with this task. In the present chapter, studies made on bistatic radar image based ATR, will be elaborated.

Some of the conventions used in this report in general and in this chapter in particular are noted below.

- Synthetic aperture radar (SAR) imaging is the most widely prevalent form of radar imaging, and radar image based ATR is the major type of ATR, using radar. In the present

work, radar image based ATR has been studied. Hence in the report, radar based ATR, and SAR ATR will be used interchangeably.

- This work addresses the classification problem. As has been mentioned before, the classification task comes after the target detection step. The detection phase in SAR image analysis, consist of determining the region of interest (ROI), and verifying for false alarm [65, 71]. In the case when a genuine target is concluded, the target image with some surrounding background is given as the output. The classification phase mostly deals with this small part of the larger SAR image (of the scene), containing the (suspected) target image and some amount of background. This smaller piece of image is termed as a *target image clip*.

The next section explains the various issues related to SAR ATR in general and bistatic SAR ATR in particular. The section after that, describes the basics of principal component analysis (PCA) and how they closely correspond to the scattering centre analysis of radar images. The following section explains the PCA based nearest neighbour (NN) algorithm, the new ATR algorithm used in this project. This is followed by notes on one of the most successful conventional ATR algorithms in the open literature, namely the conditional Gaussian model based Bayesian classifier. The section next to it explains the algorithms used in this work, in deriving the receiver operating characteristics (ROC) of an ATR algorithm. The next section deals with bistatic ATR and various aspects of it. The following section deals with the comparison of ATR in bistatic and monostatic scenarios. This is followed by the section compiling the results of applying the present PCA based NN algorithm on the standard MSTAR monostatic SAR image database. The chapter ends with a summary of the major achievements and a concluding remark.

4.2 Bistatic SAR ATR: challenges

Radar ATR is basically an image domain classification problem. However, there are certain situational peculiarities of the ATR problem, which make it extremely difficult to tackle [2, 3].

- The ATR algorithms are used mostly on-line in battle fields. This operating condition (battle field) is almost always beyond the exact prediction of the ATR designer. Hence, radar ATR field needs special study and the analysis of many other factors than what is

deemed necessary in conventional optical image domain pattern recognition fields.

- Problem definition is mostly vague in the task of ATR algorithm design. For example, while the training dataset might contain the image clips of one particular make of a main battle tank (MBT), the ATR algorithm might be expected to classify any type of main battle tank.

- The amount of training data available is mostly limited. This is partly because of the cost of missions to collect training datasets. Another part of the problem is due to the fact that an exhaustive database of most types of battle targets in all different poses and in most of representative battle field environments, is almost impossible. Not only do the battle field targets come in a vast number of types, even the same type of target can come with different types of special features. For example, an MBT can come in large number of combinations. Even the turret and canon of some MBTs are detachable.

- Radar is a coherent instrument and hence like laser, radar images have the typical speckle noise. Speckle noise is a multiplicative noise, modelling and filtering of which is a major challenge in radar image analysis.

Compared to monostatic SAR ATR, bistatic SAR ATR is much more challenging. Some of the features of the bistatic configuration, complicate the whole problem.

- In a monostatic radar system, the transmitter and the receiver are co-located. For a given position of the imaging platform, rotating the target through 360^o gives an exhaustive set of images of the target. However, in bistatic case, the transmitter and the receiver are on different platform. For a given position of transmitter, the receiver could be positioned in another position and then the target rotated through 360^o. Let it be assumed that for a given position of the transmitter, M different positions of the receiver, give a decent sampling of the space around the target to be imaged. Then, if N image clips of the target are needed for the monostatic case, $M * N$ image clips are needed for the bistatic case to represent the target to a similar level. This is not only expensive, but sometimes an almost impossible exercise to be carried out. Hence the training dataset available in bistatic ATR algorithm design would be much more limited.

- Compared to a monostatic configuration, in a bistatic configuration, detailed study and modelling of various phenomena of imaging are still under development. In other words,

the monostatic field is now an almost mature field. Hence bistatic ATR algorithms would be expected to be much more robust, if they have to compete with their monostatic counterparts.

Taking these points into consideration, it will be attempted in the present work to show the robustness of the proposed ATR algorithm, in different aspects of bistatic ATR.

4.3 PCA and scattering centres

Principal component analysis (PCA) [114, 115] has been used as a statistical tool in data analysis and data compression for a long time. This belongs to the wide class of tools, exploiting the information in eigenspace, consisting of similar methods of data compression, like the method of factor analysis and singular value decomposition (SVD). In the present section, a brief introduction to PCA, and its relation to the scattering centre model of radar data, will be presented.

4.3.1 Introduction to PCA

Let $\overline{x}$ be the observation vector of a set of p variables.

$$\overline{x} = [x_1, x_2, x_3, ..., x_p]^T \tag{4.1}$$

Principal component analysis tries to get a set of derived variables from the original set of variables. In doing so, the cross correlation between the derived variables is kept at minimum. Along with this, the new variables, also called the principal components, maintain as much second order statistical information (variance, and correlation or covariance) as possible of the original set of variables. This is done, based on the assumption that all the information of the observed variables is contained in the first or the second order statistics. Hence by preserving the variance, the new set of derived variables preserve as much information as possible, from the original set of variables.

PCA is an established method of statistical analysis. There are two major theoretical advantages of PCA. First of all, this generates a set of *uncorrelated* variables. The variables in most of the multi-variable signal analysis problems, are correlated. Hence by deriving a set of non-correlated variables, the same information could be represented by a reduced number of variables. The number of principal components to represent almost the same amount of infor-

mation as the original set of variables, is in most cases significantly less. This is the second major advantage of PCA. This results in data compression and speed of data-processing. Mathematically speaking, the aim in PCA is to look for some linear function $\overline{\alpha}_1^T\overline{x}$ of the elements of $\overline{x}$, which would give maximum variance. Here $\overline{\alpha}_1$ is given by

$$\overline{\alpha}_1 = [\alpha_{11}, \alpha_{12}, ..., \alpha_{1p}]^T \tag{4.2}$$

Next look for $\overline{\alpha}_2$, so that $\overline{\alpha}_2^T\overline{x}$ will be uncorrelated to $\overline{\alpha}_1^T\overline{x}$, and will have as much variance as possible. This can be carried on for k such searches, so that, the initial set of variables are projected into a different space. This is the process of principal component analysis (PCA). The new set of variables (which are termed as principal components) have the following characteristics:

- The dimension of the new variables can be less than the original number of variables, at the same time maintaining as much as information (variance) as possible.
- The new set of variables are uncorrelated to each other.
- The new set of variables are arranged as per their information content (i.e. contribution to the original variance), hence making it easy to pick up more significant variables.

As could be found in any standard book on statistics [114], it can easily be derived that:

- If $\mathbf{Q}$ is the covariance matrix of the observed dataset (computed from the *available* dataset), then the k^{th} PC is given by $\overline{z}_k = \overline{\alpha}_k\overline{x}$, where $\overline{\alpha}$ is the eigenvector of $\mathbf{Q}$, corresponding to the k^{th} largest eigenvalue λ_k.
- If $\overline{\alpha}_k$ is chosen to have unit length, i.e. $\overline{\alpha}_k^T\overline{\alpha}_k^T = 1$, then $var(\overline{z}_k) = \lambda_k$. Here $var()$ represents the variance of the argument. Hence the eigenvalue of the sample covariance matrix, give the indication about the variance contributed by the corresponding PC, or the information content of that PC.
- In matrix notation, the operation of PCA could be performed in a single matrix multiplication:

$$\overline{z} = [z_1, z_2, ..., z_k]^T \tag{4.3}$$

$$= \mathbf{A^T}\overline{x} \tag{4.4}$$

Here, $\mathbf{A}$ is the matrix of size $p \times k$ of k eigenvectors corresponding to the k largest eigenvalues of the covariance matrix $\mathbf{Q}$.

An important parameter to be decided in PCA is the *number of PCs to calculate*. There are many criteria which can be taken into account for deciding how many PCs to calculate [114]. Two of the major and widely accepted ones (and used in the present work) are:

Cumulative percentage of total variation: This is one of the most accepted criterion, which decides the order depending on a parameter t_k defined as:

$$t_k = 100\frac{\sum_{j=1}^{k}\lambda_j}{\sum_{j=1}^{p}\lambda_j} \tag{4.5}$$

If k largest eigenvectors of the covariance matrix are used to find k PCs, t_k represents the percentage of variance preserved from the original variables, in the reduced set of PC variables. p is the number of variables in the original dataset. For a particular application, a thresh-hold τ could be chosen, so that the minimum k satisfying the condition $t_k \geq \tau$, is taken as the number of PCs to be calculated.

Cross validatory choice of k: This criterion tries to exploit the singular value decomposition (SVD) principle from linear algebra, in back-predicting the values in the original dataset, from a reduced amount of principal components. Let $\mathbf{X}$ be the dataset of dimension $m \times p$ (m values taken by p variables), $\mathbf{A}$ be the matrix of k eigenvectors corresponding to the k largest eigenvalues of the covariance matrix $\mathbf{Q}$. Because there are p variables, the eigenvector will each be of dimension $1 \times p$. Hence $\mathbf{A}$ will be of dimension $p \times k$. Following the analysis of SVD, it can be shown that:

$$\widetilde{\mathbf{X}} = \mathbf{ULA^H} \tag{4.6}$$

Here, $\widetilde{\mathbf{X}}$ is the estimated value of $\mathbf{X}$,
$\mathbf{L}$ = a diagonal matrix of size k, with the k^{th} diagonal element given by $\lambda_k^{-\frac{1}{2}}$,
$\mathbf{U} = p \times k$ matrix with $\mathbf{U}(:, \mathbf{n}) = \lambda_{\mathbf{n}}^{-\frac{1}{2}}\mathbf{XA}(:, \mathbf{n})$.
If the rank of $\mathbf{X}$ is k, then $\widetilde{\mathbf{X}} = \mathbf{X}$, else there is an error in the estimation, given by:

$$PRESS(k) = \sum_{i=1}^{m}\sum_{j=1}^{p}(x_{ij} - \widetilde{x}_{ij})^2 \tag{4.7}$$

PRESS is the PREdictive Sum of Squares index. This can be taken as a parameter for deciding the value of k.

4.3.2 PCA applied to radar signal

The operation of principal component analysis of radar data could be done at the range profile (RP) stage or after the formation of the synthetic aperture radar (SAR) image. All the data points in one observation, could be assumed as different variables. For example, if the observation vector is a range profile (RP), the range bins could be taken as variables, and if the observation is a SAR image, the image pixels are taken as the variables. PCA would reduce the number of variables and make them uncorrelated. The steps involved in the PCA of the SAR image type observation will be discussed in this subsection. Steps for range profile type observation, would be similar. SAR images can be represented as a two dimensional matrix of the pixels in the image. The two dimensional image matrix is converted into a one dimensional vector by stacking the image matrix. This step was done to generate the observation vector $\overline{x}$, with the SAR-image pixels as the observation variables. To apply PCA on the data, the first step is to calculate the covariance matrix of the observation vector. When subsequent SAR-images are collected (for consecutive locations of the transmitter and/or the receiver), the variables (image pixels) take different values. Hence statistically speaking, the image pixels can be assumed to be the variables, taking different observation values for different consecutively collected SAR images of the same scene. The data collected from m consecutive SAR images, hence represent m observational values of the observation vector $\overline{x}$. Let the complete set of observation be represented by the matrix $\mathbf{X}$ of size $p \times m$. In it, each column represents a value taken by the observation vector. The approximate covariance matrix is:

$$\widetilde{\mathbf{Q}} = \mathbf{X}^{\mathbf{H}}\mathbf{X} \tag{4.8}$$

$\mathbf{X}^{\mathbf{H}}$ represents the Hermitian of the observation matrix $\mathbf{X}$. Let λ_is be the eigenvalues and α_is the corresponding eigenvectors of the covariance matrix. By using any of the methods described above, let it be decided to take k PCs, and hence k eigenvectors. Let $\mathbf{A}$ be the matrix with columns equal to the k most significant eigenvectors. The PCA domain observation vector $\overline{z}$ can be derived now as:

$$\overline{z} = \mathbf{A}^{\mathbf{T}}\overline{x} \tag{4.9}$$

4.3.3 Experiments on PCA-scattering centre relevance

Historically, PCA has mostly been applied to social science data [115]. Hence finding a direct correspondence between the derived principal components and some observable or quantifiable features, is quite difficult. However, in science and engineering, principal components could sometimes be linked to certain tangible features.

Mostly radar image analysis is based on the scattering centre model [81, 116]. This has been one of the most successful models in radar image analysis. The scattering centre model is based on the geometrical theory of diffraction (GTD) principle, which states that if the wavelength of the incident EM wave is small compared to the physical features of the object getting imaged, then the backscattering consists of isolated scattering centres. At present, for most of the radar imaging exercises, GTD approximation could be assumed to hold true. Hence a scattering centre model is a successful model both for radar signal and image analysis and classification [81, 82, 103, 117–120]. Because scattering centres are the major features in a radar image, it was envisioned that maybe PCA of a radar image could give us information about the scattering centres.

In an initial set of experiments on PCA and scattering centre correspondence, bistatic SAR images were collected for a simple scene with distinct discrete scatterers (using Matlab simulation). The next step was to decide on how many PCs are needed to represent the dataset, without much loss of information. For that the cumulative percentage of total variance parameter was used. This was repeated for data collected from scenes with different number of scatterers (Figure 4.1). In the figure, the X axis represents the number of principal components and the Y axis represents the percentage of energy (variance) of the original dataset, represented by the given number of PCs. The steps have been repeated for different scenes, and different curves in the figure represent the analysis for different scenes. As can be observed, the number of PCs accounting for above 95% of the variation is equal to the number of scatterers in the scene.

The next activity was to see if the variables in the PC domain in some way correspond to the scattering centres. After PCA only k variables are required to represent the data. It was found from the last set of experiments that k is equal to the number of scattering centres in the scene. Could it be that the new variables (principal components) represent the scattering centres? To study this possibility further, another set of experiments were performed using Matlab simulation. Six scenes were simulated for radar image datasets. Of these, one scene had five scatterers present at positions given by $(0,0)$,$(50,50)$,$(50,0)$,$(0,50)$ and $(25,25)$, where the numbers give the X and Y coordinates of the points in metres. The remaining five scenes were simulated

with one scatterer in each scene. The scatterer position was fixed at the same positions as the position of one of the scatterers in the first scene (with 5 scatterers). The SAR images of the scenes were collected using Matlab simulation, and PCA was applied on the dataset from each scene. As has been shown, the dimension of data for the first scene (with five scatterers) would be reduced to 5, while the same for others (with one scatterer each) would be reduced to one. After applying PCA, the data (both phase and amplitude) of the principal components were plotted (figures 4.2 and 4.3).

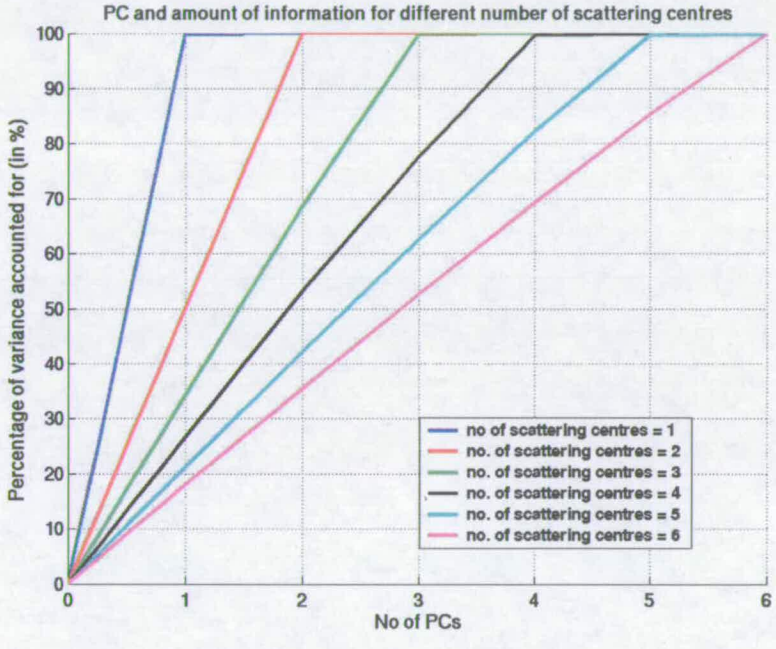

Figure 4.1: *Percentage of total variance accounted for versus the number of principal components*

As can be observed, the phase data show a lot of variance. On watching the phase data more closely, some interesting observations could be made:

- For the five-scatterer scene, although amplitude information is almost the same for all the PCs, the phase data vary.
- For one-scatterer scenes, the phase data again vary from one scene to the other (while the amplitude of the principal components remain the same).

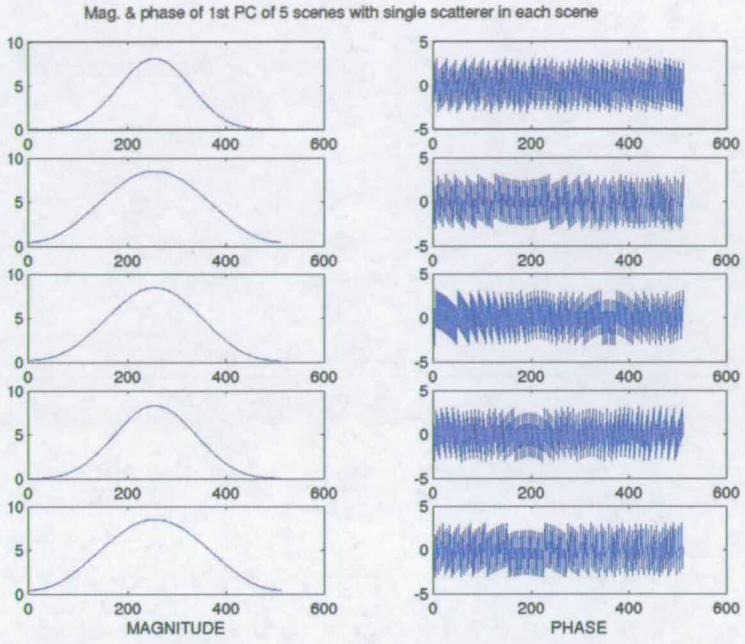

Figure 4.2: *PC domain data for the first PC for 5 scenes with 1 scatterer in each*

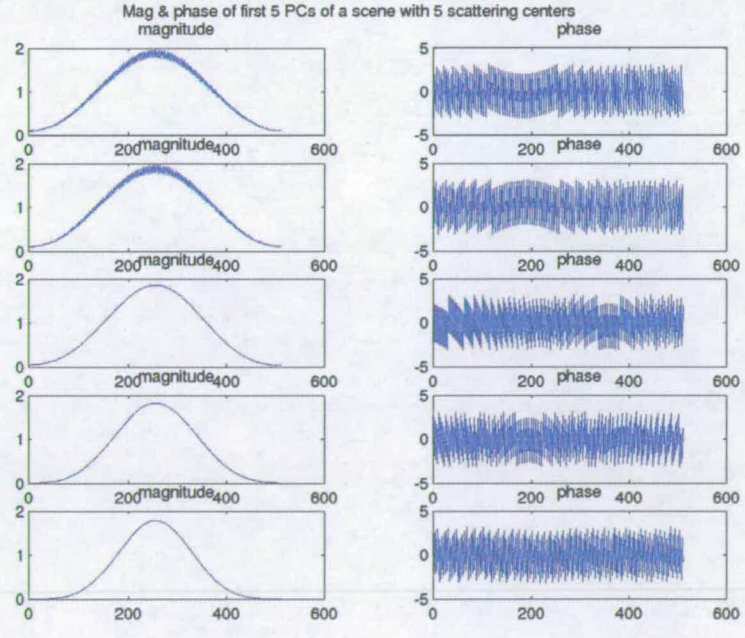

Figure 4.3: *PC domain data for the first five PCs for a scene with 5 scatterers*

- On close observation, a one to one link could be established between the one-scatterer scene PCs and the PCs of the five-scatterer scene.

From this it could be concluded that:

- After the application of PCA, each principal component seem to represent one scattering centre.
- The phase of the principal components contain more information than the amplitude.

To analyse more of PCA and scattering centre correspondence, PCA was performed on the SAR image-clips from the MSTAR database [1]. PCA was applied on one set of the image clips from the MSTAR database. The criteria mentioned above were examined to see how many PCs might be required to represent the information in the image set.

- Looking at the cumulative percentage of total variation index, if the threshold is taken to be 90%, around 40 PCs are needed to represent the data (figure 4.4).
- Looking at the PRESS index, again it seems around 30-40 PCs are needed to represent the dataset (figure 4.4).

However for real radar data, it is almost impossible to examine the targets and point out the scattering centres [116]. Hence, to verify if in this real data too, the PCA domain data corresponds to the scattering centre model, a usage can be examined which uses the scattering centre model. The performance as obtained from the scattering centre model and PCA could be compared. One such use is the SAR image based ATR, where the scattering centres are extracted form a SAR image in order to characterise the target in the image. In the works in the open literature, discussing the use of scattering centre model in ATR on MSTAR database, it has been stated that around 40 scattering centres give the best performance to the classifier [103]. A PCA based ATR algorithm (which will be explained in the next section) was applied on the present set of data for different number of PCs. The results are plotted in figure 4.5. In it, each subplot shows the variation of ATR performance for different number of PCs taken to represent the dataset. It

[1] Moving and stationary target acquisition and recognition (MSTAR) program is a DARPA supported project for collecting a standardised monostatic SAR image database, collected using the Sandia National Laboratories Twin Otter SAR sensor payload operating at X-band. The targets used for the present experiments are the 2S1 tank (t000), D-7 land clearing vehicle (t005), T62 tank (t016), ZIL131 APC (t025), and ZSU-23 (t026).

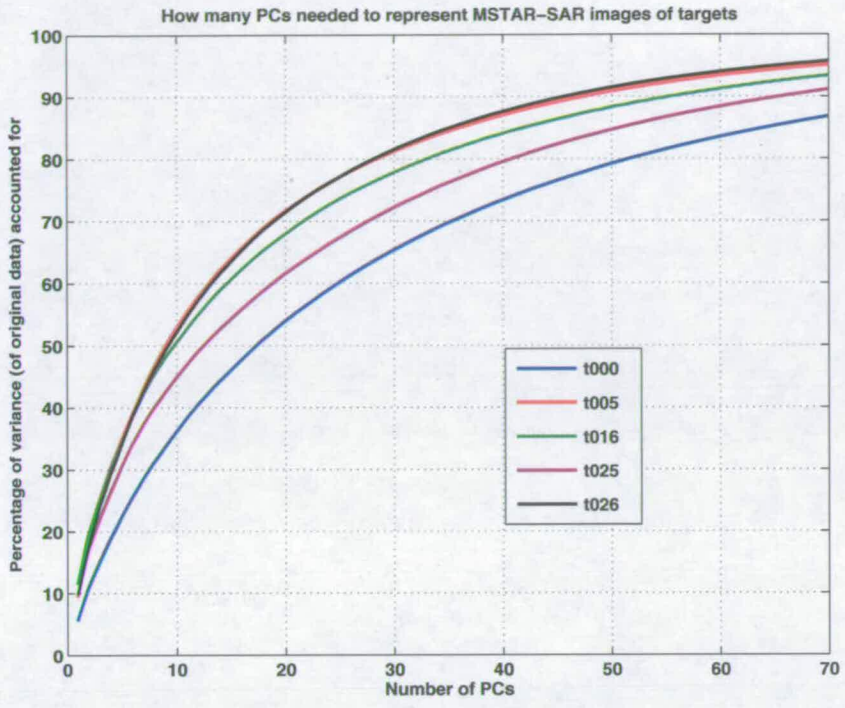

Cumulative percentage of total variance

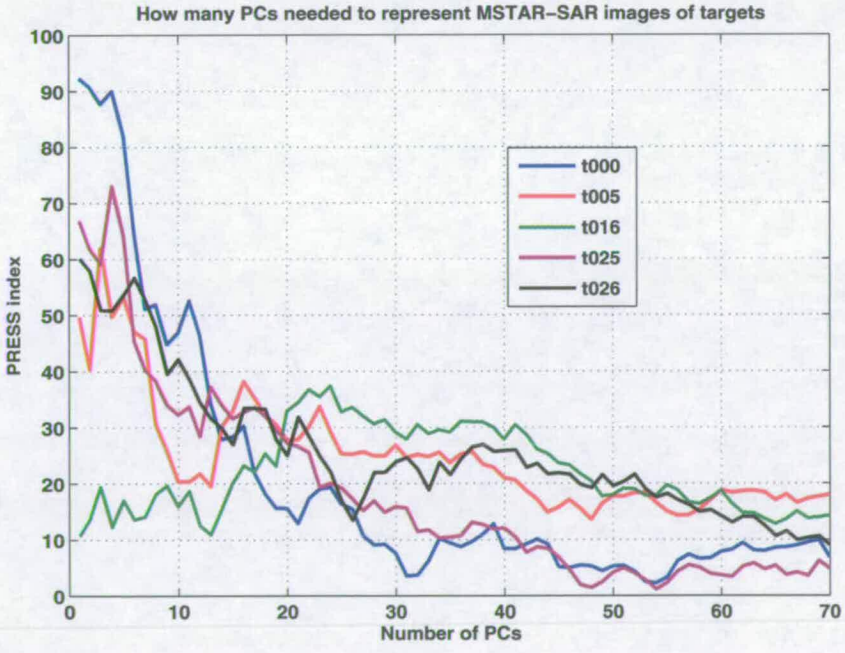

PRESS index

Figure 4.4: *Cumulative percentage of total variance index and PRESS index methods of finding how many PCs needed to represent SAR images from the MSTAR database*

could be marked that 30 to 40 principal components give optimum performance. This implies that, 30 to 40 principal components give almost all the information from the SAR image (as required by an ATR exercise).

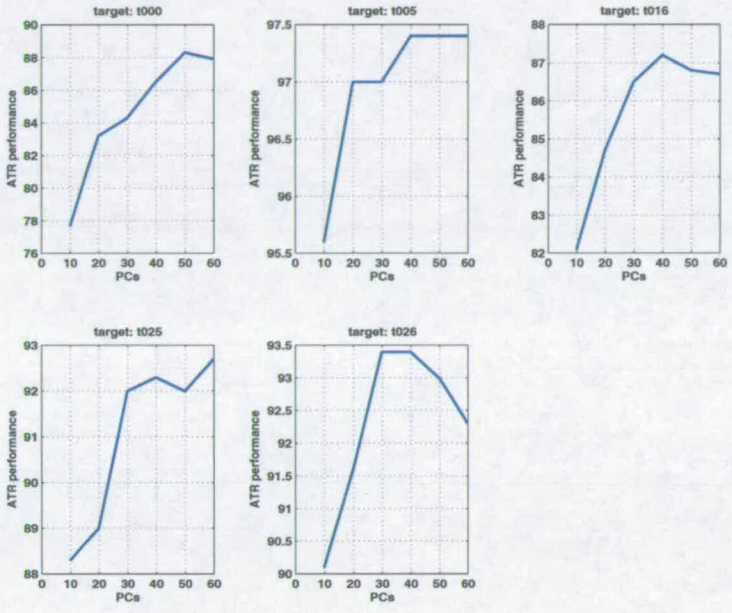

Figure 4.5: *Classification performance for MSTAR data using PCA, for different number of PCs*

Hence, for MSTAR database too, the PCA and scattering centre models are shown to bring forth an almost similar amount of information, and can prove to be equally effective in specific uses. Even though this does not positively confirm that PCs exactly represent the scattering centres, it highlights that the two models are highly correlated.

4.3.4 Some theoretical analysis on PCA-scattering-centre correlation

In the above subsection, some of the observations from the application of PCA on radar data, were presented. All the observations seemed to point towards a strong correlation between the principal component analysis and the scattering centre analysis. In this section eigenvalue analysis of the radar image data is presented to show that within standard SAR imaging assumptions, principal components do represent the scattering centres from a SAR image.

Radar imaging traditionally has depended on the scattering centre assumption. According to

this, if the wavelength of the illuminating EM wave is smaller than the object dimensions, the scattered return could be modelled as coming from distinct scattering centres. This model when applied to radar imaging, gives the scattering centre modelling of radar images, where the radar image is modelled to be a summation of distinct scattering centres. The theoretical representation of an ideal scattering centre is the two dimensional Kronecker's delta function. Practically, more approximate mathematical functions can be taken for the ease of handling. In this subsection a two dimensional sinc function is taken as the model for an ideal scattering centre in a radar image. In a simple radar image, let there be a single scattering centre in the scene, at the centre of the scene, and let the size of the scene be $N \times N$ pixels. The image can be represented by a matrix of pixel values $\mathbf{A}$, which according to the scattering centre model would be a two dimensional sinc function. It can be observed that:

$$\mathbf{A} = \overline{u}\mathbf{S}\overline{v}^{H} \tag{4.10}$$

Here $\overline{u}$ and $\overline{v}$ are two one dimensional sinc vectors (vectors of dimension $N \times 1$), and $\mathbf{S}$ is a diagonal matrix with the diagonal set to the value one [2], and of dimension 1×1. $(\cdot)^{\mathbf{H}}$ represents the Hermitian operation on a matrix. Two of the important characteristics of a scattering centre are its amplitude, and position. It can be observed from the above equation that:

- To change the intensity of the scattering centre, the value of the diagonal elements of the $\mathbf{S}$ matrix need to be changed.
- To shift the position of the scattering centre, the sinc vectors, viz. $\overline{u}$ and $\overline{v}$ are to be shifted appropriately.

Similarly, a scene with k scattering centres at different positions can be represented as:

$$\mathbf{A} = \mathbf{U}\mathbf{S}\mathbf{V}^{\mathbf{H}} \tag{4.11}$$

Here [3] $\mathbf{U} = [\overline{u}_1\ \overline{u}_2\ ...\ \overline{u}_k]$, and $\mathbf{V} = [\overline{v}_1\ \overline{v}_2\ ...\ \overline{v}_k]$. Each element vectors $\overline{u}_i$ and $\overline{v}_i$ are sinc-function-vectors of length N, and appropriately shifted to represent the position of the i^{th} scattering centre. $\mathbf{S}$ is a diagonal matrix of size $k \times k$, with the i^{th} diagonal element representing the intensity of the i^{th} scattering centre.

[2] unit matrix

[3] Dimension of $\mathbf{A}$ is $N \times N$, of $\mathbf{U}$ is $N \times k$, of $\mathbf{S}$ is $k \times k$, and of $\mathbf{V}^{\mathbf{H}}$ is $k \times N$

Because the vectors $\overline{u}_i$'s and $\overline{v}_i$'s are sinc functions, the matrices $\mathbf{U}$ and $\mathbf{V}$ are unitary and orthonormal. This conclusion holds true for most of the mathematical functions which could be taken to model an ideal scattering centre. Given these facts, equation 4.11 is in the same form as the famous singular value decomposition of the image pixel matrix!
Hence, it can be observed that radar images can be decomposed as per SVD (provided the scattering centre assumption is true). Few points worth noting are:

- The numbers of scattering centres determine the number of elements in $\mathbf{S}$, and hence the rank of the final image matrix .
- The position of the scattering centres is determined by the elements of $\mathbf{U}$ and $\mathbf{V}$ matrices.
- The strength of the scattering centres is determined by the singular values (i.e. The elements of the diagonal matrix $\mathbf{S}$)
- The i^{th} element of $\mathbf{S}$ can be shown to be equal to $\lambda_i^{1/2}$, where λ_i is the eigenvalue of the covariance matrix of $\mathbf{AA^H}$ [114, 121].
- Columns of $\mathbf{U}$ are the eigenvectors of $\mathbf{AA^H}$, and those of $\mathbf{V}$ are the eigenvectors of $\mathbf{A^HA}$ [114, 121]. Let it be assumed that in the image matrix $\mathbf{A}$, the rows represent range and columns represent cross-range vectors. Then $\mathbf{AA^H}$ is the covariance matrix (assuming the image has been zero-centred) of the cross-range pixel variables, and $\mathbf{A^HA}$ represents the covariance matrix (assuming the image has been zero-centred) of the range pixel variables. Hence, pre-multiplication of the image matrix with $\mathbf{U^H}$ represents the principal component analysis with respect to cross-range pixels and multiplication of the image matrix with $\mathbf{V}$ represents principal component analysis with respect to range pixels [114]:

$$\mathbf{U^HAV} = \mathbf{U^H(USV^H)V} \tag{4.12}$$

$$= \mathbf{ISI} = \mathbf{S} \tag{4.13}$$

The second step can be explained as both $\mathbf{U}$ and $\mathbf{V}$ are unitary, i.e. $\mathbf{U^H} = \mathbf{U^{-1}}$ and $\mathbf{V^H} = \mathbf{V^{-1}}$, $\mathbf{U^HU} = \mathbf{V^HV} = \mathbf{I}$. Here $\mathbf{I}$ is the identity matrix and $\mathbf{U^{-1}}$ represents the inverse of the matrix $\mathbf{U}$. Hence, applying PCA in one dimension is equivalent to extracting the position of the scattering centres in that dimension. Hence the result of applying PCA, is a two dimensional matrix with information about the scattering centre intensities.

- In real images, there is the presence of noise. Hence, the choice of the dimension of $\mathbf{S}$, $\mathbf{U}$ and $\mathbf{V}$, depends on the choice of k, the number of the largest eigenvalues of $\mathbf{AA}^{\mathbf{H}}$, to be taken. This is similar to the super-resolution algorithms [121], which have been applied by some researchers in filtering the noise from the radar images [122–124].
- When PCA is performed on a radar image, matrices $\mathbf{U}$ and $\mathbf{V}$ are calculated. These matrices not only help to reduce the dimension of the matrix D, but *represent the position of the scattering centres in the image matrix* $\mathbf{A}$.
- The eigenvectors chosen in forming $\mathbf{U}$ and $\mathbf{V}$ correspond to the largest eigenvalues, and hence correspond to the brightest scattering centres in the image matrix $\mathbf{A}$.
- Hence, applying PCA is equivalent to extracting the position and intensity information of the scattering centres.

Use in classification: In the training phase, given images of target of a particular class, the $\mathbf{U}$ and $\mathbf{V}$ matrices are found out,

- which correspond to the positions of the scattering centres in the target image, and
- which when applied on an image of the target, should give a matrix $\mathbf{S}$, which would be a diagonal matrix with elements in the diagonal, corresponding to the intensity of the brightest scattering centres.

Given a test image, applying $\mathbf{U}$ and $\mathbf{V}$ on that and finding the distance (Euclidean distance for simplicity) of the resulting matrix from $\mathbf{S}$, in essence represents the task of *comparing the position and intensities of the test image with the target class* with whose training the matrices $\mathbf{S}$, $\mathbf{U}$ and $\mathbf{V}$ have been found.

The above analysis shows the strong correlation between PCA of radar images and scattering-centre analysis of the radar images. However, the analysis is limited in a few aspects. First of all it does not hold, if the scattering centre model of the image does not hold absolutely correct [116]. Secondly, here the two dimensional PCA has been presented, where PCA is applied both to the range and the cross-range dimensions of the radar image. In the current project, a stacking operation is performed on the radar images to form one dimensional vectors, and then one dimensional PCA is applied. However the stacking operation is linear. Hence the results derived in the current analysis would still hold true. Moreover it has been checked

by applying the two dimensional and one dimensional PCA to radar images, that both ways of applying PCA result in same ATR performance [125].

4.3.5 Multi-mode PCA and relevance to radar signal processing

It is a common problem in social science to take observations from different subjects for different parameters and under different conditions. Hence, an observed variable can vary with the subject, the parameter of choice or the condition under which the observation was taken. This finally gives rise to a dataset which is three dimensional in nature. PCA originally was also invented to deal with the huge amount of data collected from practical field work. However, PCA deals with one dimensional dataset (variables all shown in one vector). Extending the philosophy of PCA based data reduction to the three dimensional datasets in social science, there were methods which came to be known as three-mode PCA (and this idea can be extended to multi-mode PCA). One of the key works in this area is the book by Kroonenberg [115]. In simple terms, this deals with reduction of size of the final three dimensional observation data matrix from all three dimensions, by applying the simple one dimensional PCA in three dimensions. The simplest case of this is to independently deal with the three dimensions and find PCs independently and apply them to finally get hold of the reduced size principal components. As a basic rule of PC analysis, the variables again are uncorrelated and preserve as much variance of the original data, as possible. The pertinence of this sort of analysis could be well seen in radar signal processing:

- With more complicated radar systems in practice, there is always the scope of imaging the same scene from two or more different antennas. This makes the final data dimension more than a simple two dimensional image.
- If there is facility of multi polar system, the final output is data or image in more than one polarisation. This again results in a higher dimension of data than the simple case of two dimensional images.

In the present project, multi polar returns have already been collected in the database simulation step. Hence, the three-mode PCA seems to be a new and effective tool of analysing the multi-polar data classification exercises. Given the success of PCA based algorithms in single polarisation classification algorithms, this option looks encouraging.

4.4 PCA based NN classifier

PCA has been applied to optical image recognition and target recognition, with success [126, 127]. In optical image recognition, all the pixels of the image are assumed as variables. If there are N pixels, each image could be represented by a point in the N dimensional space. After applying PCA on this data, the dimension is reduced, and each image in turn could be represented as a point in the reduced principal component space (more popularly termed as the *eigenspace* in image processing literatures). Because PCA is a linear operation, the mapping from the original image domain point to the PC-space point is one to one. In optical image processing, the PC-space points representing images of the same object taken with successive camera positions, have been shown to form a smooth manifold [126, 127]. A smooth manifold in PC-space has two major implications:

1. For different classes of objects or targets, mostly the PC-space manifolds are disjoint and hence representative of the particular class.
2. Because it forms a close manifold, a coarse sampling of the manifold is mostly representative enough. In the image domain, this implies a reduced demand for training data.

Both the above advantages of dealing in PC-domain, are useful in radar ATR problem. Hence, experiments were performed to observe if PC-space points for radar images, can also form a continuous and smooth manifold.
To examine the manifold created by the PC-space points of radar images, a preliminary experiment was designed. In the collection of bistatic image clips of the various targets, the simulated transmitter platform was kept fixed and the simulated receiver platform was moved round the target to be imaged, keeping the receiver azimuth at a fixed angle. Similarly collected optical images form smooth and continuous manifold in PC-space. Hence these images were mapped to their PC-space, and the first three PCs were taken to plot the manifold. This was because it is hard and involved to visualise points in more than three dimensions. Figure 4.6 shows the PC-space points of of different targets. Each subplot has the PC-space representation for the radar images collected for two different classes of targets.

For radar images, the manifold was found to be neither smooth nor continuous. This might be attributed to following reasons:

- Resolution of radar image is coarser, when compared to the optical counterpart. Hence

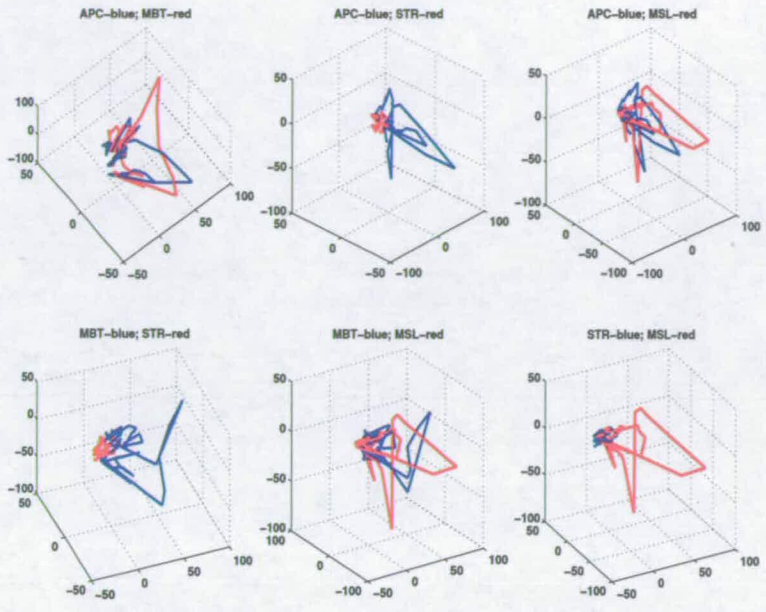

Figure 4.6: *The bistatic targets as represented in the 3D space formed by the three most significant PCs*

the manifold is not expected to be smooth either.

- As has been mentioned before, a radar image (with today's technology) is best modelled with a scattering centre model. However, scattering centres are highly unstable and sometimes change unpredictably. The correspondence between scattering centres and the principal components of a radar image, has been discussed in the previous sections. Hence, if the PC-domain points represent scattering centres and scattering centres change unpredictably with rotation of the imaging platform, the PC-domain manifold is not expected to be smooth.

- Another difference between optical and radar imaging is the coherent nature of radar imaging, which creates speckle like features in radar images. Speckles are hard to model, and hence might be one of the reasons why the PC-space manifold of a radar image, is not smooth.

However, even though the manifolds are not smooth or continuous, they are disjoint enough for pairs of different targets. Hence, these manifolds in PC-space can be taken to be representative of particular classes. Given a test image, it could be mapped as a point in the same PC-space

as the training images (which form different clusters for different classes). This test image would be declared depending on which cluster it is nearest to. The simplest algorithm to do this is the kNN (k nearest neighbour) algorithm. To decide how many nearest neighbours should be taken into account, to get an optimal decision, the performance of the classifier was tested with various values of k. $k = 1$ was found to be the best from classifier performance and classifier fastness points of views. This combination of PCA and nearest neighbour (NN) algorithm was termed as the PCA-NN algorithm. Not only is it robust (due to dealing with the data in PC-space, where they tend to form a well defined cluster or a rough manifold), it is also extremely fast when compared to many of the present ATR algorithm. The speed can be completely contributed to the PCA operation, which achieves both **feature extraction** and **data compression** in a single step.

4.5 Conditional Gaussian model based Bayesian classifier (CGBC)

This classification algorithm proposed and analysed by O'Sullivan *et al.*, is one of the most successful ATR algorithms in the open literature [72, 73]. In this, each pixel of the image clips is assumed to be from a Gaussian distribution, conditioned or depending on some of the variables of the scene. In the original work dealing with monostatic images, the image pixels were assumed to be conditioned on target type (a_m) and target pose Θ_m [4]:

$$\overline{r}_m = \overline{s}_m(\Theta_m, a_m) + \overline{w}_m \tag{4.14}$$

Signal $\overline{s}_m$ is the conditional Gaussian signal, and $\overline{w}_m$ is the Gaussian noise. However, unlike the monostatic case, in the bistatic case the variables can be quite large. Because the bistatic image will depend on the target and the position (azimuth and elevation) of both transmitter and receiver. This makes for five controlling variables. To keep the analysis and the final algorithm simple, the controlling variables were fixed at two, target type and receiver platform azimuth. Some classification experiments were done keeping the second controlling variable as the bistatic angle of imaging, but the classification performance was seen to either deteriorate or not to change at all. Hence this simplistic conditional model was maintained.

$$\overline{r} = \overline{s}(\Theta, a) + \overline{w} \tag{4.15}$$

[4]The subscript m is for monostatic, to differentiate it form the bistatic case equations, which are of similar form

Here , $\overline{r}$ is the observed intensities of the pixels arranged in a one dimensional vector, $\overline{w}$ is additive Gaussian noise, and $\overline{s}$ is the signal conditioned on Θ the receiver azimuth angle, and $\overline{a}$ the target type. The log-likelihood of an observed $\overline{r}$, given (Θ, a) can be shown to be proportional to [72, 73]:

$$-\sum_{i=1}^{N}\left[log(\sigma_i) + \left(\frac{r_i - \mu_i}{\sigma_i}\right)^2\right] \tag{4.16}$$

where r_i is the i^{th} pixel of the test-image-clip. σ_i and μ_i are the standard deviation and mean of the pixel, respectively (as estimated from the training data), and N is the total number of pixels in the test-image-clip. In this method, the recognition is done as per the Bayesian rule of maximising the probability.

$$P(a|\overline{r}) = P(\overline{r}|a)P(a) \tag{4.17}$$

For the current project, $P(a)$ the probability of each type of vehicle was taken to be equal.
In the training phase, the image clips within a window of receiver azimuth angles were assumed to be stationary. Hence, image clips from this window were used to find parameters, i.e. σ_i and μ_i for that window of receiver azimuth angle. A test image clip is classified as belonging to the class, which give maximum likelihood.

4.6 Receiver operating characteristics (ROC) curves

Automatic target recognition is one of the most difficult pattern recognition tasks. It is mainly because the operating conditions are never known with certainty while designing the ATR systems. One such uncertainty is the encounter of a new type of target. It is almost impossible to design an ATR algorithm which would have been trained with all the classes of targets. Hence, it is a major design problem to decide the action in encountering a vehicle which has not been there in the training dataset. This makes the misclassification performance of an ATR algorithm, extremely crucial. There are two major approaches to test the performance of a classifier for its misclassification. If the dataset has many different types of targets, then a subset of the targets could be treated as unknown targets. Those classes would not be taken in the training phase. In the test phase, data from all the targets are to be kept. The ATR algorithm could be tested to see how efficiently it could classify unknown targets. The prevalent trend in the open literature in this case is to have an option for *unknown target* for the ATR algorithm [72, 73]. These unknown targets are mostly targets not present in the training dataset. This is a con-

venient way of testing the ATR algorithm, if handling huge amount of data, like the MSTAR database (which has datasets of more than 10 different types of land targets). For a limited dataset, like the present case (with just four targets), the above method is not the best one. In this case, the classification problem could be taken as a detection-problem, and the receiver operating characteristic is a convenient representation of the ATR algorithm's misclassification performance. In a detection problem, the ROC curve is plotted between the probability of false alarm and the probability of detection. From a classification problem point of view, the terminologies could be changed to the probability of misclassification and the probability of correct classification. It should be noted here that, though the ROC curves in an ATR context are inspired by the detection problem ROC curves, the exact definitions change with the way of handling the whole problem. Two different philosophies in generating the ROC curves for an ATR algorithm, were found in the literature [72, 73, 128].

4.6.1 Threshold of classification based ROC curves

This is the classical open-classifier approach [128]. Let it be assumed that the ATR algorithm in question is a nearest neighbour classifier. A threshold distance τ is set. The decision could be given as:

$$a_{tst} \in C_i \Leftarrow \|a_{tst}, C_{n,i}\| \leq \tau \tag{4.18}$$

a_{tst} is the test image clip, C_i is the i^{th} class, and $\|a_{tst}, C_{n,i}\|$ is the Euclidean distance between the test image clip and the nearest test image clip from the i^{th} class. Given a test image clip, there can arise three conditions:

1. It is classified to be of a certain class, if condition 4.18 is fulfilled for only one class of targets.
2. In case the condition in equation 4.18 is fulfilled for more than one class, it could be declared as belonging to more than one class, and hence a confusing target.
3. In case the condition in equation 4.18 is fulfilled for none of the classes from training set, it is declared as a new target.

For a given τ, and for a given target-type, the ATR exercise could be performed to find the number of targets correctly classified and the number of targets misclassified as that class. If there are N image clips in the test-set belonging to a particular class, and out of them M are

correctly classified as belonging to this class, then the probability of correct classification (P_{cc}) is defined as:

$$P_{cc} = \frac{M}{N} \tag{4.19}$$

In running the ATR exercise for the given τ, let there be $N1$ number of image clips in the test dataset, not belonging to this particular target class, and out of the image clips which do not belong to this class, $M1$ image clips are decided as to belong to this particular target type. Then the probability of misclassification or false alarm (P_{fa}) is defined as:

$$P_{fa} = \frac{M1}{N1} \tag{4.20}$$

The performance of the ATR algorithm could be marked for different values for τ. Plotting the P_{cc} versus P_{fa} for a given target gives the ROC curve for that target for the ATR algorithm followed.

In the present work, two different ATR algorithms have been tested, one is the PCA based nearest neighbour (PCANN) algorithm, and the other is the classical conditional Bayesian model based Gaussian classifier (CGBC). The CGBC algorithm depended on the log-likelihood for its decision. Equation 4.18 has been used to extract the ROC curves for the CGBC ATR and PCA NN algorithms. In rest of the report, this algorithm of extracting ROC curves will be termed as ROC_1.

4.6.2 Class-specific risk factor based ROC curves

Another way of looking at ROC curves is to examine the performance of the ATR algorithm to see how efficient it is in classifying a particular class [72, 73]. This could be analysed by assigning a risk factor to each target type. For a nearest neighbour (PCANN) ATR algorithm,

$$a_{tst} \in \underset{i}{\operatorname{argmin}}(\|a_{tst}, C_i\| - \gamma_i) \tag{4.21}$$

Here γ_i is the risk factor assigned to the i^{th} class. The higher the risk factor γ_i for a class, the more difficult is it to miss that class. At the same time, the easier it is to misclassify another target as belonging to this class. An example in an airborne radar ATR scenario would be to classify stinger targets with utmost efficiency. Even anything slightly resembling a stinger should not escape surveillance. In this case assigning a high risk factor for the stinger type target class is an expected decision. For a given value of γ_i and a given target class, the probability

of correct classification and of false alarm are defined as in equation 4.19 and equation 4.20. By varying the value of γ_i, the ROC curve of a particular type of target is determined for a given ATR algorithm. Similar expressions and analysis were done for CGBC ATR algorithm. In the rest of the report, this algorithm for extracting ROC curves will be termed as ROC_2.
The present project examines two different types of ROC curves extractable for the ATR performance validation. They are developed on two different paradigms and the choice is best left to the end user.

4.7 Bistatic ATR

PCA-NN and CGBC classification algorithms, as reported in the previous sections, were applied for ATR exercises in the bistatic scenario, using the synthetic database generated in this project. In PCA-NN algorithm, 20 PCs are extracted for all the ATR exercises described below. This is because, from different ATR exercises with different numbers of PCs, the classification performance was found to be optimal with 20 PCs. To maintain uniformity, similar test and training datasets were used for all the ATR experiments detailed in this section. The test data consisted of all the data collected with receiver platform elevation angle at 15^o, and the test database consisted of all the data collected with receiver platform elevation angle at 10^o.

4.7.1 Classification performance for different polarisations

The synthetic database generated in the present project has a dataset for all four combinations of polarisation, viz. HH, VV, HV and VH. Hence it was an interesting experiment to see the difference in classification performance for different polarisations. The confusion matrices for different polarisations using the CGBC classifier algorithm are presented in table A.1 through table A.4 in appendix A. The confusion matrices for different polarisations using the PCA-NN classifier algorithm are presented in table A.5 through table A.8 in appendix A.

A note on the representation of these tables (as presented in appendix A) for bistatic ATR experiments: Due to the interest in observing the variation of performance with bistatic angle of image formation, the classification results are presented in three sub groups. One for low bistatic angles (0^o to 60^o), next for medium bistatic angles (60^o to 80^o), and the last one for high bistatic angles (60^o to 100^o). Images for bistatic angle greater than 100^o

were found to be too unintelligible and hence not included in classification exercises. The bistatic angle range is larger for low bistatic angle (60^o to 100^o, i.e. 40^o) as compared to higher bistatic angle windows (60^o to 80^o or 80^o to 100^o, i.e. range of 20^o). This is due to the fact that, data in the EM simulation were collected for increasing receiver azimuth angle, keeping the elevation fixed. As the receiver platform moves from the transmitter platform, keeping the elevation fixed, the increase in bistatic angle is not the same as the increase in receiver azimuth angle. There is a nonlinear mapping, and this results in the collection of fewer image clips from the same bistatic angle window for lower bistatic angle, as compared to the same from higher bistatic angle. To keep the amount of data available in each bistatic angle window the same, the window for lower bistatic angle is higher as compared to the same from higher bistatic angles.

Analysing the results, as shown in figures 4.7 and 4.8, it can be observed that, performance is almost the same for all the polarisations. Some variations in performance can be observed for some polarisations, showing as if some particular polarisation is more suitable for classifying a particular type of target. This is to be expected, due to the fact that some type of polarisations tends to bring out certain type of physical features more clearly in the SAR image domain than the others. Hence, it can be predicted that fusing the data from different polarisations, should give us an enhanced classification performance, irrespective of the classification algorithm used.[5]

The above observations are valid for both the CGBC and the PCA-NN algorithms. For the rest of the experiments, where the effect of other parameters are tested on classification performance, only the HH dataset would be taken for simplicity.

4.7.2 Classification performance with the addition of clutter noise

Due to the novel method used in the current project for adding ground clutter to the images, the effect of clutter on classification performance could be studied easily. For this two sets of experiments were run, one with the dataset with no clutter energy added to the images, and the other with a fixed amount of clutter energy added to each image clip. The confusion matrices (for experiments with clutter) are given in table A.9 (CGBC algorithm) and table A.10 (PCA-NN algorithm) in appendix A. The overall classification rates are compared in the more

[5] the next chapter describes this type of multi-polar data fusion for better classification performance.

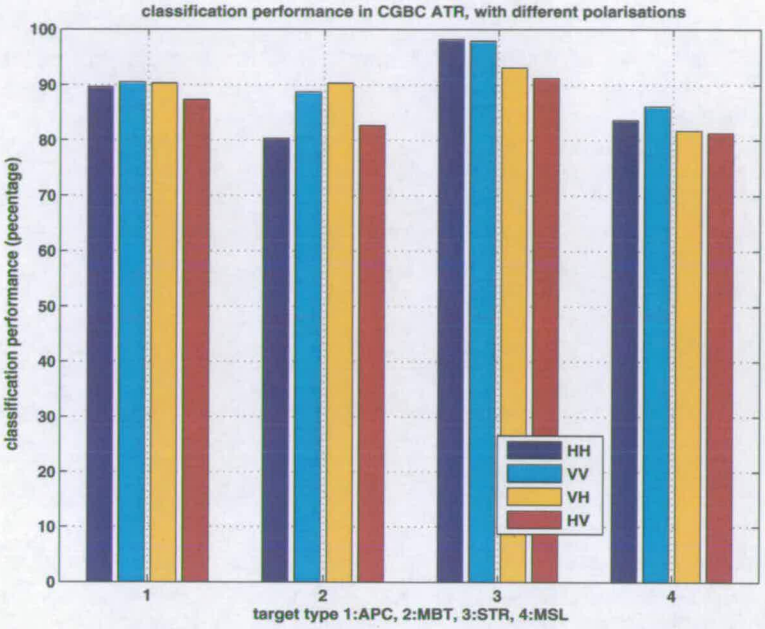

Figure 4.7: *CGBC performance for different polarised databases*

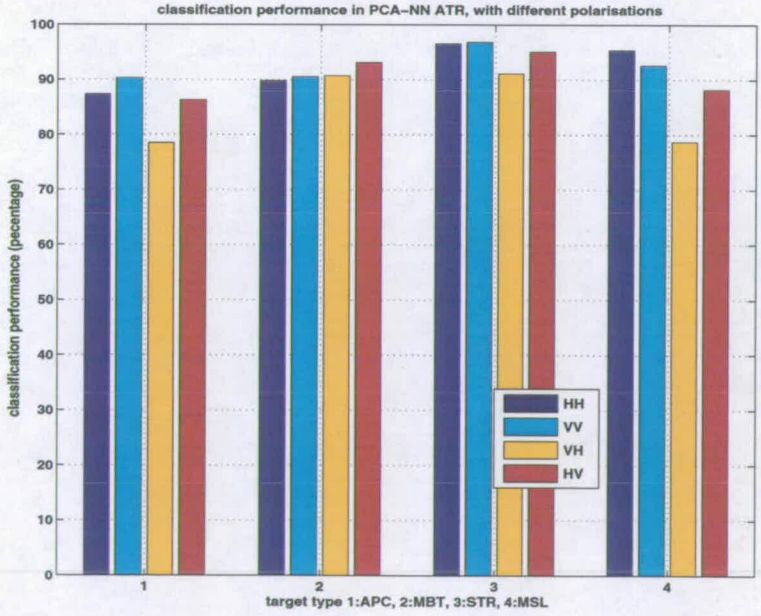

Figure 4.8: *PCANN performance for different polarised databases*

conventional bar-graph in figure 4.9 and 4.10.

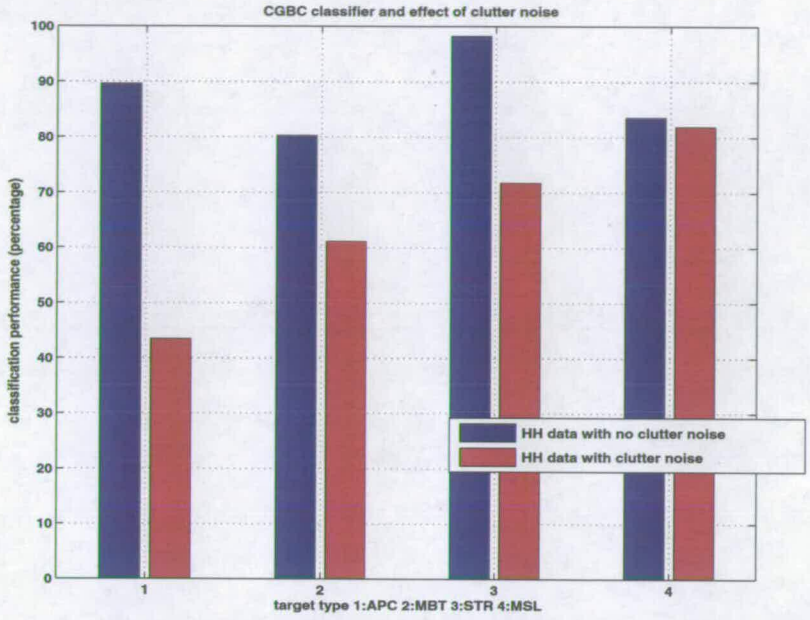

Figure 4.9: *CGBC performance with the addition of clutter*

Some observations are:

- Performance invariably deteriorates with the addition of clutter energy.
- The deterioration of performance is more severe for CGBC algorithm.
- The deterioration of performance is quite moderate for PCA-NN type classifier.

This shows the robustness of the PCA-NN algorithm in performing better with clutter, as compared to the conventional CGBC algorithm.

4.7.3 Classification performance for different ranges of bistatic angle

One of the questions that might arise in a study into this new domain of bistatic ATR, is the performance deterioration of classifiers with an increase in the bistatic angle. To study the performance change of classifiers with increase in the bistatic angle of imaging, the dataset was divided into three subsets as per three ranges of bistatic angles, as described in the beginning of

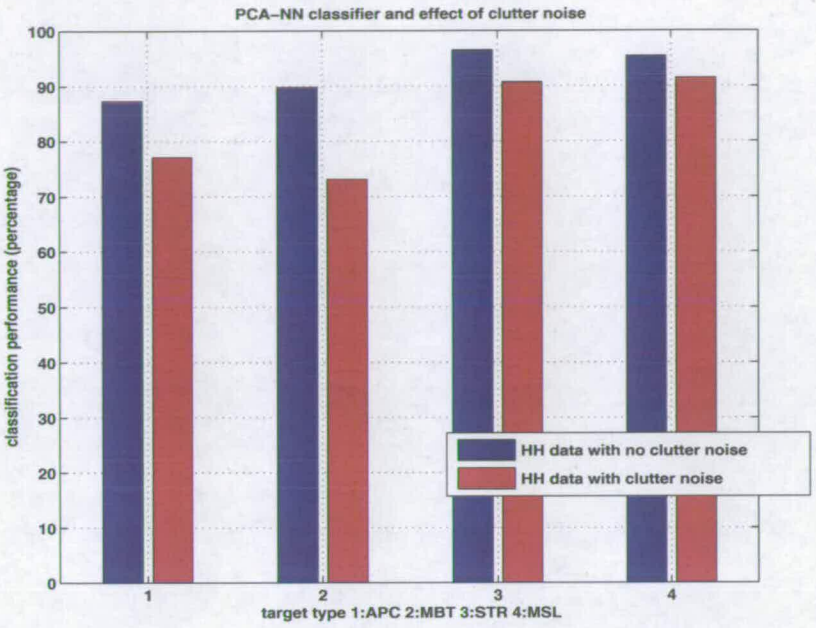

Figure 4.10: *PCANN performance with the addition of clutter*

this section. The performance of the two classifiers are plotted in the bar charts in figure 4.11 and 4.12. As can be observed, the degradation of performance with bistatic angle is less severe for the PCA-NN type classifier when compared to the CGBC type classifier.

However there is invariably a drop in performance of the classifier with increased bistatic angle of imaging, irrespective of the classifier used. This can be traced mainly to the fact that with increased bistatic angle, the frequency or k space support for the image decreases (figure 3.12). This in turn reduces the resolution of the images. Hence, in normal imaging conditions, images from a higher bistatic angle of imaging would be of lower resolution than the same taken with lower bistatic angle.

4.7.4 Classification with normalised k space support

As observed in the last subsection, the ATR performance deteriorates with increasing bistatic angle of imaging. One of the obvious reasons for this is the reduction of k space support of imaging with increase in bistatic angle of imaging, which in turn results in lower resolution images. To make up for this loss of resolution, in the present set of experiments, all the images are formed with same amount of k-space support. To perform this, for the images with lower

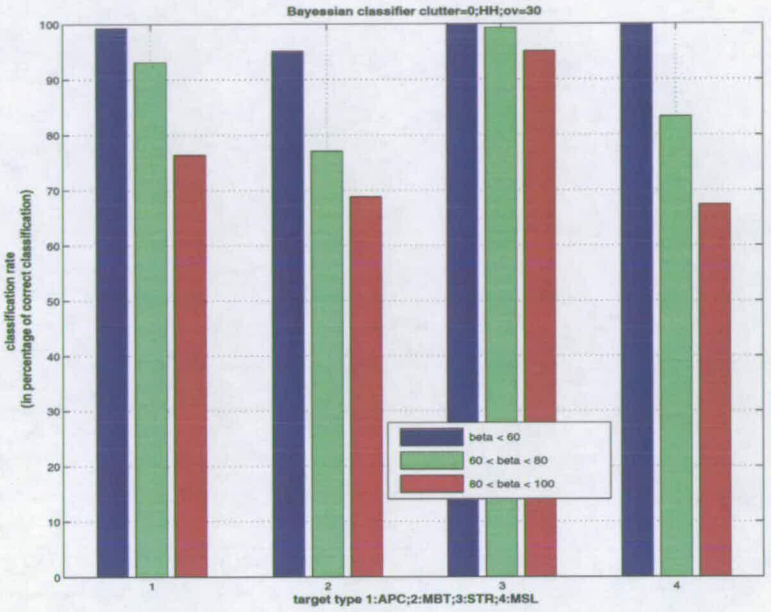

Figure 4.11: *CGBC based ATR performance for different bistatic angles of imaging*

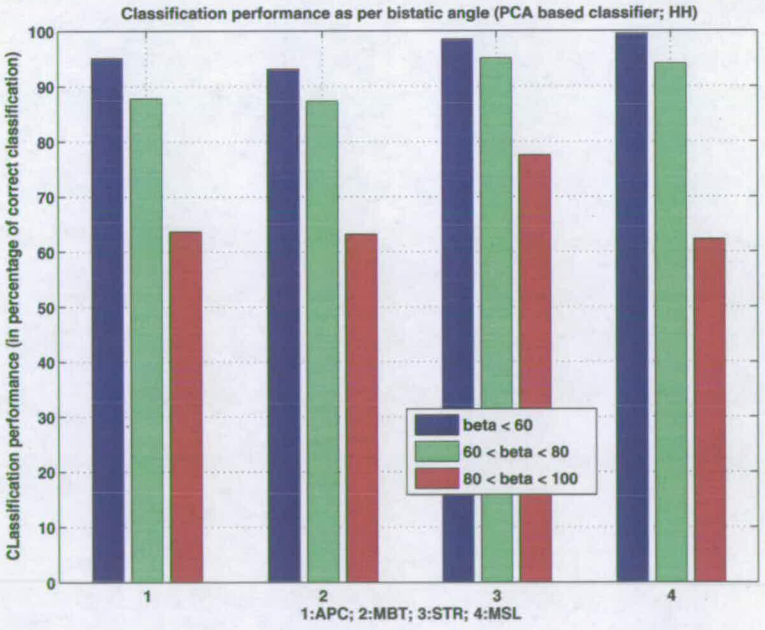

Figure 4.12: *PCANN based ATR performance for different bistatic angles of imaging*

bistatic angle, only a subset of the available the k-space data was taken. This was done so as to use the same amount of k-space for imaging, as is available for the maximum bistatic angle condition of bistatic angle of 100^o. The result was the database of images of almost similar resolution for any bistatic angle. The ATR performance observations are noted in the confusion matrices in table A.11 and A.12 in appendix A. Graphically the results are presented in figure 4.13 and figure 4.14.

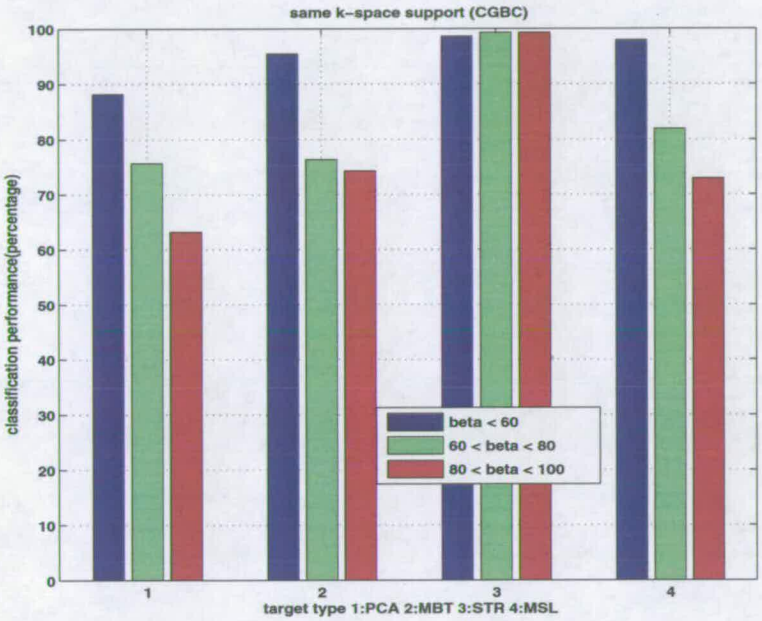

Figure 4.13: *CGBC ATR performance for different bistatic angles of imaging, when the k space support for imaging has been normalised to almost the same area*

In this case also, the PCA-NN algorithm showed less drop in performance when compared to the CGBC type classifier. However the other important point to be observed is that, if the images are formed with almost the same resolution, then classification performance does not deteriorate that much with increase in bistatic angle. Two of the important conclusions from this are:

1. Bistatic ATR performance does not deteriorate due to the lack of information in bistatic data, rather due to the lack of resolution in the bistatic images.
2. If the bistatic system can be designed so as to use higher bandwidth with increasing bistatic angle, the ATR performance would stabilise.

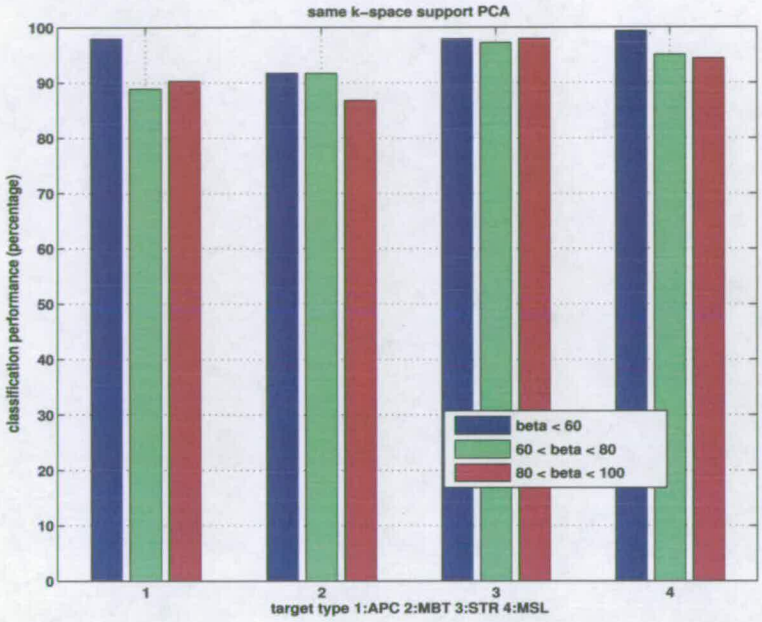

Figure 4.14: *PCANN ATR performance for different bistatic angles of imaging, when the k space support for imaging has been normalised to almost the same area*

4.7.5 ROC curves

As has been discussed previously, in the present work, two different algorithms for finding the receiver operating characteristics (ROC) curves for the ATR process, have been used. This is due to the two different types of algorithms found in the open literature.
The ROC_1 curve for CGBC algorithm, drawn using the first ROC curve algorithm, is displayed in figure 4.15. Figure 4.16 displays the ROC_1 curve for PCANN algorithm, drawn using the first ROC curve algorithm. The ROC_2 curves for both CGBC and PCANN ATR algorithms are plotted in figure 4.17. In it, each subplot is for one type of target and gives both the ROC curves for that target.

One important observation from these curves is that, for the same algorithm, ROC_2 shows better performance than ROC_1. This shows the striking difference between the underlying philosophies of the two ROC curves. A second observation from the ROC_2 curves is the fact that except for the target APC, the PCA-NN algorithm performs as good as or better than the CGBC ATR algorithm (as can clearly be noted from figure 4.17).

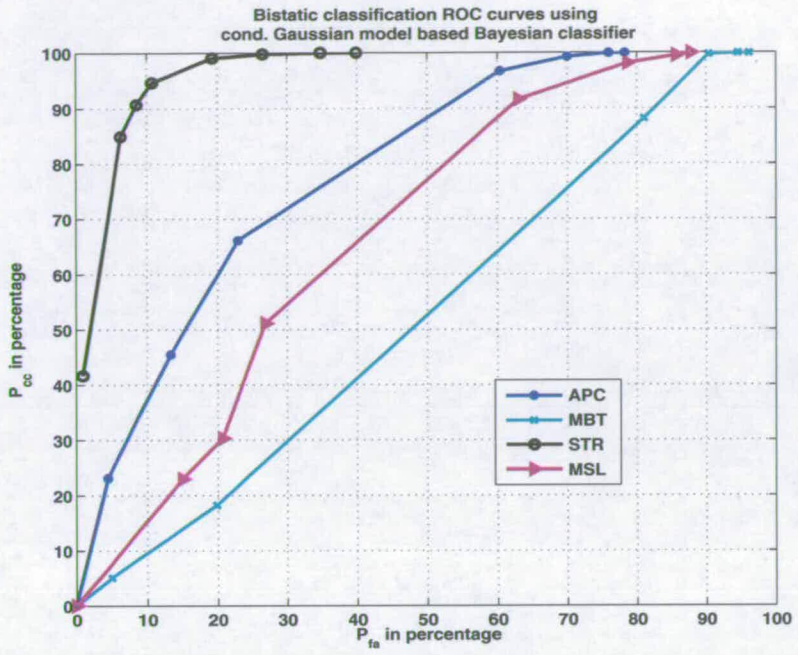

Figure 4.15: *ROC_1 curves for CGBC ATR algorithm*

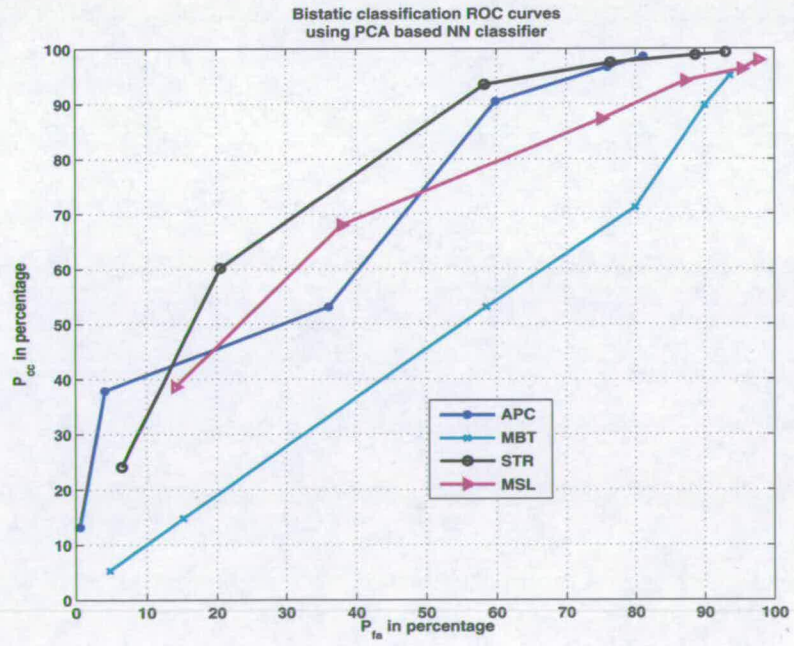

Figure 4.16: *ROC_1 curves for PCANN ATR algorithm*

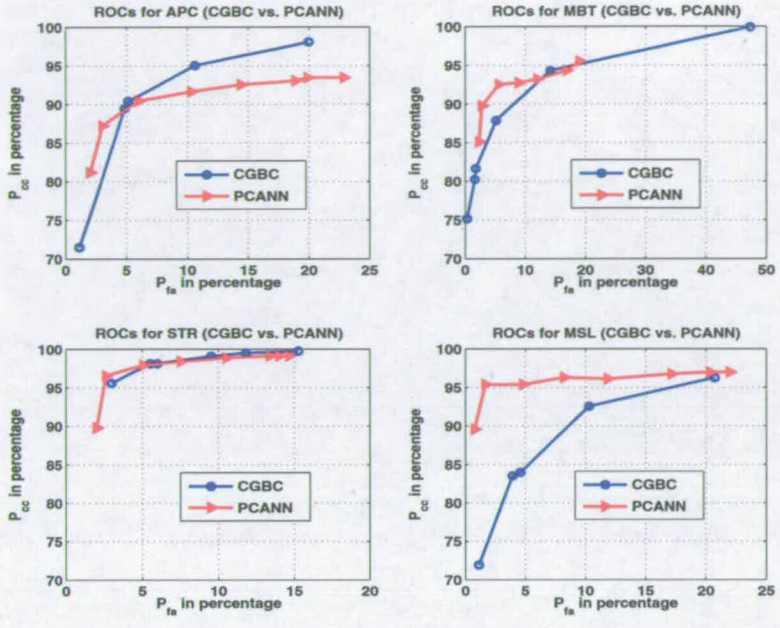

Figure 4.17: *Performance comparison between CGBC and PCANN ATR algorithms, based on ROC_2 curves*

4.7.6 Classification performance with reduced training data

One of the major challenges in bistatic ATR is the huge amount of different views of the target that can be formed. While in the monostatic case, the platform can move through the solid angle of 4π steradians, in the bistatic configuration for each position of transmitter the receiver can trace the solid angle of 4π steradians. Hence, when compared to the monostatic configuration, in the bistatic configuration there are several orders more different ways of imaging the same target. This in turn demands an equally huge amount of training datasets, for a robust classifier. In any practical system, the collection of all possible views of the target (for the training phase), is impossible. Hence, in practice, there is always a demand for a classifier which can perform comparably well with a smaller training database. In this subsection the performance of the two classifiers will be studied with a smaller training dataset. As has been explained in the last chapter, images of a target are collected with varying azimuth of the receiver. Keeping this in view, the reduction of the training dataset was designed in two ways:

1. Taking each alternate image clip from the original training dataset. In this method, the amount of training data is reduced to half. (This variety of experiments were referred to

as data-reduction at level 1)

2. Taking image data, only from a limited amount of receiver azimuth angles (approximately from 0^o till 180^o). This is a more severe limitation on training dataset (hence termed as data-reduction at level 2). To test classifier performance in this experiment, the test datasets were divided into two subsets. The first set consisted of images collected with the receiver azimuth angles, for which a training dataset is available (test set 1). The second test dataset consisted of images collected with the receiver azimuth angles, for which a training dataset is not available (test set 2).

Experiments with dataset reduced at level 1: The training dataset reduced to half and then to one third of the original size (of 432 image clips from each target type). Results for CGBC ATR algorithm are given in table A.13 and A.14 in appendix A, and the same for PCA-NN classifier are given in table A.15 and A.16 in appendix A.

Experiments with dataset reduced at level 2: In experiments for dataset reduction at level 2, the dataset was reduced to half and the effect was noted for both types of classifiers. The confusion matrices of this experiment, are given in table A.17 for CGBC algorithm, and in table A.18 for PCA-NN classifier (as presented in appendix A).

The results have been plotted in bar-chart format in figure 4.18 and figure 4.19.

The main observations are:

- For level 1 type reduction, there is an observed degradation in classification rate for both types of classifiers.
- With the reduction of the dataset to one third, the classification performance further decreases.
- For level 2 type training data reduction, the deterioration of classification performance is more severe.
- The most striking difference between the two classifiers can be observed by noting the confusion matrices, for level 2 type dataset reduction. In the PCA-NN classifier, the deterioration of performance (in level 2 type training dataset reduction) is almost of the same degree both for test set 1 and test set 3. However in the CGBC algorithm, the

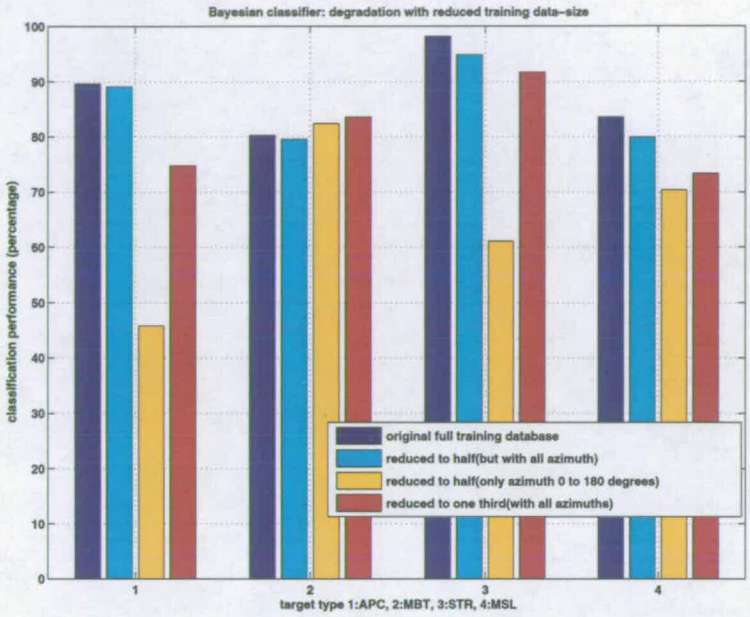

Figure 4.18: *Performance of CGBC ATR algorithm with reduced training dataset (bistatic)*

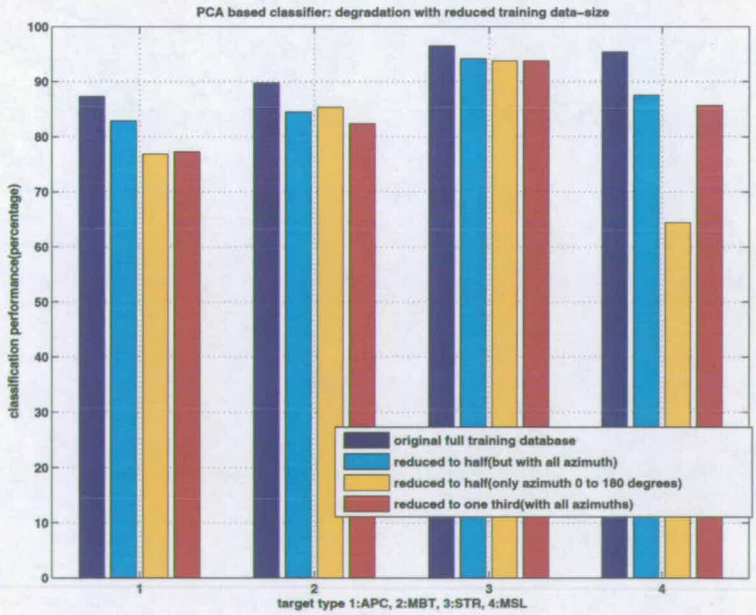

Figure 4.19: *Performance of PCANN ATR algorithm with reduced training dataset (bistatic)*

classification performance for test set 2 (the group of image clips, for which there was no representative training data available), there is almost no classification at all. All the test data were mostly classified as MBT. This can be explained based on the fact that MBT is the biggest target modelled in this project, and hence with maximum RCS energy (and hence have brightest image clips).

These results establish the utility of a PCA-NN classifier as a choice for applications with reduced training dataset. In practical military scenarios, training data is mostly expensive and sometimes impossible to collect in large quantity.

The reason for the drastic difference in performance of the two algorithms can be explained on the basis of the inherent working principle of the two algorithms. CGBC is a statistical Bayesian classifier, and hence will perform the best in the ideal situation of availability of all the possible dataset in the training phase. However PCA based algorithms use the PCs of the dataset, which were shown to give almost the same information as the scattering centres of the radar-image. Scattering centres in turn depend upon the physical features of the target. Being a feature based classifier, a PCA-NN classifier is expected to outperform a Bayesian classifier for a reduced training dataset situation. (This experiment further strengthens the thrust on the relation between PCA-extracted data and scattering centres, for radar data.)

4.7.7 Observations

Both from confusion matrices and from the ROC curves, it is observed that the PCA-NN algorithm outperforms the CGBC algorithm for bistatic ATR. Many of the typical demands in bistatic ATR exercises, are also answered more effectively by the PCA-NN algorithm. This consists of less performance deterioration with clutter addition, and with increasing bistatic angle. The performance of the PCA-NN algorithm was also found to be better than the CGBC algorithm for ATR with reduced training dataset. The unavailability of exhaustive data being a major problem in bistatic ATR, makes PCA-NN a strong candidate for bistatic ATR. Above all, due to operation in the PCA-domain, the whole ATR operation is done in a more highly reduced dimension than the original image-domain. Hence the operation time is several orders less than the conventional CGBC algorithm. Moreover, unlike other feature based ATR algorithms, extracting the features in a PCA-NN algorithm is just mapping the image domain data into the PCA-domain, which is a one-step matrix multiplication. All this makes a strong case for PCA-NN to be the ATR algorithm of choice for any implementable bistatic system.

4.8 Comparison of ATR performance in monostatic and bistatic scenario

One major piece of work in the current project is the comparison of the SAR-ATR performance for a bistatic configuration with that in a monostatic configuration. Even though a field-generated monostatic database is available, the ATR performance using that database could not be compared with the ATR performance on the synthetic bistatic database. Hence, the EM-simulator was used to generate a monostatic database for the same modelled targets and in operating conditions as similar as possible to the bistatic data generation process. The image formation process was also made as similar as possible to the one used in the bistatic case. Given the efficiency of the PCA-NN ATR algorithm, and the speed with which it could produce the results, the comparison of ATR performance was done using this algorithm. For more exhaustive comparison, the receiver operating characteristic (ROC) curves were plotted (following the ROC_2 algorithm) showing the probability of false alarm on the horizontal axis and the probability of correct classification in vertical axis (figure 4.20). For each target type, three ROC curves were plotted for:

1. The performance on monostatic data.
2. The performance on bistatic data, where the bistatic angle of imaging was limited to below 30^o.
3. The performance on bistatic data, where the bistatic angle of imaging was limited to below 60^o.

The ROC curves for all the four targets are shown in figure 4.20.

Some generic comments on the results are:

- In general the ROC curves look near optimal. This is because of the limitations of the ATR exercise. In this set of ATR exercises, the training and the test datasets are collected from the same radar elevation. Hence, the classifiers perform much better than the previous ATR exercises. However, this set of result has to be considered for the comparison between the monostatic and the bistatic ATR, in a qualitative manner. No quantitative comment can be made from this set of observations.

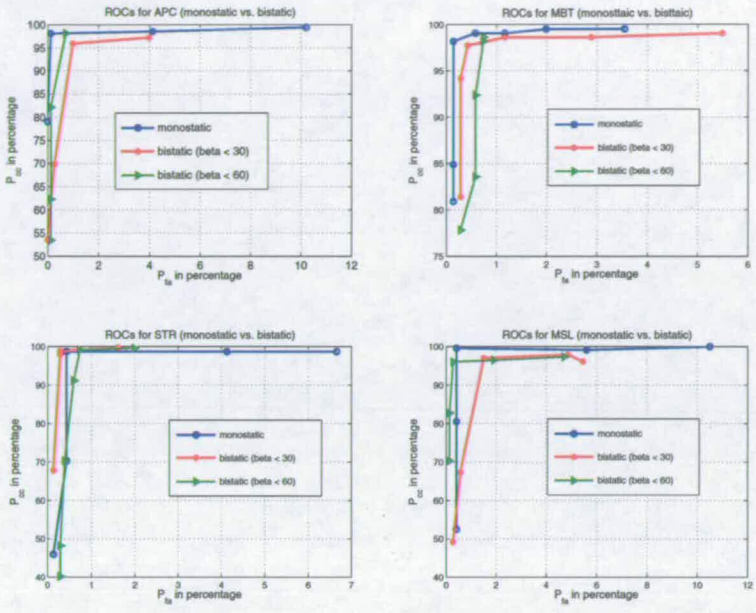

Figure 4.20: *Comparison of ATR algorithm (PCANN) performance on bistatic and monostatic database*

- The scales of the four ROC curves are not the same. This is mainly to magnify the curves. The ROC curves are close to each other, hence unless magnified it would not be possible to observe the differences between the curves.

- The ROC curve for bistatic data as shown in figure 4.20 is different from that in figure 4.17. This is because figure 4.17 gives the ROC_2 curve as extracted from ATR exercises performed on all the bistatic data available. Whereas for the ROC curves in figure 4.20, the dataset is a subset of the original amount of data (to make it similar to the available monostatic dataset).

The monostatic ATR performance is the best, as expected. However, contrary to what might be expected, the bistatic ATR performance is not drastically worse. Another important observation (again contrary to what might have been expected) is that, with increasing bistatic angle the ATR performance does not goes down. Performance seems to be more or less the same for the two types of bistatic data used in these validation experiments. This might be due to the following reason:

In the present work, the target models used are fairly simple and have distinct major physical

features. Hence, the coarse resolution image clips from even 60^o *bistatic angle bistatic configurations, might contain most of the major features needed for classifying that target. This is not a drawback of the simulation activity. Because as discussed before, the ATR performance should not depend on small details of the features of a target.*

4.9 Monostatic ATR

In this section, the results of applying the new PCA-NN algorithm to the problem of monostatic ATR, are discussed. Even though the main theme of the current project is bistatic ATR, the study of the performance of the ATR algorithm developed for monostatic ATR was necessary. The reasons for this can be attributed to the following main factors:

- Bistatic configuration is the superset of monostatic configuration. Hence, it is possible that the algorithms developed for bistatic ATR might use certain characteristic features of the bistatic configuration only, and hence may not perform well for the monostatic case. This would be a limitation of the ATR algorithm. To check for this limitation it is necessary to check the performance of the ATR algorithm on monostatic data.

- Monostatic ATR algorithms have been appearing in the open literature for the past two decades. The moving and static target acquisition and recognition (MSTAR) programme undertaken by the defence advanced research projects agency (DARPA), has collected turntable monostatic SAR image clips for a range of battle field targets. The MSTAR database has been in the public domain for a long time (except for a small break during 2003 and 2004), and hence is the established database for the ATR algorithm development engineers. One of the drawbacks of the present project is the use of synthetic database. Hence, it is necessary to check that the ATR algorithms developed are not database dependent [6]. The MSTAR database is an established and field-collected SAR image database, therefore testing the current ATR algorithms on the MSTAR monostatic database is deemed to give more credibility to the developed ATR algorithms.

- From an application perspective, even though futuristic systems are predicted to have some sort of bistatic capability this is not certain. Purely monostatic systems are never

[6] giving good performance only for certain types of database

going to be fully replaced. Hence the algorithms developed in this project will be such that, they should work equally well (or better) in the monostatic ATR environments.

The database used for the validation of the classifiers proposed, is the SAR images of five battle field targets. The dataset has been collected by the MSTAR programme. The targets used for the present experiments are, 2S1 tank (t000), D-7 land clearing vehicle (t005), T62 tank (t016), ZIL131 APC (t025), and ZSU-23 (t026). Figure 4.21 shows the optical image of the above targets, and figure 4.22 shows the SAR image of the targets at 15^o of radar elevation and 0^o of mean radar azimuth. The target clips collected at an elevation of 17^o were taken to train the classifiers and those taken at the elevation of 15^o were taken as test images. The image clips are of size 96×96 pixels.

Figure 4.21: *Optical images of the targets from MSTAR database, used in the present ATR exercises (not to scale)*

As has been pointed out before, for MSTAR database target images, around 30 principal components give the optimum ATR performance. Hence in all the ATR exercises done on MSTAR database using PCA-NN, 30 PCs have been used. A similar set of experiments were run on the monostatic database, as has been run on the bistatic database. The main aim was to validate if PCA-NN ATR algorithm can still prove to be better than the CGBC ATR algorithm.

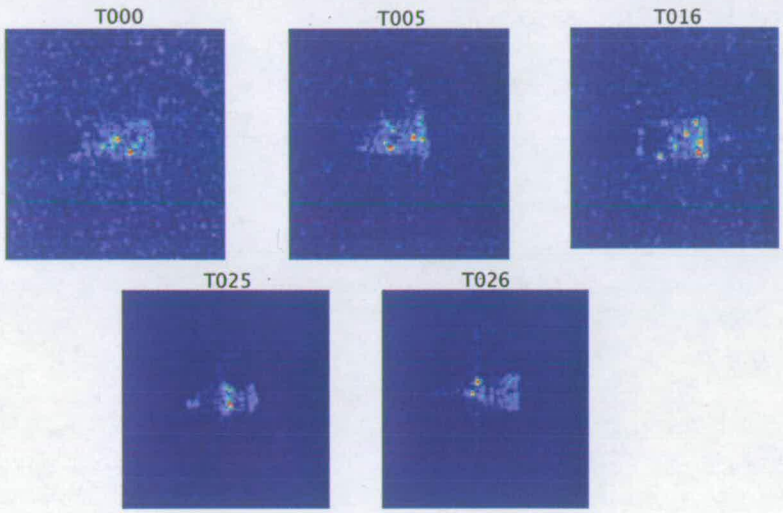

Figure 4.22: *SAR image of the targets from MSTAR database, used in the present ATR exercises, at* 15^o *of radar elevation and* 0^o *of mean radar azimuth (top row from left to right: t000, t005 and t016; bottom row from left to right: t025 and t026)*

4.9.1 Confusion matrices

Tables A.19 and A.20 in appendix A, are the confusion matrices of the ATR performance of the CGBC and the PCA-NN algorithm respectively. For targets t000 and t005, PCA-NN outperforms the CGBC algorithm. For rest of the targets too, the performance is comparable to that of the CGBC algorithm. Another important observation is that the variation of ATR performance from target to target, is greater in the CGBC algorithm. This shows that PCA-NN performance is less affected by the target type.

4.9.2 ROC curves

As the second criteria of comparison, the receiver operating characteristics (ROC) of the two classifiers were compared. The comparison for the two algorithms for the five targets is shown in figure 4.23.

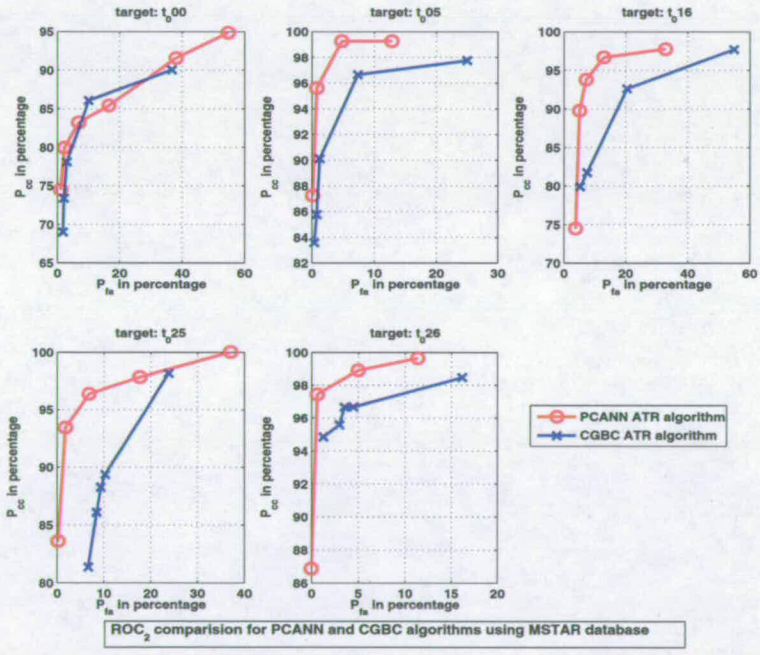

Figure 4.23: *Comparison of CGBC and PCANN algorithms based on ROC_2 curves on MSTAR database*

They show the percentage of correct classification (P_{cc}), versus the percentage of false alarm (P_{fa}) in a binary hypothesis test between the target of interest and all of the remaining targets. The probabilities of false alarm and correct classification have been calculated as has

been explained in the ROC_2 algorithm in previous sections. The performance of the PCA-NN classifier is similar (target t000) or better (targets t005, t016 and t025) than the CGBC classifier.

4.9.3 Performance with reduced training data

As the last criterion of comparison, the performances of the classifiers were studied with reduced amount of training data. As in the case of bistatic ATR, the reduction in training data was done in two different ways. First of all, the training dataset was made sparse by discarding each alternate training clip. In the second method, training data consisted of image clips with imaging platform azimuth from 0 to 180 degrees, while the test set had images from all azimuth angles. To analyse this more difficult test, the test dataset was divided into two subsets, the first set (set1) consisting of images collected with azimuth 0 to 180 degrees and the second (set 2) from azimuth 180 to 360 degrees. The confusion matrices (table A.21 and A.22 in appendix A) give the results for both the test data sets. All the results have been presented in figure 4.24 and 4.25 in bar-chart form.

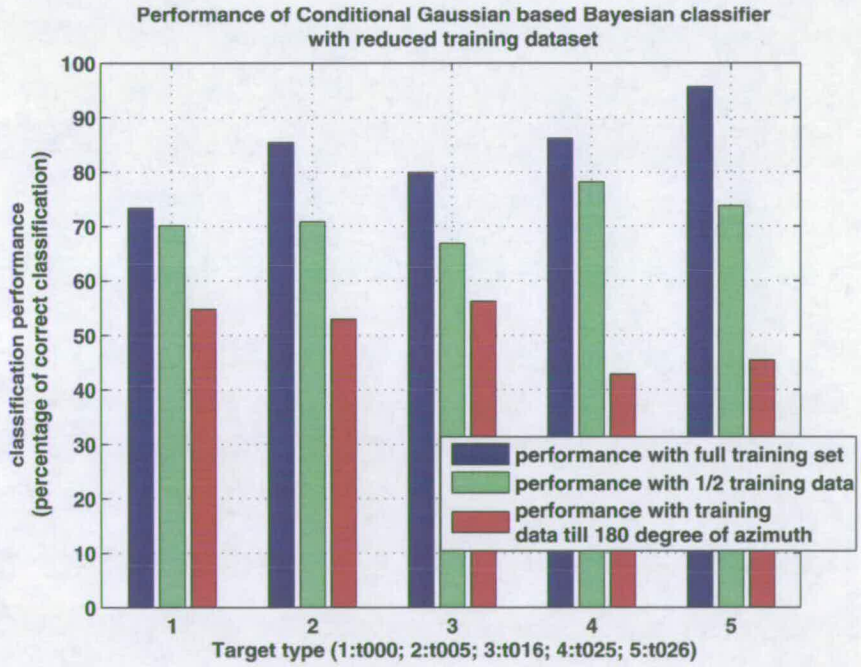

Figure 4.24: *Performance of CGBC ATR algorithm with reduced training dataset (monostatic)*

Looking at the overall performance of the classifiers with training data reduction, the loss of performance was more severe for the CGBC classifier than for the PCA-NN classifier. The con-

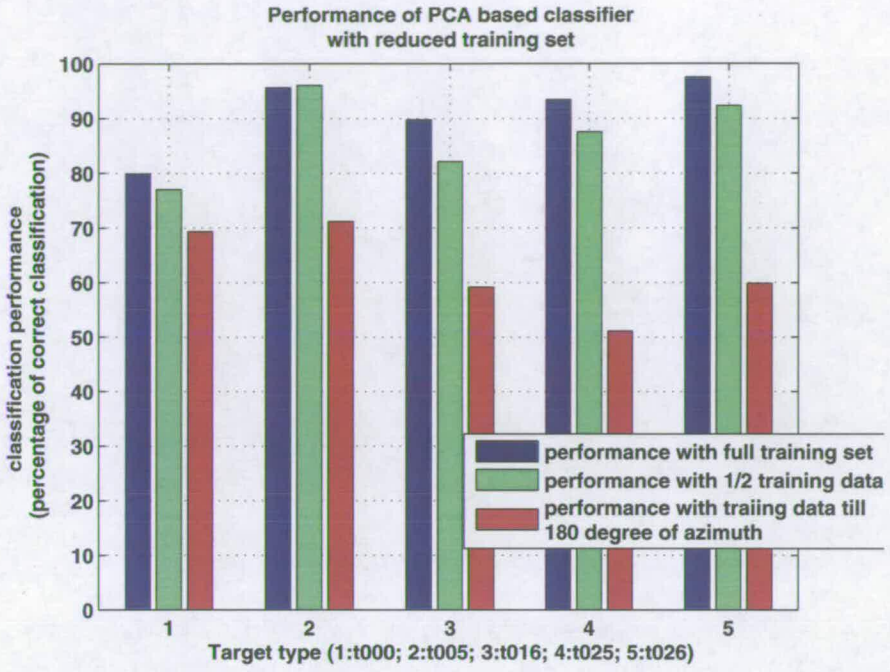

Figure 4.25: *Performance of PCANN ATR algorithm with reduced training dataset (monostatic)*

fusion matrix for the reduced training case show that both CGBC and PCA-NN perform almost similar with the set-2 data (which was not there in the training set), with PCA-NN slightly outperforming CGBC. However, for the bistatic case, PCA-NN had clearly outperformed CGBC in performance with reduced training dataset. This could be attributed to two reasons. Firstly, in the monostatic case, the images of a symmetric target would be almost similar for 0^o to 180^o azimuth case and 180^o to 360^o azimuth case. This is not the case for the bistatic configuration. Hence the ATR algorithm has to be robust enough to perform well in bistatic case. Secondly, in the bistatic case, the images are synthetic and models are simple. Hence, scattering centres are more prominent. This could have led a scattering-centre based algorithm like PCA-NN to outperform a CGBC algorithm.

4.9.4 Observations

PCA-NN performs as well as CGBC in the monostatic case. According to a recent report in the open literature [86], PCA based kNN algorithm has been shown to outperform moment based and support vector machine (SVM) based classifiers for ATR on monostatic radar images. The

major advantage of the PCA-NN algorithm is that, as far as computing time is concerned, it outperforms CGBC algorithm by several orders. Hence, even for a monostatic ATR exercise, PCA-NN is a practical and efficient algorithm.

4.10 Summary

This chapter presented the work done regarding the development of the PCA-NN ATR algorithm and the analysis of the various aspects of bistatic ATR.

Automatic target recognition in general and radar ATR in particular is a highly challenging exercise. Bistatic ATR is still more challenging and demanding due to the large number of transmitter-receiver combinations possible. To have a robust ATR algorithm, a feature based classifier is the best suited. Scattering centres have been shown to be stable and reliable features of radar images. However, extracting scattering centre characteristics from radar images is involved. Principal component analysis of radar images was shown to give informative information about the scattering centres in the image. Because, PCA is a linear and one-step operation, it was used to get the features from the image and the nearest neighbour classifier was used to classify the targets. This PCA-NN algorithm was compared in its performance as an ATR algorithm, with the conventional conditional Gaussian model based Bayesian classifier. PCA-NN proved to be a powerful ATR algorithm in the bistatic domain and also in the monostatic domain. Due to the speed of the PCA-NN algorithm, it is also expected to be extremely useful as a real-time ATR classifier.

Among the studied properties of bistatic ATR, one of the major observations was that the bistatic ATR is not significantly worse than the monostatic ATR. Hence, for any futuristic bistatic system, ATR is a feasible operation to be implemented. Secondly, it was observed that bistatic ATR performance does deteriorate with increasing bistatic angle of operation. This was found mainly due to the deterioration of the resolution of the radar image taken with increasing bistatic angle of operation. Hence, if the bistatic system could be designed to use wider bandwidth of imaging with increase in bistatic angle, it would maintain the frequency (k) space support of imaging stable. This in turn will give similar image resolution irrespective of the bistatic angle. In such a case, the ATR performance deterioration is almost negligible with increase in the bistatic angle of operation. Hence the current work not only proved that ATR is an application integrable in a futuristic bistatic radar system, but also suggested practical ways of improving the bistatic ATR performance with increasing bistatic angle.

The current work is limited from a few dimensions. First of all, for all the bistatic ATR exercises, synthetic data has been used. Hence not much could be concluded about the performance of the algorithms, in a quantitative manner, and most of the conclusions drawn from the present work are of qualitative nature. Secondly, the ATR problem addressed in the current work is of relatively simple nature, in the sense that the training and test environments are well controlled. Even the real MSTAR database has been collected within a strict controlled environments. This is not the case in practical. And, this is a loophole not only in the present work, but also in most of the ATR related reports in the open literature. Hence, this work only gives a qualitative conclusion. However, as has been discussed in the first chapter, a qualitative conclusion was what has been the aim of the present work.

Chapter 5
Use of multipolar data for ATR

5.1 Introduction

As has been discussed in chapter 2, polarisation is one of the important characteristics of an electro-magnetic wave. From the basic theories of wave transmission and dispersion, the scattered wave is not the same wave as the one transmitted. The scattered wave gets a stamp from the scatterer. Characteristics of the scattered wave are modified as per the properties of the scatterer. One of the characteristics to be modified in such manner, is the polarisation (as compared to the frequency of the wave) of the transmitted wave. Each scattering phenomenon is associated with a change in the polarisation of the wave. This **change in polarisation depends on the electro-magnetic properties of the scatterer**. It has also been proved that certain features of the target become more prominent at certain polarisations of the EM wave used [111]. The polarisation-changing property of a scatterer is completely characterised by the scattering matrix for the scatterer, S [1].

Reviewing the fundamentals of the scattering matrix [99,101], let us assume that the transmitted wave is represented in a certain polarisation basis as:

$$[E^t] = \begin{bmatrix} E_1^t \\ E_2^t \end{bmatrix} \tag{5.1}$$

Here E_1^t and E_2^t represent the complex magnitude of the transmitted wave in two mutually orthogonal polarisation bases. Similarly the scattered wave can be represented in the same polarisation bases as:

$$[E^s] = \begin{bmatrix} E_1^s \\ E_2^s \end{bmatrix} \tag{5.2}$$

[1] While collecting data for the simulations done in the present chapter, the planes of polarisation for the transmitter and the receiver, have been kept the same. Most of the theoretical analysis of multipolar data assume such a standard plane of polarisation for both the transmitter and the receiver. In the lack of such an assumption, much of the theoretical results for multipolar radar data would not hold true. This is one of the reasons for which multipolar radars are still at a developmental stage.

The incident and scattered wave are related as follows:

$$[E^s] = \begin{bmatrix} E_1^s \\ E_2^s \end{bmatrix} = \begin{bmatrix} S_{11} & S_{12} \\ S_{21} & S_{22} \end{bmatrix} \begin{bmatrix} E_1^t \\ E_2^t \end{bmatrix} = [S][E^t] \tag{5.3}$$

Here, the matrix S, called the scattering or Sinclair matrix, is the ratio between the scattered and the incident wave, for a pair of polarisation bases. More formally, its elements are defined as:

$$S_{11} = \left.\frac{E_1^t}{E_1^s}\right|_{E_2^t=0} \tag{5.4}$$

$$S_{12} = \left.\frac{E_2^t}{E_1^s}\right|_{E_1^t=0} \tag{5.5}$$

$$S_{21} = \left.\frac{E_1^t}{E_2^s}\right|_{E_2^t=0} \tag{5.6}$$

$$S_{22} = \left.\frac{E_2^t}{E_2^s}\right|_{E_1^t=0} \tag{5.7}$$

Polarimetry [2], since its inception, has remained a field of active research and development. In spite of much work on the theoretical analysis of radar polarimetry, fully polarimetric radars have come to be used in practical systems, only recently. This is mainly due to two bottlenecks regarding polarimetric radar implementation:

- Design of antennas with pure polarimetric characteristics is a major challenge. In simple terms, an antenna of pure polarimetric characteristics means the least amount of energy transmitted in cross polarisation state. For example, if the antenna is supposed to be horizontally or H polarised, then it should emit as little vertical or V polarised wave, as possible.
- Another bottleneck is the correct measurement and calibration of polarimetric antenna and radar-systems [129].

Polarimetric information has been shown to be of importance, in characterising the physical properties and the shape of the scatterers, and fully polarimetric information has been used in extracting information from remote-sensing data [19,75,92,96]. The usage of fully polarimetric data for target recognition has not been covered sufficiently in the open literature. This might be

[2] the Greek meaning of *polarimetry* is *measuring orientation and object shape*!

due to the practical issues of the implementability of a fully polarimetric radar in an air-borne platform. However, according to some of the recent reports, it seems fully polarimetric radars on air-borne platforms are going to be quite common in the coming future [4, 5, 130].
In the present project, the data used for the automatic target recognition (ATR) exercises, have been simulated using an EM simulator. Hence a set of fully polarimetric datasets were simulated, taking horizontal (H) and vertical (V) polarisation as the orthogonal bases. With the desired data (finding which, is another bottleneck for research into ATR using fully polarimetric data [3]) in hand, it was felt pertinent to analyse the different methods of using the extra information, in improving the ATR performance. There are two major studies done in the present area:

1. First of all we looked for existing algorithms in the open literature, to have a better ATR performance using the information from multipolar data. Using various ways of extracting information from the scattering matrix S, a group of new algorithms were developed to fuse this information, so as to have better SAR ATR performance.

2. The second thrust was on the *bistatic* nature of the present dataset. In radar polarimetry the bistatic polarimetric analysis is the superset of the monostatic polarimetry analysis. In a bistatic configuration, the usual transmitter receiver reciprocity of monostatic system, is lost. Hence, the cross polarised terms are no longer equal. $S_{12} \neq S_{21}$. This makes the problem more complicated. Some of the earlier works have even speculated, that the extra data in the bistatic S matrix, has no extra information. This view point is disproved in the present work.

The rest of the chapter is arranged as follows. The next section reviews some of the major reported methods of extracting information from the multipolar data. The section next to it, discusses the algorithms (both previously reported and new) used in the present work, to better the ATR performance, using the multi-polar data. The next section discusses another new algorithm developed in the present work, in which it is shown that using fully polarimetric data to train the ATR algorithm, can make the ATR performance robust to the polarisation of the test data. In the next section, the experiments and observation with bistatic polarimetric ATR exercises, are discussed. The chapter ends with a summary of the works handled and discussion of the major observations.

[3] because a database of fully polarimetric data is quite difficult to find in the public domain

5.2 Information extraction from multipolar data

A complete polarimetric information (in any convenient polarimetric bases), gives a new dimension to the knowledge available about the scattering phenomena. There has been many studies and reports on how intelligible information can be extracted from the polarimetric data, and used in practical applications [131, 132]. In this subsection, a few of the major ways of extracting information from the polarimetric data will be discussed. The discussed methods are in no way exhaustive, as there are an ample number of review papers in this field [99–101]. Instead, only those methods of extracting information from polarimetric data will be discussed, which in turn will be used for the ATR algorithms discussed in the subsequent sections.

5.2.1 Huynen's polarimetric phenomenology and Kennaugh matrix

A powerful representation of the fully polarimetric information, is the Stoke's vector, which has been popular since the times of optical polarimetry. This is given by:

$$g(E_{HV}) = \begin{bmatrix} g_0 \\ g_1 \\ g_2 \\ g_3 \end{bmatrix} = \begin{bmatrix} |E_H|^2 + |E_V|^2 \\ |E_H|^2 - |E_V|^2 \\ 2\Re(E_H^* E_V) \\ 2\Im(E_H^* E_V) \end{bmatrix} \tag{5.8}$$

Here E_{HV} represents the field in terms of linear bases of horizontal and vertical polarisation. $\Re()$ represents the real part of the argument, and $\Im()$ represents the imaginary part of the argument. $()^*$ is the complex conjugate operator. In some applications, this form of representation is more convenient. Because, all its elements are real-valued (as compared to the complex-valued elements of the Sinclair matrix). Secondly, this representation is more helpful for representing partially polarised waves (where $g_0^2 \neq g_1^2 + g_2^2 + g_3^2$).

In the backscattering case, the scattered and the transmitted Stoke's vectors are connected by the Kennaugh matrix K (in forward scattering case, this is called the Muller's matrix M).

$$g(E^s) = [K]g(E^t) \tag{5.9}$$

Elements of the K matrix have been linked to the Huynen's parameters. These are represented by $A_0, B_0, B, C, D, E, F, G, H$ and have been shown to represent specific physical properties

of the scattering object [6].

$$[K] = \begin{bmatrix} A_0 + B_0 & C & H & F \\ C & A_0 + B & E & G \\ H & E & A_0 - B & D \\ F & G & D & B_0 - A_0 \end{bmatrix} \tag{5.10}$$

In similar lines, Germond *et al.* [31] have shown that, for bistatic case, the K matrix could be decomposed as follows:

$$[K_{bi}] = \begin{bmatrix} A_0 + B_0 + A & C + I & H + N & F + L \\ C - I & A_0 + B - A & E + K & G + M \\ H - N & E - K & A_0 - B - A & D + J \\ F - L & G - M & D - J & B_0 - A_0 - A \end{bmatrix} \tag{5.11}$$

In addition to the nine monostatic parameters, the bistatic K_{bi} has seven new parameters, viz. A, I, J, K, L, M, N. The elements of the K matrix were expressed in terms of the elements of the Sinclair matrix. Let the Sinclair matrix be represented in the linear HV basis, as follows:

$$[S] = \begin{bmatrix} S_{HH} & S_{HV} \\ S_{VH} & S_{VV} \end{bmatrix} \tag{5.12}$$

Then the monostatic parameters are expressed as:

$$A_0 = \frac{1}{4}\left(|S_{HH} + S_{VV}|^2\right) \tag{5.13}$$

$$B = \frac{1}{4}\left(|S_{HH} - S_{VV}|^2\right) - \left|\frac{S_{HV} + S_{VH}}{2}\right|^2 \tag{5.14}$$

$$C = \frac{1}{2}\left(|S_{HH}|^2 - |S_{VV}|^2\right) \tag{5.15}$$

$$D = \Im(S_{HH}S_{VV}^*) \tag{5.16}$$

$$E = \Re\left(\left(\frac{S_{HV} + S_{VH}}{2}\right)^* (S_{HH} - S_{VV})\right) \tag{5.17}$$

$$F = \Im\left(\left(\frac{S_{HV} + S_{VH}}{2}\right)^* (S_{HH} - S_{VV})\right) \tag{5.18}$$

$$G = \Im\left(\left(\frac{S_{HV} + S_{VH}}{2}\right)^* (S_{HH} + S_{VV})\right) \tag{5.19}$$

$$H = \Re\left(\left(\frac{S_{HV} + S_{VH}}{2}\right)^* (S_{HH} + S_{VV})\right) \tag{5.20}$$

$$B_0 = \frac{1}{4}\left(|S_{HH} - S_{VV}|^2\right) + \left|\frac{S_{HV} + S_{VH}}{2}\right|^2 \tag{5.21}$$

The bistatic parameters are expressed as:

$$A = \left|\frac{S_{HV} - S_{VH}}{2}\right|^2 \tag{5.22}$$

$$I = \frac{1}{1}\left(|S_{VH}|^2 - |S_{HV}|^2\right) \tag{5.23}$$

$$J = \Im(S_{VH}S_{HV}^*) \tag{5.24}$$

$$K = \Re\left(\left(\frac{S_{HV} - S_{VH}}{2}\right)^* (S_{HH} + S_{VV})\right) \tag{5.25}$$

$$L = \Im\left(\left(\frac{S_{HV} - S_{VH}}{2}\right)^* (S_{HH} + S_{VV})\right) \tag{5.26}$$

$$M = \Im\left(\left(\frac{S_{HV} - S_{VH}}{2}\right)^* (S_{HH} - S_{VV})\right) \tag{5.27}$$

$$N = \Re\left(\left(\frac{S_{HV} - S_{VH}}{2}\right)^* (S_{HH} - S_{VV})\right) \tag{5.28}$$

It can be observed that, the bistatic parameters exploit the difference between the cross polarised elements, viz. S_{HV} and S_{VH}. Hence, these parameters would be zero for monostatic configuration (where $S_{HV} = S_{VH}$).

5.2.2 Pauli's spin-matrix based scattering feature vectors

Scattering feature vector representation of the Sinclair matrix, is a method to represent the information in the 2×2 Sinclair matrix, in a complex vector format, known as the feature vector $\mathbf{f}_4$.

$$\mathbf{f}_4 = F([S]) = \frac{1}{2} Trace([S]\psi) = [\ f_0 \quad f_1 \quad f_2 \quad f_3\ ]^T \tag{5.29}$$

ψ is a set of 2×2 basis matrices, conditioned on the limitations that the vectorisation process should leave the norm of the scattering feature vector invariant. One such powerful basis is the Pauli basis, formed by the Pauli's spin matrices:

$$\psi_P : \left\{ \sqrt{2}\begin{bmatrix} 1 & 0 \\ 0 & 1 \end{bmatrix}, \sqrt{2}\begin{bmatrix} 1 & 0 \\ 0 & -1 \end{bmatrix}, \sqrt{2}\begin{bmatrix} 0 & 1 \\ 1 & 0 \end{bmatrix}, \sqrt{2}\begin{bmatrix} 0 & -i \\ i & 0 \end{bmatrix} \right\} \tag{5.30}$$

The factor $\sqrt{2}$ is added, to maintain the norm invariant. Applying this, the Pauli feature vector is:

$$\mathbf{f}_{4P} = \frac{1}{\sqrt{2}} \left[\ S_{HH} + S_{VV} \quad S_{HH} - S_{VV} \quad S_{HV} - S_{VH} \quad i(S_{VH} - S_{HV})\ \right]^T \tag{5.31}$$

While in the monostatic case, the last element of the Pauli vector vanishes, in the bistatic case, all the elements of the vector remain. It has been shown that the Pauli's spin matrices represent different types of scattering-phenomena involved [133]. Hence, the Pauli's scattering feature vector is expected to contain much information about the scatterers, and hence could be of immense use in ATR exercises.

5.2.3 Polarimetric filters

One of the oldest approach to exploit polarimetric information for a better SAR ATR performance, is to use the polarimetric information, to have a better SAR image. Image using coherent radiation, like laser or radar, have the multiplicative noise, termed as speckle. It has been shown that, by using a particular polarisation state, the energy of a particular type of features in SAR image could be improved, while degrading the energy of other types of features. This basic philosophy was utilised in the polarimetric whitening filter (PWF) [65, 68, 131] to suppress the speckle type features and at the same time to improve features of the target like regions. This helps to improve the image in two ways:

- This reduces the speckle noise level.
- This also makes the target features sharper.

With a better SAR image, the performance of all stages of an ATR algorithm improves.
In the present project, PWF type ATR enhancement could not be implemented because of two major reasons:

- The input to the ATR algorithms in the present project, are the well defined areas of SAR image, with the targets in the centre. Hence the CFAR stage and detection stages of the ATR algorithm are skipped. As per the literature, these pre-classification stages are where the PWF-enhanced images show their major performance.
- Secondly, the data base used for the present project is synthetic, in which the clutter is statistically simulated. It lacks any polarimetric information. Hence it is meaningless to apply polarimetric algorithms to filter such clutter.

5.2.4 Sensor fusion approach

In addition to the above methods of extracting information from the polarimetric data, and using them as features for ATR exercises, the polarimetric data can simply be assumed to be from four different sensors [134]. Some of the simple sensor fusion approaches can then be used to extract as much information as possible from the data, from all the polarimetric channels.

5.3 Algorithms for ATR using multipolar data

The algorithms tested in this work are as follows:

1. Non-coherent addition of pixel amplitudes
2. $Det([S])$ as feature
3. Multi-dimensional PCA
4. Minimum distance algorithm
5. Maximum vote algorithm

6. Decomposition to Pauli's vector elements
7. Odd-even bounces
8. Using the K-matrix elements

These algorithms can be divided into the following three groups:

Image domain algorithms: Algorithms 1 and 2 belong to this category. Here the aim is to use all the four mono-polarised image-data, to form a single image of better quality or with more information. The classical PWF algorithm can also be put in this category.

Sensor fusion-based algorithms: Algorithm 3, 4 and 5 belong to this category. The approach here is that of a sensor fusion one. Data from different single polarisation channels are taken as if from different sensors and hence form different variables. These in turn are used to extract features, which would characterise the targets (algorithm 3, which is a novel output of the current project).

Another approach is to use the monopolar data from each polarisation for classification and use the decisions from each polarisation types. These decisions are in turn fused, to get an overall (better) decision about the class of the test image-clip (algorithms 4 and 5).

Scattering matrix synthesis-based algorithms: Algorithms 6, 7 and 8 belong to this category. Many works have been reported, discussing different ways to decompose the scattering matrix, in order to obtain the information about the scattering phenomena (which include the properties of the scatterers and of the wave-propagation media) [101, 135–137]. Given the SAR images of all the four polarisations, we have the approximate scattering matrix for each pixel. Because, if we neglect higher order effects in the imaging process, and assume a strictly far-field approximation, then as has been described in Chapter 3, the image pixels in a SAR image are directly proportional to the reflectivity of that scattering centre. Hence the elements of the scattering matrix are directly proportional to the image pixel in the SAR image.

The scattering matrices of all the individual pixels can then be decomposed, by any of the methods for scattering matrix decomposition. The resulting features are in turn used as features for ATR. Though methods of decomposition are not novel, this approach of using polarimetric information for better ATR results, has never been published in the open literature. All these algorithms are novel outcomes of this project.

5.3.1 Explaining the algorithms

Throughout the present work, the orthogonal polarisation bases used are, the horizontal (H) and the vertical (V) polarised components. The Sinclair matrix then becomes:

$$\begin{bmatrix} S_{HH} & S_{HV} \\ S_{VH} & S_{VV} \end{bmatrix}$$

The convention adopted here for notation, is to represent the receiver antenna polarisation by the first subscript and the transmitter antenna polarisation by the second subscript. For example, for the scattering coefficient, when the transmitter antenna is horizontally polarised (H) and the receiver antenna is vertically (V) polarised, the scattering matrix element would be represented as S_{VH}. In the rest of this section, the algorithms used in the present project to exploit the multipolar data for better ATR, will be discussed.

5.3.1.1 Non-coherent addition of pixel-amplitudes

In this algorithm, the image amplitudes of all the four polarisation images are added to form the new image. The pixel amplitude of a particular pixel in the new image is calculated as follows.

$$I_{new} = |S_{HH}| + |S_{HV}| + |S_{VH}| + |S_{VV}| \tag{5.32}$$

Once a set of new images has been derived from the four polarised images, they are used for the classification exercise using the PCA-NN ATR algorithm (as discussed in the last chapter).

5.3.1.2 Det([S]) as feature

Determinant of the Sinclair matrix is invariant to the polarisation bases in use. Hence, det([S]) is taken in the present algorithm, as the polarimetric-feature, to classify the target [4].
In the present algorithm, a new image is formed so that the pixels of the new image are derived by taking the determinant of the S matrix of the corresponding pixels.

$$I_{new} = Det[S] \tag{5.33}$$

[4]It should be noted here that, this feature or any such features extracted from the polarimetric data is the extra feature from the polarimetric data. The other set of features, which are the 20 most prominent principal components of the SAR image clip, are also used as before for the ATR task.

5.3.1.3 Multidimensional PCA

To handle different polarisation data, the dimension of data increases by one more degree than that in a monopolar dataset. One way of looking at this increased dimension data is to handle it as if it were obtained from different sensors. PCA is a powerful tool to fuse the data together, so that the resulting data is of lower dimension and has least correlation and hence maximum information. In the present project, the main ATR algorithm is based on PCA. Hence the over all procedure becomes like a multi-dimensional PCA application. Multi-dimensional PCA has mainly been used in data analysis in social science experiments (where data collected are huge and mostly of multiple dimensions). A limited piece of work has also been done in the present project, on the possibilities of 2D PCA in SAR-ATR. In the present case, PCA was used in two phases:

1. Reducing the multi-polar dimension from four to a lower number, preserving as much information as possible.
2. Reducing the number of pixel dimension from the total number of pixels to a much lower value, preserving as much information as possible.

One important observation from the experiments was that, by reducing the four dimensional data set (for the four polarisations) to just two dimensional data using PCA, gives almost similar results as reducing it to three or four dimensions. Hence in the further experiments, the four-polarisation data (HH, HV, VH, and VV) are fused into two dimensions using PCA. As this step in real-time means just one matrix multiplication, hence resources-wise even if multipolar data is used, the hardware requirements for the ATR algorithms are almost the same as monopolar ATR implementation.

5.3.1.4 Minimum distance algorithm

The present and the next algorithms are inspired by a similar work in the open literature [138]. This is a decision level data-fusion algorithm, where the decisions from each data channel are taken into account for a better final decision. For the present case, the PCA-NN algorithm was applied as before, to each individual single polarised training dataset, to get the training feature vectors. Given the test image clip in all the four polarisations, the four image clips are tested using the training feature vectors from the corresponding polarisations. In a NN classifier, the

output from each single polarisation classifier, is the Euclidean distance of the test clip to the nearest neighbour in that polarisation. Out of these four Euclidean distances (from the four different tests performed on the four different polarisations), the shortest one is chosen, and the class corresponding to that is declared as the target class of the test clip. The algorithm is expounded in the flow chart of figure 5.1.

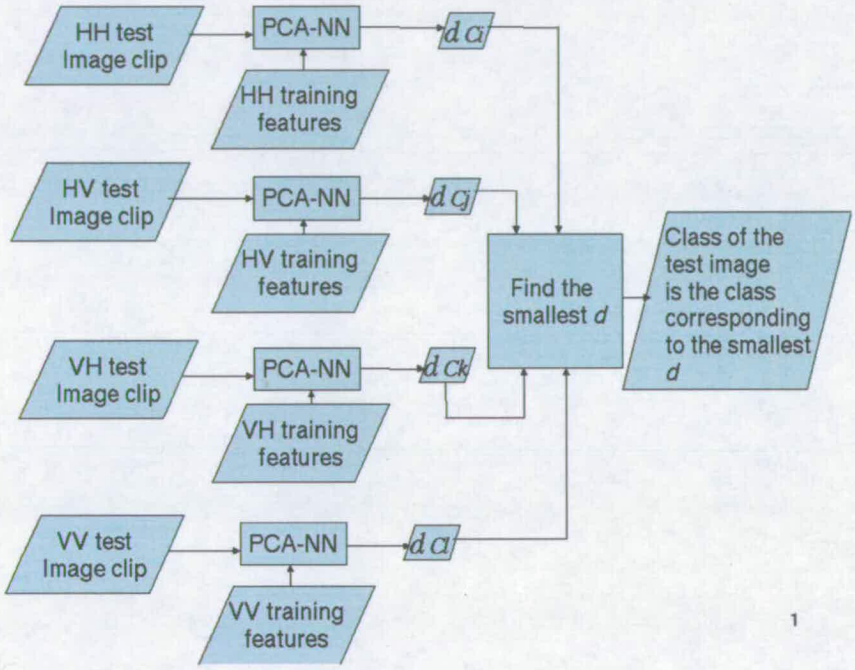

Figure 5.1: *Flowchart for the minimum distance algorithm for multipolar ATR*

5.3.1.5 Maximum vote algorithm

In this algorithm, the classification is done separately for separate polarised data. The class types decided by the four polarised channels, are fed to the final decision algorithm. The declared class is the one favoured by the maximum number of polarisation channels. One draw back of this maximum-vote algorithm is the case when a tie occurs, or when the same number of votes are obtained for two or more targets. In that case, the Euclidean distances are taken from the monopolar channels, and the decision is done as in the previous *minimum distance algorithm*. From the implementation point of view, the above two algorithms are most computationally intensive and do not give as good results as many of the other algorithms tested in the present work. However, as this depends on the individual monopolar data, it is more implementable if less than all four polarisation channel data are available.

5.3.1.6 Decomposition to Pauli's vector-elements

As has been discussed in the last section, the elements of Pauli's feature vector give insight into the physical features of the scattering centre. In the present algorithm, the four elements of Pauli's feature vector, are taken as the features.

The first step was to map each pixel into a four dimensional set of Pauli's feature vector, which is calculated as below:

$$\frac{1}{\sqrt{2}}\left[\begin{array}{cccc} S_{HH}+S_{VV} & S_{VV}-S_{HH} & S_{VH}+S_{HV} & j(S_{HV}-S_{VH}) \end{array}\right] \tag{5.34}$$

This in turn is used in a multi-dimensional PCA-NN ATR algorithm.

5.3.1.7 Odd-even bounce

Another set of useful features extracted from the S-matrix is the percentage of energy in that scatterer-response, from an odd or even number of bounces [65, 137]. Basically this is due to the fact that the receiver and transmitter antenna should be of exactly same polarisation to get the maximum return from an odd number of bounces. This set of features has been used in the ATR process, by Novak *et al.*, and has been studied as a potential candidate for ATR, in another work by Bennett *et al.* [139]. In the present algorithm, these two pieces of information (the percentage of energy in that scatterer-response, from an odd and from an even number of bounces) are taken as the features. The first step is to map each pixel into a two dimensional feature space of pixel energy from odd and even bounces. This in turn is used in a multi-dimensional PCA-NN ATR algorithm.

5.3.1.8 Using K-matrix elements as features

To look for the information content in the parameters derived from the K-matrix, those parameters are extracted for each pixel of the SAR image. These derived parameters are in turn used as features of the target for the ATR exercise. The algorithm used for ATR is that of the multi-dimensional PCA. The initial SAR image can be assumed as a two dimensional matrix. After generating the K-matrix parameters from each pixel from the four polarised images, it results in a set of n two-dimensional matrices (where n is the number of K-matrix elements used in the ATR exercise). The final dataset can now be treated as a three dimensional matrix, and by using PCA, its dimensions are reduced to generate only the uncorrelated data. That in

turn is used in the ATR exercise, using the nearest neighbour recognition algorithm.

5.3.2 Results and discussions

In this subsection, the results from the multipolar SAR ATR algorithms [5] are presented. Figure 5.2 shows the performance for the PCA-NN ATR algorithm applied on the four types of single polarised data (viz. HH, HV, VH, and VV), as compared to using all the different polarised data. In using multi-polar data, the multi-dimensional PCA based approach has been used. The results are displayed in the form of a bar-chart, where each group of bars represent the ATR performance for one target type. It can be observed that:

- The polarisation of the data, which gives the best performance (among the single polarised dataset results) is not the same for different targets. This implies that, there is no particular choice of polarisation of the radar system antennas, using which a uniformly good performance could be achieved across the target types.
- In general the performance of the multi-polar data based ATR is better than single polarised data based ATR, for all the targets.

With this initial positive observation that handling ATR in the multipolar domain does increase the performance of the ATR system, the performance of the various multi-polar ATR algorithms will be discussed next. In addition to comparing the results as the percentage of correct classification, the present comparison will also involve comparison of the error bars. While comparing the result from two or more different ATR algorithms, it is crucial to note how these performances would vary for a different set of training and test databases. For this purpose, the ATR exercise was run using the different algorithms for 100 times, choosing a random set of images as the test and the training datasets, for each run. From these simulations, the statistics of the ATR performances was found for each type of ATR algorithm. Due to the lack of exhaustive amount of datasets, simulation-runs and the synthetic nature of the database, the performance was assumed to follow a Gaussian distribution. If P_{cci} represents the probability of correct classification (in percentage) for one class of target for the i^{th} iteration, then the mean value of

[5] except for the K-matrix element based algorithm, which will be discussed in a different section, because of its significance for bistatic polarimetry!

the probability of correct classification P_{ccm} for that class is given by:

$$P_{ccm} = \frac{1}{N}\sum_{i=1}^{N} P_{cci}. \tag{5.35}$$

N is the total number of iterations run. The standard deviation of the probability of correct classification P_{ccsd} is given by:

$$P_{ccsd} = \sqrt{\frac{1}{N}\sum_{i=1}^{N}(P_{cci} - P_{ccm})^2} \tag{5.36}$$

In comparing the results, the mean value of performance was plotted along with an error bar of width, which is thrice the standard deviation.
Figure 5.3 shows the mean value of the performances along with the error bars. There are quite a few major observations from this set of results:

- The performance of the ATR algorithms using HV dataset and VH dataset, are not the same. This is in line with the classical fact that cross polar components in a bistatic system are different (and carry different information).
- Almost all the multi-polar ATR algorithms perform better than the single-polarisation ATR performance.
- Multipolar ATR algorithms based on Pauli's feature vector and multidimensional PCA, outperform all other multipolar algorithms and have almost similar performance.
- These two algorithms also have the minimum error bar.
- These two algorithms differ only in the implementation phase, where the PCA-based approach reduces the fully polarimetric data dimension from four to two, while the Pauli's feature vector based algorithm converts the four dimensional polarimetric data into a four dimensional Pauli's feature vector. Hence, even though they have the same performance, due to implementation ease, the PCA-based algorithm would be the algorithm of choice.
- Error bars for the single polarised ATR algorithms are mostly greater than that for the multipolar ATR algorithms.

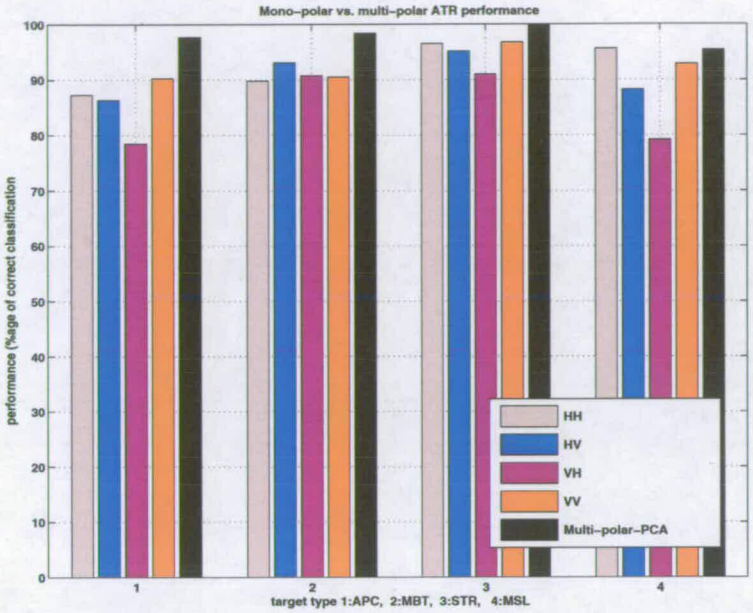

Figure 5.2: *Comparison of ATR performance using single polarised data versus the performance using all the four types of polarised data*

5.4 Train all test any (TATA) algorithm

This is another novel way of handling multi-polar data for the purpose of ATR. The guiding principles behind this algorithm are:

- Fully polarimetric data represents the complete information about a scatterer.
- Information-content of a monopolar image is the subset of the information in the multipolar image.

The major problems targeted by this algorithm, are three fold:

1. A major concern behind the reluctance in accepting fully polarimetric systems is the cost involved in replacing all the existing systems with fully polarimetric systems. Even by crude calculations, a fully polarimetric system would be at least twice as costly as its monopolar counterpart. Hence it can be concluded that it will take a while before fully polarimetric systems find their place in all running systems. So is there any way

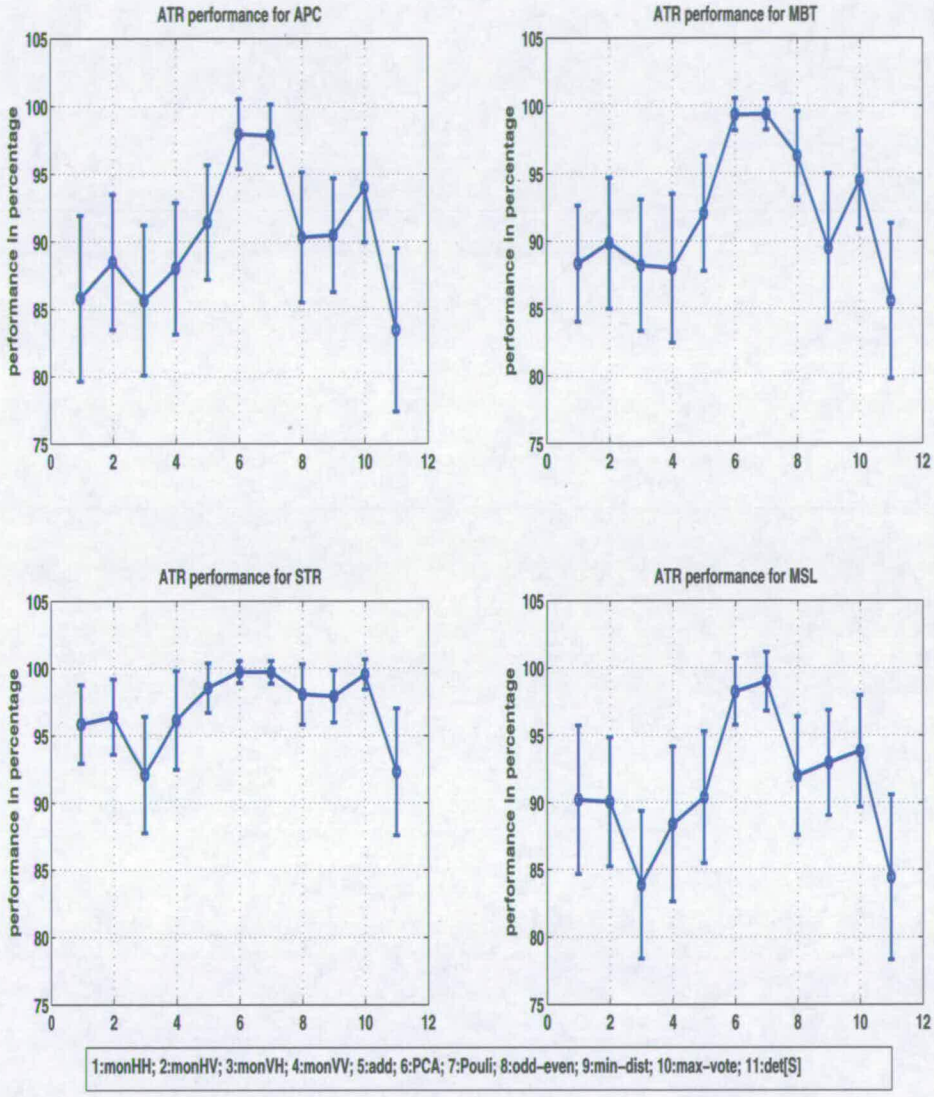

Figure 5.3: *Performance of different multipolar ATR algorithms, along with the error bar of each algorithm*

to obtain even some limited advantages of a fully polarimetric system, by some partial implementation?

2. A second concern is the stability of a monopolar antenna in a running system. For example, the ATR algorithm might have been trained for a HH polarised database. Hence, the running system has to be HH polarised, to give the best performance. If the transmitter or receiver antenna polarisation gets changed, then as would be discussed in this subsection, the ATR performance drops drastically. Can this limitation of a monopolar system be overcome by some partial implementation of multi-polar data?

3. Thirdly, there has been extensive work done on the advantages of using the optimal polarisation in radars [76, 77], which uses a particular antenna polarimetry to reduce the speckle in the scene. This combination may change from flight to flight, and even from scene to scene. Hence, unless the ATR system has been trained with that particular combination of polarisation, including the advantages of the optimal-polarisation antenna to the ATR facility, is impossible. Is there any scope of getting optimum polarimetry and good ATR performance in the same system?

The answer to all the above concerns was found to be quite simple, which is to use fully polarimetric data to train the ATR system, and to use any polarimetric data in the test phase.
The multipolar ATR algorithm to be followed, has to be such that it does not depend on the extra information extracted from the elements of the Sinclair matrix. Because, in that case monopolar test image information can not be used effectively. However, the *non-coherent addition of the pixel amplitudes* algorithm and the *multi-dimensional PCA* algorithm, do not depend on any particular information from the Sinclair matrix, unlike the *Pauli's feature vector* based algorithm. The steps taken in this algorithm, are as follows:

- The training phase is carried out with all the four polarised databases. For the *non-coherent addition of the pixel amplitudes* algorithm, the first step is a pixel by pixel addition to get the new data, on which PCA was applied. For the *multidimensional PCA* based approach, the four dimensional data (HH,HV,VH and VV) is reduced to two dimensions.

- In the test phase, the test image clips of only a single polarisation, are processed. To match the test phase with the training phase, the single polarised image clip is copied into four image matrices. This four dimensional data is then handled like a multipolarised

dataset. For the *non-coherent addition of the pixel amplitudes* algorithm, it is a pixel by pixel addition to get the new data, on which PCA is applied. For the *multidimensional PCA* based approach, the four dimensional data (same polarised data copied four times) is reduced to two dimensions.

- The rest of the steps are the same, as those for the multidimensional case.

The first set of experiments performed was to observe the performance of single polarised training database ATR algorithms (PCA-NN was the ATR algorithm used), and of the TATA algorithm, when the polarisation of the test data varies. Figure 5.4 shows the results for the four targets. In each subplot, the indices in the x-axis represents the polarisation of the test data. Major observations, from this set of results, are:

- For single polarised dataset, the performance is the best when the test dataset is of the same polarisation as the training dataset.
- For any difference in polarisation, such algorithms mostly perform poorly.
- For the *non-coherent addition of the pixel amplitudes* based TATA algorithm, the performance is less than the best performance obtainable, if a single polarised case is used, with the test and the training datasets of the same polarisation. However, with a change in the polarisation of the test-data, the performance remains extremely stable.
- The *multidimensional PCA* based TATA algorithm performs only slightly worse than the best performance obtainable using the single polarised cases (when the test and training database are of the same polarisation). In addition to this, the performance is almost independent of the polarisation of the test-data.

To further study the sensitivity of the ATR performance, to the polarisation of the training and the test datasets, another set of simulation-experiments was designed. In practice, the radar systems used are mostly co-polarised, and in linear bases the polarisations would be HH or VV. When the antenna are co-located, which is the classical monostatic configuration, there is very little chance of polarisation mismatch, between the transmitter and the receiver antenna. However, for the bistatic case, the transmitter and the receiver antenna are on different platforms. One fact mostly not given enough thrust while dealing with bistatic systems, is the fact that along with time synchronisation, the antenna should also be polarisation synchronised,

in a bistatic configuration. Unsynchronised polarisation on the two antenna might not affect the immediate system performance, but will affect severely the performance of the system in ATR exercises. As was discussed in last section, ATR performance is the best, only when the training and the test data polarisation are the same. Let us assume a bistatic ATR system, which has been trained with HH polarised data. It would perform the best for HH polarisation, and hence the test system has been set to HH polarisation. However, there is every possibility that due to certain shocks or aerial-manoeuvres, the receiver antenna polarisation plane will get mis-aligned to the transmitter antenna polarisation plane. Let us further assume that the receiver antenna is shifted by an amount $\delta\theta$ with respect to the supposed H axis. The received signal by this antenna can be represented in terms of the orthogonal bases as:

$$E_{new} = E_H \cos(\delta\theta) + E_V \sin(\delta\theta) \tag{5.37}$$

Using this equation, the new image formed using this offset receiver antenna will be:

$$I_{HH\delta\theta} = S_{HH} \cos(\delta\theta) + S_{VH} \sin(\delta\theta) \tag{5.38}$$

ATR was performed on this new data using single polarised training data (using HH polarised data) and using TATA based algorithms. This was repeated for increasing values of the offset angle $\delta\theta$. The result is shown in figure 5.5. Similar experiments were performed with a VV polarised system, in which case, the image for offset receiver antenna will be given by:

$$I_{VV\delta\theta} = S_{VV} \cos(\delta\theta) + S_{HV} \sin(\delta\theta) \tag{5.39}$$

The results for VV polarised system are shown in figure 5.6. Certain observations, from the set of results, are as follows:

- With increase in the offset angle, the performance of the single polarisation trained ATR algorithm, decreases monotonously.
- TATA based algorithms also suffer a performance loss in certain cases with increase in the offset angle.
- However the loss of performance for the single polarisation trained ATR algorithm, is steeper.
- In some cases, with increasing offset angle, the performance of the TATA based algorithm

increases. This is because, with offset receiver antenna, the antenna collects information from both co and cross polarisation.

- For an offset angle of around 10^o, the single-polarised ATR algorithm performs better than the TATA based PCA-NN algorithm. However, after that, the TATA based PCA-NN algorithm outperforms.

Hence the new algorithm was shown to be quite efficient in handling any polarised database. This will be of a huge benefit, where the ATR system polarisation is not known in advance. Such a case might arise if the optimum polarisation theories are implemented. Secondly, implementing TATA based algorithm may allow for less strict calibration of the bistatic system antenna, as compared to the methods recommended by certain studies in the open literature [140]. Thirdly, it was shown that for an optimum ATR performance in a bistatic system, synchronisation of transmitter and receiver antenna polarisations is a must. This strict and unrealistic condition can easily be overcome, by using a TATA based algorithm.

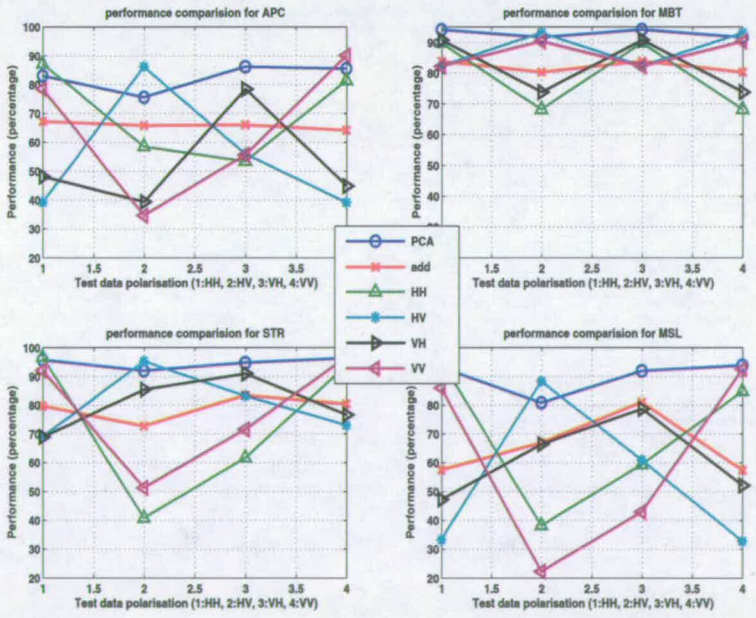

Figure 5.4: *TATA algorithm as applied on HH, HV, VH and VV testdata*

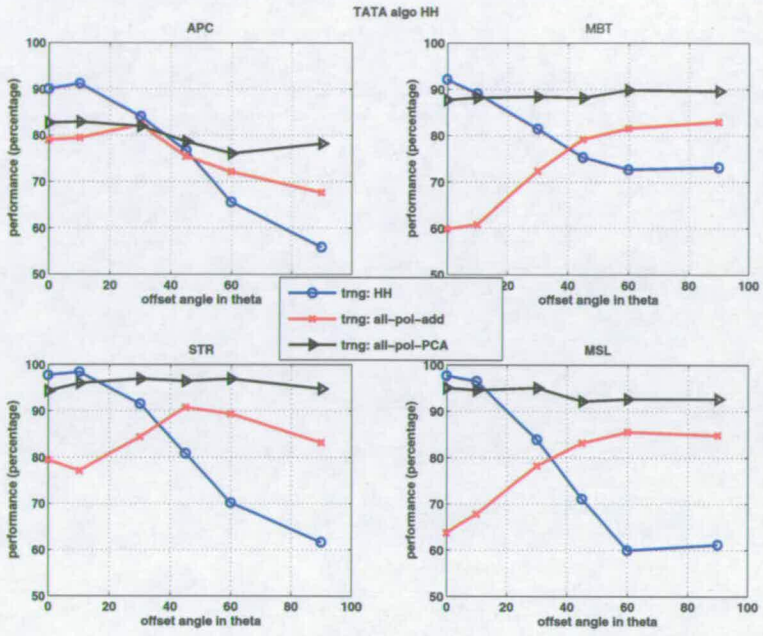

Figure 5.5: *Performance of an ATR algorithm trained with HH data, when the antenna polarisation changes*

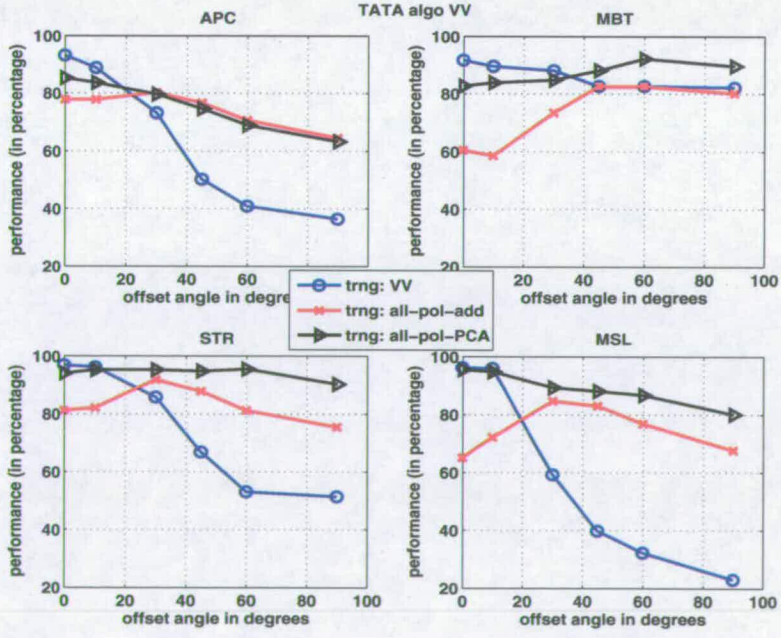

Figure 5.6: *Performance of an ATR algorithm trained with VV data, when the antenna polarisation changes*

5.5 Bistatic and monostatic polarimetric features

Fully polarimetric radar systems have been a subject of intense study and research for a long time. It has been conclusively shown that fully polarimetric data in monostatic configuration gives a lot of information about the physical features of the target. Specially remarkable is the work by Huynen [6], who gave a one-to-one correspondence between physical features of a target and parameters derived from the fully polarimetric data from a monostatic radar. However, due to the large number of scene-combinations (of transmitter and receiver) involved in the bistatic case, Huynen has expressed strict reservations against any information contained in the extra parameters derivable from a bistatic configuration. In the present project, a limited study was undertaken to predict any possible information from the fully polarimetric data in a bistatic configuration.

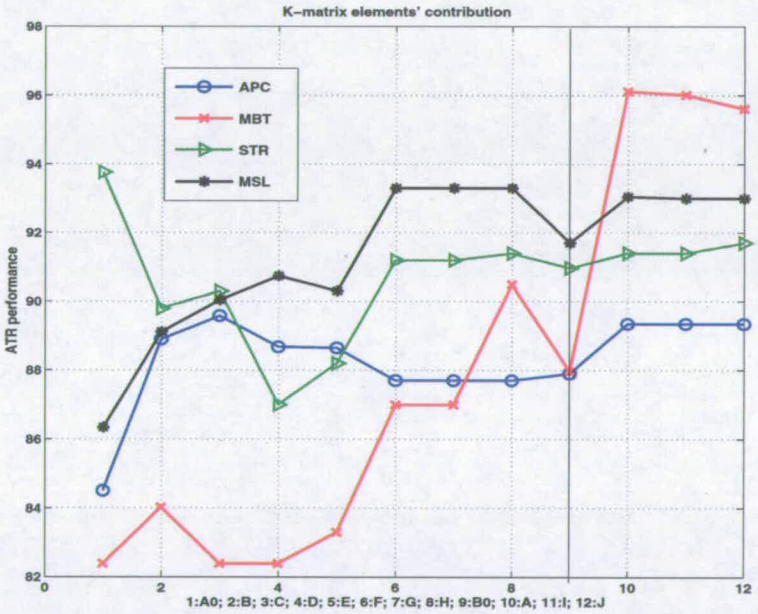

Figure 5.7: *ATR performance by taking increased number of K matrix elements*

Huynen extracted nine parameters from the K-matrix for the monostatic case, and showed their direct relation to physical features of the target. For the monostatic case, the K-matrix is symmetric, whereas for the bistatic case, it is not. Hence in a similar manner, seven more parameters were extracted from the bistatic K-matrix, by Germond *et al.* [31]. However, Huynen has stated that any such bistatic parameters would contain no information about the target. To look at the

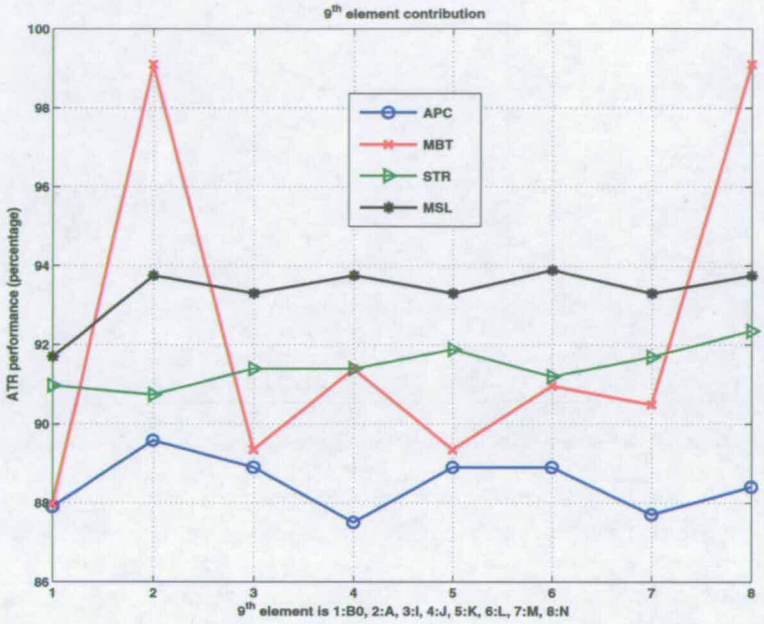

Figure 5.8: *The ninth element effect on ATR performance*

information content in the extra parameters derived from the K-matrix, those parameters were extracted for each pixel of the bistatic SAR images. These derived parameters were in turn used as features of the target, for ATR. In this piece of analysis, it was assumed that if a certain derived parameter has any physical significance, then adding that parameter as a feature should increase the ATR performance. The algorithm used for ATR is that of multi-dimensional PCA based nearest neighbour classifier. The initial SAR image can be assumed as a two dimensional matrix. After generating the parameters from each pixel from the four polarised images, it results in a set of two-dimensional matrices. The total data now, can be treated as a three dimensional matrix, and using PCA, its dimension is reduced to generate only the uncorrelated data. That in turn, was used in the ATR exercise, using nearest neighbour recognition algorithm.

Figure 5.7 shows the ATR performance for the four targets, as the number of parameters from K-matrix, were increased one by one. The first nine parameters are monostatic. The bistatic parameters are from the tenth onwards. It can be observed that:

- With an increase in the number of parameters, the ATR performance increases.
- With the addition of bistatic parameters, the ATR performance does not increase, except

for one target (MBT).

The reason, why the increase is observed only for the MBT, can be explained on basis of the complexity of the models. The MBT is the most complicated model among all the four targets modelled in this work, with the maximum amount of physical features. The other three targets are not that complicated, and hence the nine monostatic parameters are enough to represent their physical features. Whereas, for the MBT, there are features to be accounted for, by the bistatic polarimetric data.

Hence the bistatic parameters were shown to contain information.

The next experiment was done to find which bistatic parameters in particular, contain the information. For this, the ATR exercise was run with nine of the parameters from the K-matrix. Out of these, eight were kept fixed. For the ninth parameter, all the bistatic parameters were used one after the other. The results are shown in figure 5.8. As before, the performance increases only for the target MBT. The interesting observation from this experiment is that, only two out of all the bistatic parameters tested are responsible for the increase in the ATR-performance. The last experiment showed that taking more elements from the K matrix increases the ATR performance. It can be argued that taking more elements is just like adding more information. However, the present experiment showed that by simply increasing the number of K matrix elements taken, does not increase the ATR performance. Rather, the ATR performance increases only by taking certain Kmatrix elements. Hence it can be concluded that those particular elements represent certain classifiable features of the target, and hence could indeed represent certain physical features of the target. Contrary to the held belief that bistatic polarimetric data is devoid of any interpretable information, this experiment concludes that bistatic polarimetric data do represents specific information about the target, which can be used to classify the targets better.

5.6 Summary

In the present chapter the work done in this project towards exploiting multipolar data for better ATR performance, was discussed. The experiments and results are limited, in the sense that the database used was a synthetic one. However, the qualitative aspects of the results still hold and are quite significant. It was demonstrated that multipolar data do give a significant improvement in the ATR performance and reduce the error bounds of the performance, thus

making the whole system more stable and robust. Another important contribution was the development of the *train all test any* algorithm, which can be a practical answer to many issues related to the polarisation of the bistatic systems. Lastly, it was also shown that contrary to views held, the bistatic fully polarimetric data do have information about the targets and could be used effectively for a better ATR performance. Two fronts of future work from this point, are as follows:

1. All the algorithms discussed in this chapter can be tested on the field collected monostatic database available recently in the public domain.
2. Work in line with Huynen's work could be carried out to analyse the exact correlation between the bistatic fully polarimetric data and the physical features that they may be carrying the information of.

Chapter 6
Conclusions

In the introduction chapter of the thesis, the pertinence of the present work has been presented. With that, a few of the questions were discussed, which the present work has tried to answer. In the present chapter, those questions will be reviewed with the observations from the previous chapters, and the major achievements and observations will be reiterated.

Section 6.1 will review the aims of the project as discussed in the introductory chapter of the thesis. The major achievements of the project will be discussed in the section, stressing the achievement of the goals as set in the beginning. In section 6.2, limitations of the project are discussed, and it is explained how the major observations still hold in spite of the stated limitations. Section 6.3 discusses the possible future directions of the current research.

6.1 Aims and achievements of the project

One of the major interests behind the present project was to examine the possibility of bistatic ATR. It was observed that, within the limitation of simulated database-based studies, bistatic ATR performance is quite encouraging. Upon being compared to the ATR performance in the monostatic domain, the bistatic ATR performance was found to be worse. To face the strict demands of a bistatic ATR system, the principal component analysis (PCA) based nearest neighbour (NN) algorithm was used as the ATR algorithm. The PCA-NN algorithm was shown to be fast, due to the handling of the ATR exercise in the reduced PC-space. It was also shown to give almost similar performance with different targets. Degradation of ATR performance with the addition of clutter and with the reduction in training dataset, was found to be less severe using the PCA-NN algorithm than using the standard conditional Gaussian model based Bayesian classifier (CGBC). Hence, in response to the first major interest, a couple of encouraging observations, along with an efficient ATR algorithm, were contributed by the present project.

One of the most popular ways of relating monostatic and bistatic configuration is the fact that monostatic configuration is the special case of bistatic configuration with the bistatic angle equal to zero degrees. From both the understanding and implementation points of view, bistatic

angle is an important parameter of the bistatic configuration. Hence the next interest was to find out the dependence of bistatic ATR performance on the *bistatic angle* parameter. It was observed that ATR performance does degrade with an increase in the bistatic angle of imaging. However, the degradation in the case of using the PCA-NN algorithm, was found to be less severe than the degradation as observed while using the conventional CGBC ATR algorithm.

The next interest was to look for ways to improve the bistatic SAR ATR performance. One of the reasons for deteriorating bistatic SAR ATR performance, with increasing bistatic angle of imaging, is the loss of image resolution with an increasing bistatic angle of imaging. This is because the frequency (k) space support of imaging decreases by a factor of $\cos(\beta)$, which in turn reduces the resolution of the image. Observations from the experiment of using the same k space support of imaging, irrespective of the bistatic angle, suggested that the loss of ATR performance with increasing bistatic angle of imaging, can be attributed mostly to the reduction of the k space support. Hence, to make up for the loss of ATR performance, which is due to the loss of image resolution, an increasing bandwidth of operation can be chosen with an increasing bistatic angle of imaging. With a bandwidth compensation, the bistatic ATR system performance would be comparable to the monostatic ATR system. However, the loss of resolution increases with a factor of $\cos(\beta)$. For extreme bistatic angle conditions (as β approaches 180^o), an infinite increase in bandwidth of imaging is needed to compensate for the loss of resolution. Hence, depending on the system capabilities and the future research achievements in the field of bistatic imaging, the bistatic angle of operation has to be kept below a certain angle, for acceptable ATR performance.

Given the current slow revival of interest in fully polarimetric radar systems, it was also of particular interest to look into possible improvements in ATR performance, by using multipolar data instead of single polarisation radar data. Even though polarimetric studies of electromagnetic scattering, have been done for the past few decades, a thorough study of algorithms to exploit fully polarimetric data for better ATR performance, has not been found in the open literature. Due to a simulated database, the present project was successful in generating fully polarimetric database for the bistatic configuration. A range of algorithms were tested in the present project, to improve the ATR performance by using multipolar, instead of single-polarisation radar images. Such an approach, involving a thorough test of so many algorithms, is a unique work. The results were encouraging. First of all, multi-polar data was shown to significantly improve the ATR performance. It was also shown that by using PCA-based fusion of multipolar data, the ATR performance not only improves, but also stabilises (by having a very small error

bar). The novel approach of using multipolar data in the training phase of ATR and any single polarised data in the test phase, was also proposed. Such an approach was shown to be robust to transmitter-receiver antenna misalignment. Finally, contrary to popular reservations, it was shown that extracting information from bistatic fully polarimetric data is possible and analysis of fully polarimetric radar data in a bistatic configuration can give information about the target features.

The conclusions and insights gained from the present work make the case stronger for the development of bistatic and multistatic radar systems. Within a limited study, it was found that an important usage like ATR is definitely implementable in a bistatic radar system, with certain modifications in the system. Hence, the future radar system, if bistatic, need not shed any current applications to gain into other strategic applications. The current study also made a case for further detailed study into possibilities using multipolar radar systems and implementation of them.

In addition to the above achievements, one of the major achievements of the current project is the generation of the SAR image database of military ground targets. There is no current literature in the open databases, which explains the procedure towards generating a database of SAR images of man-made targets, using a generic EM-simulation tool. There have been reports stressing the need for simulated database for getting insight into SAR imaging and to help in improving performance of radar ATR algorithms [3]. Commercial electromagnetic computational tools like $XPatch$ and $Epsilon$ do claim to be capable of simulating SAR images of life-size targets. However, these softwares are restricted in their marketing, and hence not available for the wider research community. In the current project, a generic EM modelling software has been used. Using the physical optics (PO) approximations with multiple-bounces, the SAR images of the CAD models of the targets, were simulated. A theoretically sound and computationally simple procedure was also introduced to simulate the ground clutter and shadow regions in the SAR images of the targets. The overall procedure is computationally fast, generic enough to be adaptable to any EM-simulation tool, and is supposed to help any future researcher working in fields related to radar signal modelling and classification.

6.2 Limitations of the present project

One of the limitations of the present work is the dependence on a synthetic database. Even though the simulated database has performed encouragingly in all the tests it has been put

through, there is always a chance that it might give rise to some subtle flaw in the final conclusions. However, as all the conclusions made in the present work, have been kept at a qualitative level, the overall observations are expected to be immune to the synthetic nature of the database. The work on using fully polarimetric radar data for improved ATR, has used only the synthetic database for bistatic configuration. However, all the algorithms used in that piece of work are generic and could be applied on monostatic data as well. Hence another limitation of the present work is that, even though the applied algorithms are generic, the results could only be claimed to be true, strictly for the bistatic case. The next section discusses the proposed future research which could establish the results for both bistatic and monostatic cases.

6.3 Future extension of the work

There are quite a few proposed directions for further research.

The PCA-NN ATR algorithm could be fine-tuned further. One obvious path would be to implement the PCA-NN algorithm in an FPGA, and to note the issues in implementation and final performance. Secondly, kernel principal component analysis could be tested for its performance as an ATR tool. Even though it will both be memory intensive and more time taking than the PCA-NN algorithm, the performance might be higher.

Among other possible ATR approaches, one novel approach which can be tried, is the projective geometry based feature extraction. Projective geometry [141] based features are more robust to target pose and the angle of imaging [142], and hence may prove as the right answer in the search of ATR algorithms, which can be trained with minimum data.

The observations from the work concerning the use of fully polarimetric radar data for ATR, are based on simulated bistatic data. Recently, a database of fully polarimetric monostatic SAR image clips has been made public [143]. Hence similar algorithms can be applied on the real data, to establish the observations more firmly.

Appendix A
Confusion Matrices for the Experiments from Chapter 4

	Low bistatic angle				Medium bistatic angle				Low bistatic angle				
Train (Rx at 10^o) Test (Rx at 15^o)	A	M	S	M	A	M	S	M	A	M	S	M	Overall performance (in %age)
APC	143	1	0	0	134	6	1	3	110	6	17	11	89.6
MBT	6	137	0	1	13	111	0	20	24	99	5	16	80.3
STR	0	0	114	0	1	0	143	0	2	4	137	1	98.2
MSL	0	0	0	144	1	3	20	120	16	2	29	97	83.6

Table A.1: *Confusion matrix for CGBC algorithm on synthetic bistatic data (no clutter; HH polarisation)*

	Low bistatic angle				Medium bistatic angle				Low bistatic angle				
Train (Rx at 10^o) Test (Rx at 15^o)	A	M	S	M	A	M	S	M	A	M	S	M	Overall performance (in %age)
APC	143	1	0	0	138	4	1	1	110	15	16	3	90.5
MBT	1	143	0	0	6	122	1	15	8	118	9	9	88.7
STR	0	1	143	0	0	2	142	0	2	3	138	1	97.9
MSL	0	0	0	144	1	3	12	128	13	2	29	100	86.1

Table A.2: *Confusion matrix for CGBC algorithm on synthetic bistatic data (no clutter; VV polarisation)*

	Low bistatic angle				Medium bistatic angle				Low bistatic angle				
Train (Rx at 10^o) Test (Rx at 15^o)	A	M	S	M	A	M	S	M	A	M	S	M	Overall performance (in %age)
APC	140	2	0	2	138	5	0	1	112	11	4	17	90.3
MBT	0	144	0	0	1	142	1	0	17	104	11	12	90.3
STR	0	4	140	0	1	4	137	2	2	9	125	8	93.1
MSL	6	0	1	137	20	1	5	118	32	10	4	98	81.7

Table A.3: *Confusion matrix for CGBC algorithm on synthetic bistatic data (no clutter; VH polarisation)*

	Low bistatic angle				Medium bistatic angle				Low bistatic angle				
Train (Rx at 10^o) Test (Rx at 15^o)	A	M	S	M	A	M	S	M	A	M	S	M	Overall performance (in %age)
APC	129	0	2	13	130	1	0	13	118	4	1	21	87.3
MBT	2	126	0	16	2	133	2	7	21	98	7	18	82.6
STR	12	0	131	1	7	1	135	1	7	1	128	8	91.2
MSL	4	4	0	136	18	1	11	114	31	7	5	101	81.3

Table A.4: *Confusion matrix for CGBC algorithm on synthetic bistatic data (no clutter; HV polarisation)*

	Low bistatic angle				Medium bistatic angle				Low bistatic angle				
Train (Rx at 10^o) Test (Rx at 15^o)	A	M	S	M	A	M	S	M	A	M	S	M	Overall performance (in %age)
APC	140	3	0	1	128	10	3	3	109	13	12	10	87.3
MBT	4	139	0	1	10	130	3	1	10	119	11	4	89.8
STR	0	0	144	0	2	1	141	0	5	4	132	3	96.5
MSL	0	0	0	144	3	1	0	140	6	5	5	128	95.4

Table A.5: *Confusion matrix for PCA-NN algorithm on synthetic bistatic data (no clutter; HH polarisation)*

	Low bistatic angle				Medium bistatic angle				Low bistatic angle				
Train (Rx at 10^o) Test (Rx at 15^o)	A	M	S	M	A	M	S	M	A	M	S	M	Overall performance (in %age)
APC	143	1	0	0	135	3	1	5	112	17	7	8	90.3
MBT	6	138	0	0	7	138	0	1	12	117	9	6	90.5
STR	1	0	143	0	3	1	140	0	4	4	135	1	96.8
MSL	0	1	0	143	2	4	1	137	5	11	8	120	92.6

Table A.6: *Confusion matrix for PCA-NN algorithm on synthetic bistatic data (no clutter; VV polarisation)*

	Low bistatic angle				Medium bistatic angle				Low bistatic angle				
Train (Rx at 10^o) Test (Rx at 15^o)	A	M	S	M	A	M	S	M	A	M	S	M	Overall performance (in %age)
APC	140	1	3	0	127	4	3	10	106	8	12	18	86.3
MBT	0	144	0	0	2	139	2	1	6	119	10	9	93.1
STR	4	1	139	0	4	4	134	2	3	1	138	2	95.1
MSL	0	0	0	144	7	2	0	135	19	14	9	102	88.2

Table A.7: *Confusion matrix for PCA-NN algorithm on synthetic bistatic data (no clutter; HV polarisation)*

	Low bistatic angle				Medium bistatic angle				Low bistatic angle				
Train (Rx at 10^o) Test (Rx at 15^o)	A	M	S	M	A	M	S	M	A	M	S	M	Overall performance (in %age)
APC	136	1	1	6	111	8	7	18	92	18	14	20	78.5
MBT	0	144	0	0	9	128	7	0	2	120	11	11	90.7
STR	3	0	140	1	3	6	131	4	8	11	122	3	91.1
MSL	5	1	0	138	13	3	4	122	31	21	12	80	78.7

Table A.8: *Confusion matrix for PCA-NN algorithm on synthetic bistatic data (no clutter; VH polarisation)*

	Low bistatic angle				Medium bistatic angle				Low bistatic angle				
Train (Rx at 10^o) Test (Rx at 15^o)	A	M	S	M	A	M	S	M	A	M	S	M	Overall performance (in %age)
APC	91	18	0	35	52	23	1	68	45	39	7	53	43.5
MBT	31	104	1	8	24	74	5	41	19	86	2	37	61.1
STR	2	1	130	11	8	2	99	35	10	6	81	47	71.8
MSL	6	11	0	127	12	19	1	112	10	20	0	115	81.9

Table A.9: *Confusion matrix for CGBC algorithm on synthetic bistatic data (with clutter; HH polarisation)*

	Low bistatic angle				Medium bistatic angle				Low bistatic angle				
Train (Rx at 10^o) Test (Rx at 15^o)	A	M	S	M	A	M	S	M	A	M	S	M	Overall performance (in %age)
APC	122	16	3	3	112	24	5	3	99	15	18	11	77.1
MBT	28	112	4	0	25	107	9	3	20	97	12	15	73.1
STR	1	4	139	0	4	6	132	2	10	4	121	9	90.7
MSL	3	2	0	139	1	0	7	136	7	5	12	120	91.4

Table A.10: *Confusion matrix for PCA-NN algorithm on synthetic bistatic data (with clutter; HH polarisation)*

	Low bistatic angle				Medium bistatic angle				Low bistatic angle				
Train (Rx at 10^o) Test (Rx at 15^o)	A	M	S	M	A	M	S	M	A	M	S	M	Overall performance (in %age)
APC	127	5	1	11	109	3	2	30	91	4	29	20	75.7
MBT	4	139	0	1	10	110	1	23	15	107	13	9	82.4
STR	0	2	142	0	1	0	143	0	1	0	143	0	99.1
MSL	0	3	0	141	3	2	21	118	1	3	35	105	84.3

Table A.11: *Confusion matrix for CGBC algorithm on synthetic bistatic data (no clutter; HH polarisation; same k space imaging)*

	Low bistatic angle				Medium bistatic angle				Low bistatic angle				
Train (Rx at 10^o) Test (Rx at 15^o)	A	M	S	M	A	M	S	M	A	M	S	M	Overall performance (in %age)
APC	141	3	0	0	128	8	1	7	130	6	4	4	92.4
MBT	10	132	1	1	4	132	6	2	7	125	6	6	90.1
STR	0	0	141	3	2	5	0	137	3	3	2	136	96.3
MSL													

Table A.12: *Confusion matrix for PCA-NN algorithm on synthetic bistatic data (no clutter; HH polarisation; same k space imaging)*

	Low bistatic angle				Medium bistatic angle				Low bistatic angle				
Train (Rx at 10^o) Test (Rx at 15^o)	A	M	S	M	A	M	S	M	A	M	S	M	Overall performance (in %age)
APC	140	4	0	0	136	0	3	6	109	10	16	9	89.1
MBT	4	138	0	2	9	110	0	25	23	96	4	21	79.6
STR	2	2	140	0	2	0	140	2	7	4	130	3	94.9
MSL	3	3	4	134	1	4	22	117	22	0	28	94	79.9

Table A.13: *Confusion matrix for CGBC algorithm on synthetic bistatic data (no clutter; HH polarisation; training dataset reduced to half)*

	Low bistatic angle				Medium bistatic angle				Low bistatic angle				
Train (Rx at 10^o) Test (Rx at 15^o)	A	M	S	M	A	M	S	M	A	M	S	M	Overall performance (in %age)
APC	123	20	0	1	119	8	4	13	81	17	16	29	74.8
MBT	2	141	0	1	9	116	0	19	10	104	3	27	83.6
STR	0	3	141	0	2	1	136	5	18	1	119	6	91.7
MSL	9	16	5	124	9	16	12	107	9	16	23	96	73.4

Table A.14: *Confusion matrix for CGBC algorithm on synthetic bistatic data (no clutter; HH polarisation; training dataset reduced to one-third)*

	Low bistatic angle				Medium bistatic angle				Low bistatic angle				
Train (Rx at 10^o) Test (Rx at 15^o)	A	M	S	M	A	M	S	M	A	M	S	M	Overall performance (in %age)
APC	137	7	0	0	123	20	0	1	98	31	0	15	82.9
MBT	7	135	0	2	11	124	5	4	10	106	17	11	84.5
STR	0	0	141	3	4	1	133	6	5	5	133	1	94.2
MSL	6	1	3	134	5	6	2	129	9	10	10	115	87.5

Table A.15: *Confusion matrix for PCA-NN algorithm on synthetic bistatic data (no clutter; HH polarisation; training dataset reduced to half)*

	Low bistatic angle				Medium bistatic angle				High bistatic angle				
Train (Rx at 10^o) Test (Rx at 15^o)	A	M	S	M	A	M	S	M	A	M	S	M	Overall performance (in %age)
APC	127	17	0	0	109	35	0	0	98	46	0	0	77.3
MBT	19	122	2	1	16	118	6	4	13	116	8	7	82.4
STR	0	3	143	0	1	2	140	1	10	8	122	4	93.8
MSL	10	4	1	129	7	4	3	128	12	13	10	109	84.7

Table A.16: *Confusion matrix for PCA-NN algorithm on synthetic bistatic data (no clutter; HH polarisation; training dataset reduced to one-third)*

	Low bistatic angle				Medium bistatic angle				Low bistatic angle				
Train (Rx at 10^o) Test (Rx at 15^o)	A	M	S	M	A	M	S	M	A	M	S	M	Over-all per-form-nce(in %age)
APC test set1	72	0	0	0	65	3	1	3	45	4	12	11	45.8
APC test set2	14	41	0	17	0	53	0	19	2	70	0	0	
MBT test set1	5	67	0	0	6	59	0	7	11	49	4	8	82.4
MBT test set2	4	62	0	6	5	52	0	15	4	67	0	1	
STR test set1	0	0	72	0	1	0	71	0	1	4	66	1	61.1
STR test set2	7	6	37	22	13	30	13	16	8	50	5	9	
MSL test set1	0	0	0	72	1	1	11	59	2	1	14	55	70.4
MSL test set2	2	16	0	54	2	24	0	46	5	48	1	18	

Table A.17: *Confusion matrix for CGBC algorithm on synthetic bistatic data (no clutter; HH polarisation; training dataset reduced to half (azimuth angle till* 180^o*))*

	Low bistatic angle				Medium bistatic angle				Low bistatic angle				
Train (Rx at 10^o) Test (Rx at 15^o)	A	M	S	M	A	M	S	M	A	M	S	M	Over-all per-form-nce(in %age)
APC test set1	62	10	0	0	54	15	0	3	32	23	0	17	76.9
APC test set2	66	2	0	4	63	5	0	4	55	13	0	4	
MBT test set1	2	69	0	1	11	55	4	2	11	51	3	7	85.4
MBT test set2	4	68	0	0	1	66	0	0	5	60	2	5	
STR test set1	1	0	70	1	5	0	67	0	4	7	60	1	93.8
STR test set2	0	0	72	0	2	0	70	0	70	0	66	2	
MSL test set1	8	2	13	48	8	3	22	39	8	7	18	39	64.4
MSL test set2	11	8	4	49	11	0	13	48	4	3	10	55	

Table A.18: *Confusion matrix for PCA-NN algorithm on synthetic bistatic data (no clutter; HH polarisation; training dataset reduced to half (azimuth angle till* 180^o*))*

Train (17^o) Test (15^o)	t000	t006	t016	t025	t026	Performance (in percentage)
t000	222	0	13	38	1	81.02
t005	2	263	1	5	3	95.99
t016	14	3	241	12	3	88.28
t025	4	1	4	263	2	95.99
t026	0	4	1	1	268	97.81

Table A.19: *Confusion matrix for CGBC algorithm on MSTAR monostatic data (window width = 10^o)*

Train (17^o) Test (15^o)	t000	t006	t016	t025	t026	Performance 1 (in percentage)
t000	231	0	21	19	3	84.31
t005	1	266	2	2	3	97.08
t016	8	7	237	12	9	86.81
t025	14	1	2	252	5	91.97
t026	2	5	7	4	256	93.43

Table A.20: *Confusion matrix for PCA-NN algorithm on MSTAR monostatic data (PC=30)*

Train (17^o) Test (15^o)	t000	t006	t016	t025	t026	Performance (in %age)	Overall performance (in %age)
t000 set 1	112	0	22	3	0	81.7	54.74
set 2	38	1	48	49	1	27.7	
t005 set 1	1	105	1	30	0	76.6	52.92
set 2	5	40	26	33	33	29.2	
t016 set 1	17	7	97	11	5	70.8	56.20
set 2	52	5	57	21	1	41.1	
t025 set 1	3	22	17	91	4	66.4	42.86
set 2	62	1	45	26	2	19.1	
t026 set 1	1	6	9	20	101	73.7	45.62
set 2	28	24	52	8	24	17.5	

Table A.21: *Confusion matrix for CGBC algorithm on MSTAR monostatic data(training dataset for azimuth angles 0^o to 180^o)*

Train (17^o) Test (15^o)	t000	t006	t016	t025	t026	Performance (in %age)	Overall performance (in %age)
t000 set 1	119	0	14	4	0	86.8	69.34
set 2	71	0	62	2	1	51.8	
t005 set 1	0	127	0	3	7	92.7	71.12
set 2	9	68	6	37	17	49.6	
t016 set 1	4	2	126	5	0	91.9	59.12
set 2	70	9	36	21	0	26.2	
t025 set 1	2	2	6	125	2	91.2	51.09
set 2	62	29	30	15	1	10.9	
t026 set 1	0	2	0	2	133	97.0	59.85
set 2	18	27	30	31	31	22.6	

Table A.22: *Confusion matrix for PCA-NN algorithm on MSTAR monostatic data(training dataset for azimuth angles* 0^o *to* 180^o*)*

Appendix B
Original Publications

- A.K. Mishra and B. Mulgrew, " Bistatic SAR ATR", to be submitted towards *IEE Proceedings on Radar, Sonar and Navigation.*
- A.K. Mishra and B. Mulgrew, " Bistatic SAR signature database generation for ground targets using EM simulator", submitted towards *IEEE Transaction of Aerospace and Electronics Systems and Navigation.*
- S. Papadopoulos, A.K. Mishra and B. Mulgrew, " Monostatic radar signatures of significant classes of ground targets ", *Proceedings of European Radar Conference (EuRAD) 2006*, September 2006.
- A.K. Mishra and B. Mulgrew, " Bistatic ATR: an overview", *Proceedings of third annual technical conference, EMRSDTC*, July 2006.
- † A.K. Mishra and B. Mulgrew, " Radar signal classification using PCA-based features", *Proceedings of ICASSP 2006*, May 2006.
- † A.K. Mishra and B. Mulgrew, " Bistatic SAR ATR using PCA-based features", *Proceedings of SPIE Defence Symposium, Conference on ATR XVI*, April 2006.
- A.K. Mishra and B. Mulgrew, " SAR-ATR using one and 2D PCA", *Proceedings of the International Radar Symposium (India) IRSI 2005*, December 2005.
- A.K. Mishra and B. Mulgrew, " Principal component analysis and relevance to scattering centre model of radar data", *Proceedings of the International Radar Symposium (IRS) 2005*, September 2005.
- A.K. Mishra and B. Mulgrew, " Target recognition for airborne bistatic radar using PCA", *Proceedings of second annual technical conference, EMRSDTC*, June 2005.
- † A.K. Mishra and B. Mulgrew, " Database generation of bistatic ground target signatures", *Proceedings of IEEE/ACES Conference on Wireless Communication and Applied Computational Electromagnetics*, April 2005.

- A.K. Mishra and B. Mulgrew, " Ground target classification for airborne bistatic radar", *Proceedings of first annual technical conference, EMRSDTC*, May 2004.

† Reprinted in this appendix.

RADAR SIGNAL CLASSIFICATION USING PCA-BASED FEATURES

Amit Kumar Mishra and Bernard Mulgrew

IDCOM, University of Edinburgh, Edinburgh, UK

ABSTRACT

Principal component analysis (PCA) has been used in many applications ranging from social science to space science, for the purpose of data compression and feature extraction. Usage of PCA for synthetic aperture radar (SAR) image classification, though widely reported by remote-sensing researchers, has not been exploited much by automatic target recognition (ATR) community. In the present paper, PCA has been used in SAR-ATR using the MSTAR data base, and comparison has been made with the conventional *conditional Gaussian model based Bayesian classifier* [1]. The results have been compared based on percentage of correct classification, receiver operating characteristics (ROC), and performance with limited amount of training data. By all standards of comparison, the PCA based classifier was observed to outperform the conditional Gaussian model based Bayesian classifier (CGBC) or at the worst it performs at par. And given the computational and algorithmic simplicity of PCA based classifier, the new algorithm was concluded to be a highly prospective candidate for real time ATR systems.

1. INTRODUCTION

Principal component analysis (PCA) has been used in data analysis and data compression for a long time [2, 3]. Usage of PCA for feature extraction has shown many advantages in many fields. In the current work, we discuss the usage of PCA on radar data for the recognition of ground targets from their radar images. Though PCA has been used in works reported in open literature, for remote sensing data classification [4, 5, 6], use of the same for target recognition task has not been well exploited. The novelty of the present work lies in use of PCA for ATR exercise, and the development and analysis of a simple nearest neighbor based classification algorithm based on PCA-extracted features, which is conceptually simple and computationally extremely fast.

The rest of the paper has been arranged as follows. The next section gives an overview of the database used for testing the classification algorithms, which is followed by an overview of the classification algorithms used in the present work. This is followed by a report of the results, and then the conclusion. In the appendix the confusion matrices of some of the experiments have been given as a more complete form of result display.

2. DATABASE USED

Database used for the validation of the classifiers proposed, is the SAR images of five military ground targets. The dataset has been collected by the MSTAR program [7]. Moving and stationary target acquisition and recognition (MSTAR) program is a DARPA supported project for collecting a standardized mono-static SAR image database, collected using the Sandia National Laboratories Twin Otter SAR sensor payload operating at X-band. The targets used for the present experiments are the 2S1 tank (t000), D-7 land clearing vehicle (t005), T62 tank (t016), ZIL131 APC (t025), and ZSU-23 (t026). The target clips collected at an elevation of 17 degrees were taken to train the classifiers and those collected at elevation of 15 degrees were taken as test images. The image clips were resized to 96x96 pixels.

3. EXPERIMENTAL SETUP

In the present work, the conditional Gaussian model based Bayesian classifier [1] (CGBC) was taken as the benchmark for comparing the results. This is mainly because as per results reported in open literature; this classifier is one of the most successful algorithms for SAR-ATR. Secondly, due to the use of Bayesian classification algorithm, this algorithm is the theoretically best algorithm (given there is enough training data and correct probability density function is found for the database). In this, each pixel of the image clips is assumed to be from a Gaussian distribution, conditioned or depending on the target type and target pose.

$$r = s(\Theta, a) + w \qquad (1)$$

where , r is the observed intensities of the pixels arranged in a one dimensional vector, w is additive Gaussian noise, s is the signal conditioned on Θ the target pose angle, and a the target type. The log-likelihood of an observed r, given $\{\Theta, a\}$ can be shown to be proportional to [1]:

1-4244-0469-X/06/$20.00 ©2006 IEEE

$$-\sum_{i=1}^{N}\left[\log(\Sigma_i)+\left(\frac{r_i-M_i}{\Sigma_i}\right)^2\right] \quad (2)$$

Where r_i is the i^{th} pixel of the test-image-clip, Σ_i, M_i are the standard deviation and mean of the pixel respectively (as estimated from the training data), and N is the total number of pixels in the test-image-clip. In this method, the recognition is done as per the Bayesian rule of maximizing the probability

$$P(a|r) = P(r|a)P(a) \quad (3)$$

$P(a)$, the probability of each type of vehicle was taken to be equal.

In the method of using principal component analysis (PCA) [2, 3], the image pixels are assumed to be the ***observed variables***, depending upon the target type.

$$r = s(a) + w \quad (4)$$

where, r is the observed intensities of the pixels arranged in a one dimensional vector, and w is additive Gaussian noise. The database is arranged so that all image clips collected at a 15 degree elevation are taken as training data. Each image clip in the training data-set is from the same elevation but a different azimuth angle. Pixels of image clips are assumed as ***variables***, taking different ***observations*** with changing azimuth angle. PCA is applied to the dataset to reduce the number of ***observed variables***. This is done in the following steps:

- For each image clip, the pixels are arranged into the observation vector, and consecutive image clips are taken as different observational values.
- All consecutive rearranged image-pixel vectors are stacked together to form the observation matrix.
- The observation matrix is normalized (to have unity variance), and all the observation vectors are zero centered. Let the final matrix be denoted by X.
- From this observation matrix, the covariance matrix is found for the observation vector.

$$Q = X^H X \quad (5)$$

- Then the eigen-value operation is applied on Q, to get the eigen vectors.
- Eigen vectors corresponding to k largest eigen values are stacked together to form matrix V.
- Using this matrix V, the training dataset is reduced in dimension to k. The final outputs from the training phase are the database in reduced dimension and the converting matrix V.
- In test phase, the test image clip is reduced in dimension using the converting matrix V.
- Next the Euclidean distance is found from each point in the training database, and the class giving the least distance is decided as the class of the test clip.

Hence this is a nearest neighbor (NN) classifier, taking the PCA-extracted data as features. We coined this simple classifier as PCA-NN classifier. In all the experiments reported in this paper, value of k has been kept to 20. Because, from previous experiments this number of principal components, have been shown to give the optimum classification performance [8].

4. RESULTS AND DISCUSSIONS

The classifiers will be compared based on .their performance over three criteria. Though, the more striking features will be presented in this section in the form of graphs and bar-charts, the confusion matrices from the major experiments have been given in the appendix, for more complete information on the performance of the algorithms.

The first criteria of comparison is the over all percentage of correct classification. This can be observed from table 1 and 4 in the appendix. For all the targets, the PCA-NN classifier performs better than the CGBC classifier.

As the second comparison criteria, the receiver operation characteristics (ROC) of the two classifiers were compared. The comparisons for the two algorithms for four of the targets are shown in figure 1. They show the percentage of correct classification (P_{cc}), versus the percentage of false alarm (P_{fa}) in a binary hypothesis test between the target of interest and all of the remaining targets. The probabilities of false alarm and correct classification have been calculated as per the standard works on SAR-ATR [1]. As can be observed, the performance of PCA-NN classifier is similar (target t000) or better (targets t005, t016 and t025) than the CGBC classifier.

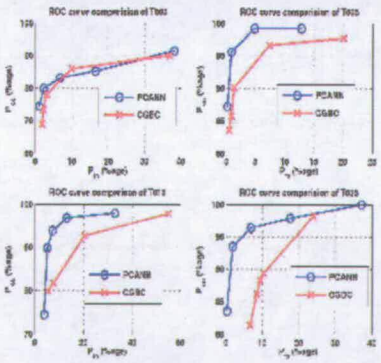

Fig.1 ROC comparisons for four of the targets

As the last criterion of comparison, the performances of the classifiers were studied with reduced amount of

training data. The reduction in training data was done in *two different ways*. First the training dataset was made sparse by discarding each alternate training clip (tables 2 and 5 in the appendix). In the second method, training data consisted of image clips with imaging platform azimuth from 0 to 180 degrees, while the test set had images from all azimuth angles. To analyze this more strong test, the test dataset was divided into two subsets, the first set (*set1*) consisting of images collected with azimuth 0 to 180 degrees and the second (*set 2*) from azimuth 180 to 360 degrees. The confusion matrices (table 3 and 6 in appendix) give the result for both test data sets. All the results have been presented in figure 2 and 3 in bar-chart form.

Looking at the over all performance of the classifiers with training data reduction, the loss of performance was more severe for CGBC classifier than for PCA-NN classifier

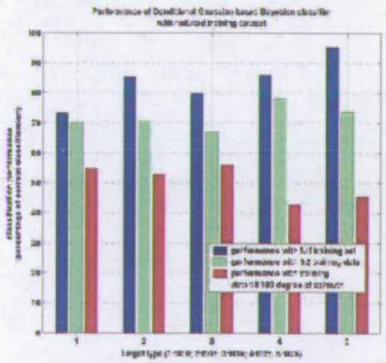

Fig.3 Performance of CGBC with reduced training dataset

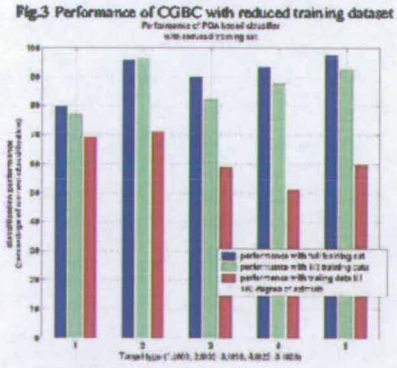

Fig.4 Performance of PCA-NN classifier with reduced training dataset

5. CONCLUSIONS

From the results found with the present work, it can be clearly concluded that the simple PCA based NN classifier out performs the CGB classifier in all the criteria of comparison. And due to the simplicity of the PCA-NN classifier, it takes several orders of less time for computation, than the CGB classifier. Given the reported success of CGB classifier, this makes a fairly strong algorithm for comparison. More over the extraction of the features of comparison (the data in PC-domain) is extremely fast for this new algorithm (just a matrix multiplication!). Hence the proposed PCA-NN classifier is a strong candidate for any real time ATR system, given its performance and computing speed.

6. ACKNOWLEDGEMENT AND DISCLAIMER

The authors acknowledge the electromagnetic remote sensing defense technology center (EMRSDTC) for funding this project and the royal academy of engineers.

Any views expressed are those of the authors and do not necessarily represent those of MOD or any other UK government department.

11. REFERENCES

[1] M.D. DeVore, and J.A. O'Sullivan, "Performance Complexity Study of Several Approaches to ATR from SAR Images", *IEEE Trans. on Aerospace and Electronic Systems*, vol.38, no.2, 632-648, April 2002.

[2] I.T. Jolliffe, *Principal Component Analysis*, 2nd Ed., Springer press, 2002.

[3] Dunteman, and H. George, *Brief Description: Principal components analysis*, Newbury Park, Calif. ; London : Sage, 1989.

[4] M.R.A. Sadjadi, S. Ghaloum, and R. Zoughi, "Terrain classification in SAR image using principal component analysis and neural networks", *IEEE Trans. On Geoscience and Remote Sensing*, vol.31, no.2, 511-515, March 1993.

[5] M.Klenke, and V.Hochschild, "Reducing the radiometric terrain effect in SAR imagery by means of principal components analysis", IEEE Geoscience and Remote Sensing Symposium, vol.2, 1288-1290, 1999.

[6] T.Feingersh, B.G.H.Gorte, and H.J.C. VanLeeuwen, "Fusion of SAR and SPOT image data for crop mapping", IEEE Geoscience and Remote Sensing Symposium, vol.2, 873-875, 2001.

[7] https://www.sdms.afrl.af.mil/

[8] A.K.Mishra, and B.Mulgrew, "SAR-ATR using one and 2D PCA", International Radar Symposium (India), Bangalore, 19-22 December 2005.

9. APPENDIX

Table 1. Confusion matrices for CGBC based algorithm (full training dataset)

	t000	t005	t016	t025	t026	Performance
t000	201	2	18	49	4	73.35%
t005	2	234	7	17	14	85.40%
t016	20	1	219	23	10	79.92%
t025	1	2	30	236	5	86.13%
t026	2	4	4	2	262	95.62%

Table 2. Confusion matrices for CGBC based algorithm (sparse training dataset to ½ original size)

	t000	t005	t016	t025	t026	Performance
t000	192	2	13	67	0	70.07%
t005	3	194	14	46	17	70.80%
t016	48	1	183	32	9	66.79%
t025	17	13	21	214	9	78.10%
t026	9	14	32	17	202	73.72%

Table 3. Confusion matrices for CGBC based algorithm (training dataset for azimuth angles from 0 to 180 degrees only)

	t000	t005	t016	t025	t026	Performance (%)	Overall performance
t000 set1	112	0	22	3	0	81.7	54.74%
set2	38	1	48	49	1	27.7	
t005 set1	1	105	1	30	0	76.6	52.92%
set2	5	40	26	33	33	29.2	
t016 set1	17	7	97	11	5	70.8	56.20%
set2	52	5	57	21	1	41.1	
t025 set1	3	22	17	91	4	66.4	42.86%
set2	62	1	45	26	2	19.1	
t026 set1	1	6	9	20	101	73.7	45.62%
set2	28	24	52	8	24	17.5	

Table 4. Confusion matrices for PCA based algorithm (full training dataset)

	t000	t005	t016	t025	t026	Performance
t000	219	0	50	5	0	79.93%
t005	3	262	2	4	3	95.62%
t016	15	2	246	8	2	89.78%
t025	8	3	5	256	2	93.43%
t026	0	4	0	3	267	97.45%

Table 5. Confusion matrices for PCA based algorithm (sparse training dataset to ½ original size)

	t000	t005	t016	t025	t026	Performance
t000	211	0	52	8	3	77.01%
t005	1	263	3	7	0	95.99%
t016	31	3	225	7	7	82.12%
t025	13	10	8	240	3	87.59%
t026	0	12	0	9	254	92.34%

Table 6. Confusion matrices for PCA based algorithm (training dataset for azimuth angles from 0 to 180 degrees only)

	t000	t005	t016	t025	t026	Performance (%)	Overall performance
t000 set1	119	0	14	4	0	86.8	69.34%
set2	71	0	62	2	1	51.8	
t005 set1	0	127	0	3	7	92.7	71.12%
set2	9	68	6	37	17	49.6	
t016 set1	4	2	126	5	0	91.9	59.12%
set2	70	9	36	21	0	26.2	
t025 set1	2	2	6	125	2	91.2	51.09%
set2	62	29	30	15	1	10.9	
t026 set1	0	2	0	2	133	97.0	59.85%
set2	18	27	30	31	31	22.6	

Bistatic SAR ATR using PCA-based features

A. K. Mishra, and B. Mulgrew
University of Edinburgh
Edinburgh, EH9 3JL

Abstract

Target recognition is desirable feature of any defence radar system. With the present revival of interest in bistatic and multi-static radar systems, the future radar systems are predicted to invariably have bistatic abilities. The present project aims at looking into prospects and limitations of bistatic target recognition and to develop efficient algorithm for the same. The work in this paper reports the development of a database of bistatic target signatures, and the application of principal component analysis (PCA) based classifiers on the same. Results are compared with the more basic conditional Gaussian model based Bayesian classifier.

Keywords: Bistatic airborne radar, target recognition, PCA.

Introduction

Airborne bistatic radar has long been recognized as offering advantages as a counter stealth and anti-jamming technology with respect to its monostatic counterpart. Algorithms for bistatic synthetic aperture image formation are now starting to appear in the open literature (Ref. 1). Given the potential of a non-monostatic configuration, bistatic and multistatic configurations may replace monostatic in some existing applications and inspire new ones. In any military radar system, a facility for robust automatic target recognition (ATR) system is desirable. In this paper we present the work undertaken by us, involving the application of principal component analysis (PCA) based classification algorithms in bistatic ATR.

There are quite a few dimensions to the novelty of the work in this paper. First of all, the study of classification performance of ATR algorithms in bistatic scenario, in itself is a novel area. Secondly, the database used for the purpose has been developed completely by indigenous efforts. Thirdly, the preferred ATR algorithm reported in this work, which is the simple PCA based nearest neighbor algorithm, also is a novel algorithm in itself. Though PCA has been used for recognition task by remote sensing community, the usage of the same by ATR community has not been found much in open literature.

In the rest of the paper, the database used for the validation of the algorithms is discussed, followed by a short note on PCA and why PCA is a suitable candidate in radar signal classification problems. Then the results from the experiments are presented followed by conclusions.

Database of airborne bistatic radar images (Ref.2)

Unlike the monostatic counterpart, in bistatic case, there are no datasets in public domain, which could be used in validation and analysis of any classification algorithm. As the next best alternative, an electro magnetic modeling tool (Ref.3) is used to model and generate a database for bistatic scenario.

In modeling the targets (military land vehicles), only the major (classifiable) features are modeled, ignoring the finer details. Based on this principle of modeling major features, four generic targets were simulated, viz. a battle field tank (MBT), an armored personal carrier vehicle (APC), a stringer missile launching vehicle (STR)

and a land missile launching platform (MSL).
In figure 1, the target models (not to scale) are illustrated and in figure 2, the corresponding synthetic aperture radar (SAR) images are shown. The SAR images are one of the realizations, with minimum bistatic angle. Figure 3 gives the SAR images of the targets with the addition of ground clutter and shadow.

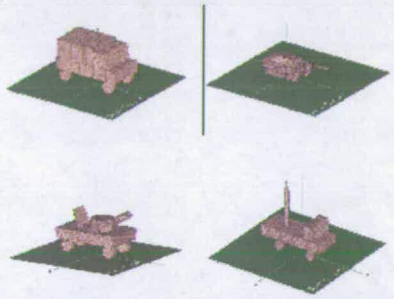

Fig.1 Models of the targets (APC, MBT, MSL, & STR in clockwise manner)

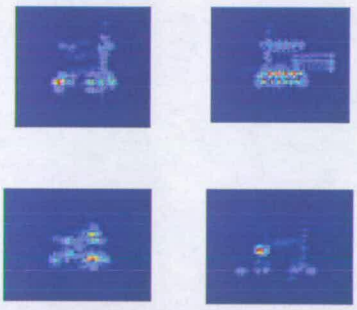

Fig.2 Bistatic SAR images of the targets (APC, MBT, MSL, & STR in clockwise manner)

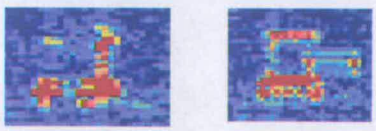

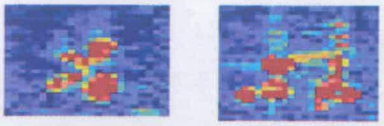

Fig.3 SAR images with ground clutter and shadow (APC, MBT, MSL & STR in clockwise manner)

PCA and its pertinence

Principal component analysis (PCA) has been used in data analysis and modeling and has a long and successful history. There has been some usage of PCA in SAR image classification in remote sensing and segmentation applications (Ref.4). But in the open literature, there have not been many reports on the usage of PCA for ATR. The use of PCA for ATR has two justifications. First of all, PCA itself reduces the amount of data to be handled, and hence can reduce computational complexity. For a time-crucial application like ATR, this is a great advantage. Secondly, from our initial experiments with PCA and radar data, there was some evidence of a link between PCA and scattering centre model for radar data (Ref.5). The scattering centre model is a well-established model in radar community as of now. In addition to these, the results reported in this paper show that PCA-based classification approach is more robust with respect to the standard conditional Bayesian classification algorithms (Ref.6).

Experimental procedure

In the present work, the conditional Gaussian model based Bayesian classifier was taken as the standard - partly because of it closeness to the conventional Bayesian approach and partly due to the excellent results reported using this method for monostatic ATR (Ref.6). In this each pixel of the image clips, is assumed to be drawn from Gaussian distribution, conditioned on

the target type and receiver azimuth[1].

$$r = s(\Theta, a) + w$$

where , r is the observed intensities of the pixels arranged in a one dimensional vector, and w is Gaussian noise and s is the complex signal conditioned upon Θ the receiver azimuth angle, and a the target type. The log-likelihood of an observed r, given $\{\Theta, a\}$ can be shown to be proportional to:

$$-\sum_{i=1}^{N}\left[\log(\Sigma_i) + \left(\frac{r_i - M_i}{\Sigma_i}\right)^2\right]$$

where r_i is the i^{th} pixel of the test-image-clip, Σ_i, M_i are the variance and mean of the pixel respectively (as estimated from the training data), and N is the total number of pixels in the test-image-clip. In this method, the recognition is done as per the Bayesian rule of maximizing the probability

$$P(a \mid r) = P(r \mid a)P(a)$$

$P(a)$, the probability of each type of vehicle was taken to be equal. In principal component analysis (PCA) (Ref.7, 8), the image pixels are assumed to be the ***observed variables***, depending upon the target type.

$$r = s(a) + w$$

The database is arranged so that all image clips collected at 10 degrees receiver elevation, are taken as training data. Each image clip in the training data-set, is from the same elevation but a different azimuth angle. Pixels of image clips are assumed to take different ***observations*** with changing azimuth angle. PCA is applied to the dataset to reduce the number of ***observed variables***. This is done in the following steps:

- For each image clip, the pixels are arranged into the observation vector, and consecutive image clips are taken as different observational values.
- All consecutive rearranged image-pixel vectors are stacked together to form the observation matrix.
- The observation matrix is normalized (to have unity variance), and all the observation vectors are zero centered. Let the final matrix be denoted by X.
- From this observation matrix, the covariance matrix is found for the observation vector.

$$Q = X^H X$$

- Then the eigenvalue operation is applied on Q, to get the eigen vectors.
- Eigenvectors corresponding to k largest eigenvalues are stacked together to form matrix V.
- Using this matrix V, the training dataset is reduced in dimension to k. The final output from the training phase is the database in reduced dimension and the converting matrix V.
- In test phase, the test image clip is reduced in dimension using the converting matrix V.
- Next the Euclidean distance is found from each point in the training database, and the class of target giving the least distance is decided as the class of the test clip.

Results

In figure 4, the results of classification algorithm performance for conditional Gaussian model based Bayesian (CGB) classifier has been displayed for both HH and VV polarized data. Figure 5 displays the results of classification algorithm performance for PCA based nearest neighbor classifier for both HH and VV polarized data.

[1]For monostatic case, its the target pose; but in bistatic case, receiver azimuth was deemed a more simple and convenient parameter

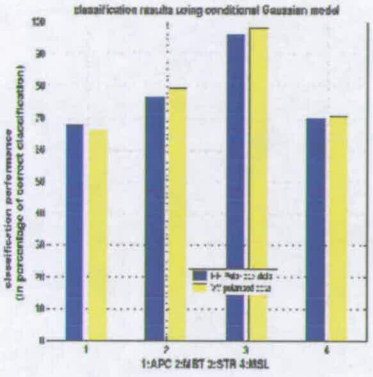

Fig.4 Bistatic ATR performance of conditional Gaussian model based classification algorithm

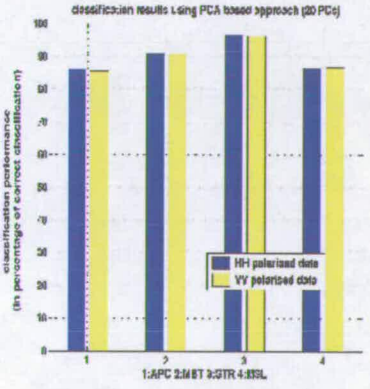

Fig.5 Bistatic ATR performance of PCA based classification algorithm

Figures 6 and 7 show the receiver operational characteristics curves for the four targets, for CGB and PCA based classifiers respectively. As can be clearly marked, the best performance is shown for one particular target, using CGB. But the ROC curves vary a lot from target to target in CGB classifier. For PCA based classifier, where as the best ROC curve is not as good as the best for CGB classifier, the ROC curves are almost similar. Hence proving the fact that classification performance for PCA based classifier is less dependent on the type of target used. This robustness to the target type is a great advantage for any ATR system.

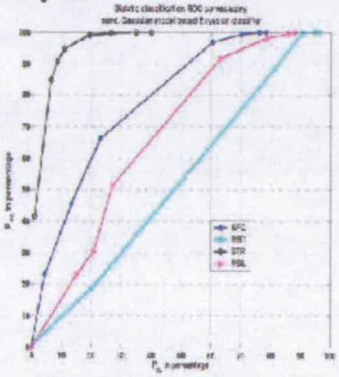

Fig.6 Bistatic ATR ROC curves of CGB classification algorithm

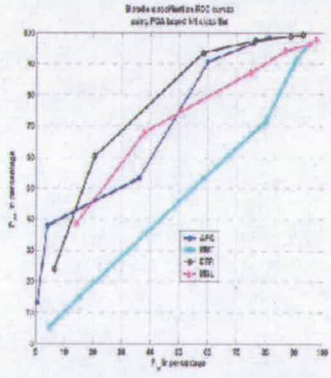

Fig.5 Bistatic ATR ROC curves of PCA based classification algorithm

To further see the usage of different classifiers for bistatic scenario, a major study was done about the performance of classification algorithms, with reduced training datasets. As has been explained in the dataset formation section, images of a

target are collected with varying azimuth of the receiver. Keeping this in view, the reduction of dataset was designed in two ways:

1. Taking each other image clip from the original training dataset. In this method, the amount of training dataset is reduced. (This variety of experiments were coined as data-reduction at level 1)
2. Taking image data, only from a limited amount of receiver azimuth angles. This is a more severe limitation on training dataset (hence termed as data-reduction at level 2). To test classifier performance in this experiment, the test dataset were divided into two subsets. The first set consisted of images collected with the receiver azimuth angles, for which training dataset is available (test set 1). The second test dataset consisted of images collected with the receiver azimuth angles, for which training dataset is not available (test set 2).

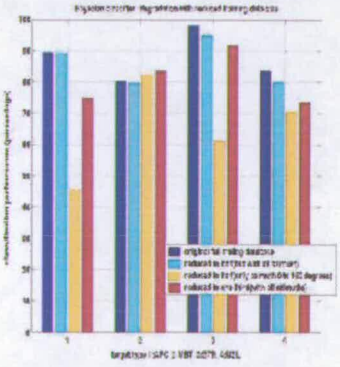

Fig.8 Performance of CGBC with reduced training data

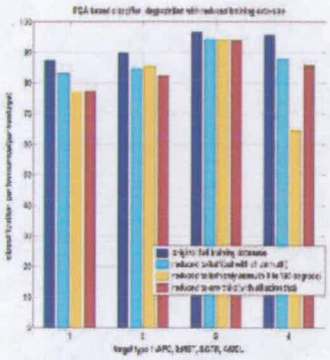

Fig.9 Performance of PCA-NN classifier with reduced training data

Experiments with dataset reduced at level 1: The training dataset reduced to half and then to one third of the original size (of 432 image clips from each target type). Results for CGBC are given in table 1 and 2, and the same for PCA-NN classifier are given in table 3 and 4 (in Appendix).

Experiments with dataset reduced at level 2: In experiments for dataset reduction at level 2, dataset was reduced to half and the effect was noted for both types of classifiers. The confusion matrices of this experiment are given in table 5, for CGBC algorithm, and in table 6 for PCA-NN classifier.

The results have been plotted in bar-chart format in figure 8 and 9. The major observations are:

- For level 1 type reduction, there is observed degradation in classification rate for both types of classifiers.
- With reduction of dataset to one third, the classification performance further decreases.
- For level 2 type training data reduction, the deterioration of classification performance is more severe.
- The most striking difference between the two classifiers can be observed by

noting the confusion matrices, in level 2 type dataset reduction.

- In PCA-NN classifier, the deterioration of performance (in level 2 type training dataset reduction) is almost of same degree both for test set 1 and test set 2.
- But in CGBC algorithm, the classification performance for test set 2 (for which type of image clips, there was no training data available) there was almost no classification at all. All the test data were mostly classified as MBT. This can be explained as because of the fact that MBT is the biggest target modeled in this project, and hence with maximum RCS energy.

The reason for the drastic difference in performance of the two algorithms can be explained on the basis of the inherent working principle of the two algorithms. CGBC is a statistical Bayesian classifier, and hence will perform the best in the ideal situation of availability of all the possible dataset in training phase. But PCA based algorithms use the PCA of the dataset, which was shown to give almost same information as the scattering centers of the radar-image. Scattering centers in turn depend upon the physical features of the target. Being a *feature based classifier*, PCA-NN classifier is expected to outperform Bayesian classifier for reduced training dataset situation. (This experiment further strengthens the theory about the relation between PCA-extracted data and scattering centers, for radar data.)

Conclusion and Discussion

Some observations drawn from the results are:

- Performance for both HH and VV polarization are almost the same, for both the algorithms.
- Highest individual performance for CGB algorithm is around 97% for the target STR.
- Highest individual performance for PCA based algorithm is around 96% for the target STR.
- Lowest individual performance for CGB algorithm is around 66% for the target APC.
- Lowest individual performance for CGB algorithm is around 86% for the target STR.

Hence even though CGB algorithm can give very high performance for some targets, this performance is sensitive to the target type. PCA based algorithms may give slightly lower performance, than the CGB algorithm for the most classifiable target. But their performance does not vary so drastically with different targets. Hence it may be concluded that PCA based algorithms are more stable and robust (both to target variation and to reduced training dataset).

REFERENCES

1. Rigling BD, Moses RL, "Polar format algorithm for bistatic SAR", *IEEE Trans. On Aerospace and Electronics Systems*, vo.40,no.4, 1147-1159 (Oct. 2004).
2. Mishra AK, Mulgrew B, "Database generation of bistatic ground target signatures", *IEEE/ACES conference on Wireless communication And Applied Computational Electromagnetics* (April 3-7, 2005).
3. FEKO User's Manual, EM Software & Systems-S.A. (Pty) Ltd. (June 2004).
4. Azimi-Sadjadi MR, Ghaloum S, and Zoughi R, "Terrain Classification in SAR Images Using Principal Component Analysis and Neural Networks,"*IEEE Trans. on Geoscience and Remote Sensing*, vol.31,no.2, 511-515 (March 1993).
5. Mishra AK, Mulgrew B, "Principal component analysis and relevance to scattering centre model of radar data", accepted for *International Radar Symposium (IRS) 2005* (September 2005).
6. DeVore MD, and O'Sullivan JA, Performance Complexity Study of Several Approaches to ATR from SAR

Images, *IEEE Trans. on Aerospace and Electronic Systems*, vol.38, no.2, 632-648, (April 2002).

7. Jolliffe I.T., "Principal Component Analysis", 2nd Ed., Springer press (2002).
8. Dunteman, and George H., "Brief Description: Principal components analysis",Newbury Park, Calif. ; London : Sage (1989).

ACKNOWLEDGEMENTS

The work reported in this paper was funded by the Electro-Magnetic Remote Sensing (EMRS) Defense Technology Centre, established by the UK Ministry of Defense and run by a consortium of BAE Systems Avionics, Thales Defence, Roke Manor Research and Filtronic.

APPENDIX

Table 1 Bistatic ATR: CGBC; no clutter; pol : HH; training set reduced to half

	Low bistatic angle				Med. Bistatic angle				High bistatic angle				Overall classification
	APC	MBT	STR	MSL	APC	MBT	STR	MSL	APC	MBT	STR	MSL	
APC	140	4	0	0	136	0	3	6	109	10	16	9	89.1%
MBT	4	138	0	2	9	110	0	25	23	96	4	21	79.6%
STR	2	2	140	0	2	0	140	2	7	4	130	3	94.9%
MSL	3	3	4	134	1	4	22	117	22	0	28	94	79.9%

Table 2 Bistatic ATR: CGBC; no clutter; pol : HH; training set reduced to one third

	Low bistatic angle				Med. Bistatic angle				High bistatic angle				Overall classification
	APC	MBT	STR	MSL	APC	MBT	STR	MSL	APC	MBT	STR	MSL	
APC	123	20	0	1	119	8	4	13	81	17	16	29	74.8%
MBT	2	141	0	1	9	116	0	19	10	104	3	27	83.6%
STR	0	3	141	0	2	1	136	5	18	1	119	6	91.7%
MSL	9	16	5	124	9	16	12	107	9	16	23	96	73.4%

Table 3 Bistatic ATR: PCA based NN; no clutter; pol : HH; training set reduced to half

	Low bistatic angle				Med. Bistatic angle				High bistatic angle				Overall classification
	APC	MBT	STR	MSL	APC	MBT	STR	MSL	APC	MBT	STR	MSL	

APC	137	7	0	0	123	20	0	1	98	31	0	15	82.9%
MBT	7	135	0	2	11	124	5	4	10	106	17	11	84.5%
STR	0	0	141	3	4	1	133	6	5	5	133	1	94.2%
MSL	6	1	3	134	5	6	2	129	9	10	10	115	87.5%

Table 4 Bistatic ATR: PCA based NN; no clutter; pol : HH; training set reduced to one third

	Low bistatic angle				Med. Bistatic angle				High bistatic angle				Overall classification
	APC	MBT	STR	MSL	APC	MBT	STR	MSL	APC	MBT	STR	MSL	
APC	127	17	0	0	109	35	0	0	98	46	0	0	77.3%
MBT	19	122	2	1	16	118	6	4	13	116	8	7	82.4%
STR	0	1	143	0	1	2	140	1	10	8	122	4	93.8%
MSL	10	4	1	129	7	4	3	128	12	13	10	109	84.7%

Table 5 Bistatic ATR: CGBC; no clutter; pol : HH; training set reduced to half (azimuth angles till 180°)

	Low bistatic angle				Med. Bistatic angle				High bistatic angle				Overall classification
	APC	MBT	STR	MSL	APC	MBT	STR	MSL	APC	MBT	STR	MSL	
APC (test set 1)	72	0	0	0	65	3	1	3	45	4	12	11	45.8%
(test set 2)	14	41	0	17	0	53	0	19	2	70	0	0	
MBT (test set 1)	5	67	0	0	6	59	0	7	11	49	4	8	82.4%
(test set 2)	4	62	0	6	5	52	0	15	4	67	0	1	
STR (test set 1)	0	0	72	0	1	0	71	0	1	4	66	1	61.1%
(test set 2)	7	6	37	22	13	30	13	16	8	50	5	9	
MSL (test set 1)	0	0	0	72	1	1	11	59	2	1	14	55	70.4%
(test set 2)	2	16	0	54	2	24	0	46	5	48	1	18	

Table 6 Bistatic ATR: PCA based NN; no clutter; pol : HH; training set reduced to half (azimuth angles till 180°)													
	Low bistatic angle				Med. Bistatic angle				High bistatic angle				Overall classification
	APC	MBT	STR	MSL	APC	MBT	STR	MSL	APC	MBT	STR	MSL	
APC (test set 1)	62	10	0	0	54	15	0	3	32	23	0	17	76.9%
(test set 2)	66	2	0	4	63	5	0	4	55	13	0	4	
MBT (test set 1)	2	69	0	1	11	55	4	2	11	51	3	7	85.4%
(test set 2)	4	68	0	0	1	66	0	0	5	60	2	5	
STR (test set 1)	1	0	70	1	5	0	67	0	4	7	60	1	93.8%
(test set 2)	0	0	72	0	2	0	70	0	4	0	66	2	
MSL (test set 1)	8	2	13	48	8	3	22	39	8	7	18	39	64.4%
(test set 2)	11	8	4	49	11	0	13	48	4	3	10	55	

Database generation of bistatic ground target signatures

Amit Kumar Mishra
IDCOM, University of Edinburgh, UK
EH9 3JL
akmishra@ieee.org

Bernard Mulgrew
IDCOM, University of Edinburgh, UK
EH9 3JL
B.Mulgrew@ed.ac.uk

Abstract: Automatic target classification has been an area of active study due to many of its significances. With the re advent of bistatic technology in radar, the research into target classification in bistatic scenario seems quite timely. But the study of any classification algorithm demands for a suitable database. Due to the unavailability of suitable field collected bistatic database, computer simulation of such a database is quite pertinent. The present work discusses the approach towards the generation of a similar database, using FEKO as the electromagnetic simulation tool. Various special needs of such a project and the answers of FEKO to those needs, have been discussed. The results conclusively show the suitability of FEKO for the project.

Keywords: Bistatic Target Signature, EM Simulation, database generation

1. Introduction

There has been an increasing interest in bistatic radars for the purpose of surveillance and detection, specifically in a military scenario. Once bistatic systems are technically established, automatic target recognition(ATR) algorithms would be a valuable addition to the system. To test and establish any ATR algorithm, an exhaustive bistatic signature database is needed. But the major problem is obtaining access to field generated database. First of all there has been hardly any bistatic operation for collecting such a database, and if any, these are highly classified for public access. Hence simulation of the database is the most viable option. In this paper we discuss and analyze the steps and flow-plan undertaken in generating such a database using the electro magnetic (EM) simulation tool FEKO [1].

The present work aims at generating bistatic synthetic aperture radar (SAR) images and range profiles of ground based military targets[1]. Some of the other EM-simulations tools which have been used for generating SAR images, are Epsilon [2] and Xpatch [3]. At the same time, there has also been some limited usage of synthetic database in validating target classification algorithms. For example, in their research [4], Bhanu and Lin use a limited amount of SAR data generated using Xpatch, in validating their classification algorithms. However both Xpatch and Epsilon, have not been so easily accessible for the international academics. While FEKO has been found quite suitable for the purpose.

1 Through out the paper, "military ground vehicles" and "ground targets" have been used interchangeably

One novelty of the present work is the usage of FEKO in generating SAR images of ground targets. Secondly, here the goal is to generate a database for the bistatic scenario, work similar to which has not been found in the open literature.

In the rest of this paper, in section 2, the modeling aspects of the military ground vehicles would be discussed. Section 3 discusses the simulation approaches undertaken using FEKO to generate the SAR images of the targets. And in section 4 we analyze some of the results generated using the present modus operandi.

2. Modeling

Military ground vehicles have highly involved and complex surfaces and features. Hence to model even a fairly approximate ground target, needs considerable expertise from the modeler and a highly efficient CAD tool. Another problem is the issue of surface alignment. Like most other EM simulation tools, FEKO replaces surfaces with small triangular facets (the dimension of these should be an order less than the central frequency wavelength). Hence for two mutually touching surfaces or sides, the respective sides of the triangles in the sides should exactly match each other. This strict condition is often extremely difficult to achieve for complex structures. But in the present work, the final objective was to generate a data base to validate classification algorithms. Hence instead of modeling the finer details of a target, the more prominent features of the target were modeled. Such features are termed as the classifiable features. For example, the prominent turret and canon of a main battle tank, and the guidance antenna of a land-to-air missile launcher.

To model such prominent features, the modeling tool of FEKO, EDITFEKO, was found suitable. It had the ability to model a lot of the basic three dimensional geometries and gives control on the type of meshing to be applied. While many CAD tools do have the feature to mesh the models, the meshing from a CAD tool needs a lot of modification to be a electromagnetically suitable meshing, because CAD tools are mostly not meant for EM-design. Two of the features of EDITFEKO, which were convenient for the current work, were the ability to

- create new geometries, symmetric to the previous geometries (SY card), and
- modify a previously defined geometry by rotation and translation (TG card).

Ground targets do have symmetric parts (if we ignore the intricate details) and exploiting this makes the modeling easier. And this information in turn can be exploited by FEKO for faster simulation. The EDITFEKO's ability to modify a geometry, can be used to translate or/and rotate a particular part of the model. This feature is handy in modeling slanting canons, turrets and also in creating multiple wheels similar to one (hence in effect just one wheel is modeled). Another significance of this ability is to generate a database of articulated or slightly modified target. For example to model the tank with the canon or turret in some different orientation, just need to apply this feature of EDITFEKO. This facility is typically important while generating databases for classification exercises. Because one of the major test of a classification algorithm is to train it on one database and test it on another database of the same target with some modifications.

In the modeling of ground targets, one extremely important part is ground modeling. Some of the major contribution of the ground are it's contribution to the ground clutter, and in generating a shadow region. FEKO has the facility to define a dielectric plane ground with user-defined parameters (BO card). Being a perfectly plane ground, this could not contribute for the ground clutter and speckles. But it very well contributed towards the shadowing effects. To taste its ability to generate shadow, a very simple wall like structure was modeled with dielectric ground and with transmitter on one side[2], the surface current on the ground was observed (Figure 1 and 2).

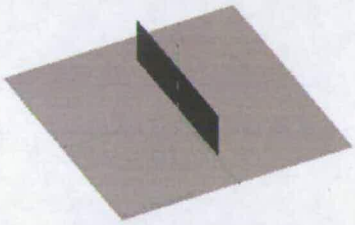

Fig.1 Model for tasting shadowing.

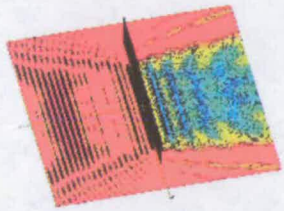

Fig.2 Surface current on the ground.

As can be observed FEKO simulates shadow region contributions on the ground plane. The interference pattern formed on the ground is also evident.

3. Simulation

Basic steps followed in generating the radar return of a target model and in forming the SAR image are:

i. Determining the frequency range over which the target scene would be simulated to get the scattered field. Also determining the frequency steps. These are determined by the spatial resolution and maximum spatial distance in range direction: $x = \frac{c}{2F}$; $f = \frac{c}{2X}$, where f is the frequency step, F is the band width, x is the range resolution and X is the maximum range to be imaged[5].

ii. Determining the angular range and step in angular dimension. These in turn are determined by the spatial resolution and maximum spatial distance in cross-range direction: $=\frac{}{2Y}$; $y=\frac{}{2}$, where is the central frequency wavelength, is the step in angle, is the total angular swath, y is the cross range resolution and Y is the maximum cross range to be imaged [5]. (It should be noted that because we intend to generate data for the bistatic case, the calculations in step i and ii

2 The exact values of position of transmitter and receiver and the exact numerical values of frequencies used would not be discussed in the paper because of strategic nature of the project.

are not exact, but could be taken just as thumb-rules.)

iii. The transmitter position to be fixed and the target illuminated with waves of the predetermined ranges of frequencies and one polarization.

iv. The scattered field collected for the range of angles as determined in step ii. (The exact way to swap the range of angles might vary.)

v. Once the scattered field is collected for the range of frequencies and for the range of angles, the two dimensional data set is to be polar-to-rectangular reformatted and windowed.

vi. After this, taking a two dimensional inverse Fourier transform gives the SAR image.

In rest of this section the utility of FEKO in carrying out the above steps would be discussed.

Life size ground targets are electrically huge. Hence even though FEKO supports the method of moments calculation of scattered field, it costs a large amount of memory and time, which is practically impossible. Hence looking for alternate methods of simulation, the method of physical optics (PO) with multiple bounces was found to best suit the present work. As has been discussed in the user manual and observed from our initial simulations, PO with multiple bounces is a good compromise between the resource utilization (time and computer memory) and accuracy.

Another advantage with FEKO is the simulation of multi-polar returns. Once the polarization of the transmitter is fixed, FEKO calculates the return in both horizontal and vertical polarization. Hence running the simulation once more, gives the full polarimetric characteristic of the target, which is a promising field in target recognition.

Because the present work focuses on generating bistatic signature, the configuration taken was, a fixed transmitter position and varying receiver position. And the main bottle neck in any EM simulation, consuming maximum time, is the calculation of the surface currents. Because surface current does not change for a fixed transmitter (given the polarization and frequency also remains fixed), FEKO's PS card was found invaluable in storing the surface currents on the target for all the frequencies, for a particular transmitter position. After one run using the PS card, the surface currents are stored in a *.str file. And this in turn can be used for any position of receiver with a simulation time several order less than the original one. This not only solves the problem of time effective simulation, but also makes the whole process suitable to generate huge amount of database which is essential for validating any classification algorithm.

4. Results

FEKO gives the far field in a output file of format *.ffe. Using an interface C-program, the data was to be converted into Matlab readable form, before further post processing.
Figure 3 and 4 show two of the models, built using EDITFEKO, showing a life size land missile launcher and a battle field tank. As can be noticed, only the classifiable features have been modeled and not all the intricate details (the meshing shown is just for better visualization, and the actual meshing is an order denser than what shown).

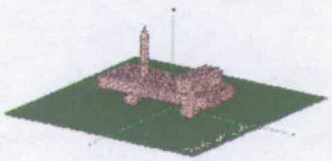

Fig.3 model of a land missile launcher.

Fig.4 model of a battle field tank.

Figure 5 and 6 show the SAR image of the target models shown before, for a bistatic angle of around ten degrees (exact bistatic angle is not an obvious parameter, as the SAR image is formed over a range of looks). As can be seen, due to a flat ground, the ground speckles are absent.

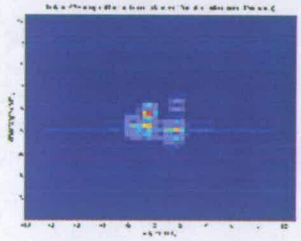

Fig.5 bistatic SAR image of the land missile launcher.

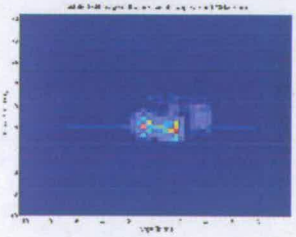

Fig.6 bistatic SAR image of the battle field tank.

5. Conclusion and future work

In the present paper we have discussed generating a database for validation of classification algorithms for bistatic SAR images of ground targets. From the results, it can be concluded that FEKO has proved to be a suitable tool for the present work, with many special features which particularly suited the problem. One of the problems remaining for future consideration is the simulation of a more realistic ground, which could account for ground clutter and speckles. Because modeling a detailed ground in the same scene proves to be a challenging task for FEKO, some suitable breakdown of the problem has to be considered.

6. Acknowledgement

The authors acknowledge the electromagnetic remote sensing defense technology center (EMRSDTC) for funding this project and the royal academy of engineers (RAE) for the equipment grant to procure FEKO.

7. Disclaimer

Any views expressed are those of the authors and do not necessarily represent those of MOD or any other UK government department.

References

[1] FEKO User's Manual, EM Software & Systems-S.A. (Pty) Ltd, June 2004.

[2] Simpson S.H.W., Galloway P., and Harman M., "Application of Epsilon a radar signature prediction and analysis tool", *International Radar Symposium* IRS'98, 1998.

[3] Andersh D., Moore J., Kosanovich S., Kapp D., Bhalla R., Kipp R., Courtney T., Nolan A., German F., Cook J., and Huges J., "Xpatch 4: the next generation in high frequency electromagnetic modeling, and simulation software", *IEEE Radar Conference*-2000, pp. 844-849.

[4] Bhanu B., and Lin Y., "Stochastic models for recognition of occluded targets", *Pattern Recognition*, 36, 2003, pp. 2855-2873.

[5] Charles V.Jakowatz, Jr., Daniel E. Wahl, Paul H. Eichel, Dennis C. Ghiglia, and Paul A.Thompson, "Spotlight-mode synthetic aperture radar: a signal processing approach", Kluwer academic publishers, 1996.

References

[1] *http://epsilon.nought.de*.

[2] B. Bhanu and T. L. Jones, "Image understanding research for automatic target recognition," *IEEE AES Magazine*, pp. 15–22, 1993.

[3] K. Augustyn, "A new approach to automatic target recognition," *IEEE Transaction on Aerospace and Electronics Systems*, vol. 28, no. 1, pp. 105–114, 1992.

[4] W. Keydel, "Perspectives and visions for future sar systems," *IEE Proc. Radar Sonar Navigation*, vol. 150, no. 3, pp. 97–103, 2003.

[5] K. Wolfgang, "Future radar systems for remote sensing," in *IEE Workshop on the Future of Radar in the UK and Europe*, vol. 7, pp. 7/1–7/6, Nov. 1999.

[6] J. R. Huynen, "Physical reality and mathematical process in radar polarimetry," in *Proceedings of the 7th IEE International Conference on Antenna and Propagation, ICAP 91*, pp. 257–261, April 1991.

[7] F. T. Ulaby, R. K. Moore, and A. K. Fung, *Microwave remotesensing: active and passive*, vol. II. Addison-Wesley, 1986.

[8] G. Franceschetti and R. Lanahari, *Synthetic aperture radar processing*. CRC Press, 1999.

[9] C. J. Oliver and S. Quegan, *Understanding synthetic aperture images*. Artech House, 1997.

[10] C. V. J. Jakowatz, D. E. Wahl, P. H. Eichel, D. C. Ghiglia, and P. A. Thompson, *Spotlight-mode synthetic aperture radar: a signal processing approach*. Kluwer Academic Publishers, 1996.

[11] G. Morris and L. Harkness, eds., *Airborne pulsed doppler radar*. Artech House Publishers, 1996.

[12] IEEE Std, *IEEE standard radar definition*, 686-1997 ed., 1997.

[13] N. J. Willis, *Bistatic radar*. Technology Service Corporation, 1995.

[14] Hawkins, "An opportunistic radar," in *Proceedings of IEE Radar Conference*, pp. 318–322, October 1997.

[15] X. He, T. Zeng, and M. Cherniakov, "Signal detectability in ss-bsar with gnss non-cooperative transmitter," *IEE Porceedings on Radar, Sonar and Navigation*, vol. 152, no. 3, p. June, 2005.

[16] R. J. Burkholder, I. J. Gupta, and J. T. Johnson, "Comparision of monostatic and bistatic radar images," *IEEE Antenna and Propagation Magazine*, vol. 45, no. 3, pp. 41–50, 2003.

[17] A. Y. Nashashibi and F. T. Ulaby, "Detection of targets above rough surfaces using millimeter-wave bistatic radar," in *Proceedings of IEEE International Symposium of Antenna and Propagation Society*, pp. 424–427, June 2003.

[18] D'Errico, M. Grassi, and Vetrella, "A bistatic sar mission for earth observation based on a small satellite," *Acta Astronautica*, vol. 39, pp. 837–846, 1996.

[19] R. A. Cordey, "Sar polarimetry: applications and understanding," in *IEE Colloquium on Polarization in Radar*, vol. 6, pp. 6/1–6/4, March 1996.

[20] A. M. Horne and G. Yates, "Bistatic synthetic aperture radar," in *Proceesings of RADAR 2002*, pp. 6–10, 2002.

[21] H. D. Griffiths, "From a different persepctive: principles, practice and potential of bistatic radar," in *Radar Conference 2003*, pp. 3–5, September 2003.

[22] R. Touzi, "A review of speckle filtering in context of estimation theory," *IEEE Transaction on Geoscience and Remote Sensing*, vol. 40, no. 11, pp. 2392–2404, 2002.

[23] L. M. Kaplan, "Analysis of multiplicative speckle models for template based sar atr," *IEEE Transaction on Aerospace and Electronics Systems*, vol. 37, no. 4, pp. 1424–1431, 2001.

[24] S. Chitrob, A. Houachine, and B. Sansal, "Statistical characterisation and modelling of sar images," *Signal Processing*, vol. 82, pp. 69–92, 2002.

[25] G. P. Kulemin and E. V. Tarnavsky, "Land clutter map development for millimeter-wave radar," in *IEEE Radar 2003*, pp. 399–404, 2003.

[26] G. Kulemin, *Millimeter-wave radar targets and clutter*. Artech House, 2003.

[27] M. Lowe, "Algorithms for high resolution bistatic sar," in *Proceedings of Radar 2002*, pp. 512–515, October 2002.

[28] J. T. Johnson, I. J. Gupta, and R. J. Burkholder, "Comparision of monostatic and bistatic radar images," in *Proceedings of Symposium of Antenna and Propagation Society*, pp. 281–284, July 2001.

[29] C. Y. Hsieh and A. K. Fung, "Bistatic multiple scattering from randomly rough surfaces," *IEE Proceedings on Microwave, Antennas and Propagation*, pp. 214–218, August 2003.

[30] D. Kahny, K. Schmitt, and W. Wiesbeck, "Calibration of bistatic polarimetric radar systems," *IEEE Transaction on Geoscience and Remote Sensing*, vol. 30, no. 5, pp. 847–856, 1992.

[31] A. L. Germond, E. Pottier, and J. Saillard, "Foundations of bistatic radar polarimetric theory," in *Proceedings of Radar 1997*, pp. 833–837, October 1997.

[32] A. L. Germond, E. Pottier, and J. Saillard, "Two bistatic target signatures: the bistatic equations and the bistatic polarisation fork," in *Proceedings of MIKON 1998*, vol. 1, pp. 123–127, May 1998.

[33] F. Comblet, F. Pellen, A. Baussard, and A. Khenchat, "Bistatic sar: theory and simulation," in *IEEE Radar Conference 2005*, pp. 664–667, 2005.

[34] M. Soumekh, "Bistatic synthetic aperture radar inversion with application in dynamic object imaging," *IEEE Trans. on Signal Processing*, vol. 39, no. 9, pp. 2044–2055, 1991.

[35] B. D. Rigling and R. L. Moses, "Polar format algorithm for bistatic sar," *IEEE Transaction on Aerospace and Electronics Systems*, vol. 40, no. 4, pp. 1147–1159, 2004.

[36] G. Franceschetti, M. Migliaccio, G. Schirinzi, and D. Riccio, "Saras: a synthetic aperture radar raw signal simulator," *IEEE Transaction on Geoscience and Remote Sensing*, vol. 30, no. 1, pp. 110–122, 1992.

[37] Y. D. Shirman, ed., *Computer simulation of aerial target radar scattering, recognition, detection and tracking*. Artech House Publishers, 2002.

[38] J. B. Keller, "Geometrical theory of diffraction," *J. of Opt. Soc. Amer.*, no. 1, pp. 116–130, 1962.

[39] L. C. Potter, D. M. Chiang, R. Carriere, and M. Gerry, "A gtd-based parametric model for radar scattering," *IEEE Transaction on Antenna and Propagation*, vol. 43, no. 10, pp. 1058–1067, 1995.

[40] S. H. W. Simpson and P. E. R. Gallow, "Complex target signature generation," in *Proceedings of ICSP 1996*, pp. 485–488, 1996.

[41] R. Bhalla, H. Ling, J. Moore, D. J. Andersh, S. W. Lee, and J. Huges, "3d scattering center representation of complex targets using the shooting and bouncing ray technique," *IEEE Antenna and Propagation Magazine*, vol. 40, no. 5, pp. 30–39, 1998.

[42] M. J. Gerry, L. C. Potter, I. J. Gupta, and A. van der Merwe, "A parametric model for sar measurements," *IEEE Transaction on Antenna and Propagation*, vol. 47, no. 7, pp. 1179–1188, 1999.

[43] S. Nadimi and B. Bhanu, "Moving shadow detection using a physics-based approach," in *Proceedings of 16th International Conference on Pattern Recognition*, vol. 3, pp. 701–704, Aug. 2002.

[44] J. M. Sturm and J. C. West, "Numerical study of shadowing in electromagnetic scattering from rough dielectric surface," *IEEE Transaction on Geoscience and Remote Sensing*, vol. 36, no. 5, pp. 1477–1484, 2002.

[45] A. K. Fung and H. J. Eom, "Multiple scattering and depolarisation by a randomly rough kirchoff surface," *IEEE Transaction on Antenna and Propagation*, vol. 29, no. 3, pp. 463–471, 1981.

[46] A. K. Fung, Z. Li, and K. S. Chen, "Backscattering from a randomly rough dielectric surface," *IEEE Transaction on Geoscience and Remote Sensing*, vol. 30, no. 2, pp. 356–369, 1992.

[47] M. Simcoe, E. Chen, R. Adve, F. Qureshi, J. Schneible, and M. Wicks, "Fopen scene generation using numerical electromagnetic analysis," in *IEEE Radar Conference*, pp. 362–369, 2003.

[48] G. Franceschetti and G. Schirinzi, "A sar processor based on two-dimensional fft codes," *IEEE Transaction on Aerospace and Electronics Systems*, vol. 26, no. 2, pp. 356–365, 1990.

[49] S. Cimmino, G. Franceschetti, A. Iodice, and D. Riccio, "Efficient spotlight sar raw signal simulation of extended scenes," *IEEE Transaction on Geoscience and Remote Sensing*, vol. 41, no. 10, pp. 2329–2338, 2002.

[50] G. Franceschetti, M. Migliaccio, and D. Riccio, "Sar simulation of natural landscape," in *Proceedings of IGARSS 1994*, pp. 1181–1183, August 1994.

[51] G. Franceschetti, A. Iodice, D. Riccio, and G. Ruello, "Sar raw signal simulation for urban structures," *IEEE Transaction on Geoscience and Remote Sensing*, vol. 41, no. 9, pp. 1986–1995, 2003.

[52] G. Franceschetti, M. Migliaccio, and D. Riccio, "The sar simulation: an overview," in *Proceedings of IGARSS 1995*, vol. 3, pp. 2283–2285, July 1995.

[53] N. N. Youssef, "Radar cross-section of complex targets," *IEEE Proceeding*, vol. 77, no. 5, pp. 722–734, 1989.

[54] E. H. Newman and R. J. Marhefka, "Overview of mm and utd methods at the ohio state university," *IEEE Proceeding*, vol. 77, no. 5, pp. 700–708, 1989.

[55] L. N. Medgyesi and D. S. Wang, "Hybrid methods for analysis of complex scatterers," *IEEE Proceeding*, vol. 77, no. 5, pp. 770–779, 1989.

[56] *http://www.saic.com/products/software/xpatch.*

[57] D. A. et al, "Xpatch 4: the next generation in high frequency electromagnetic modelling and simulation software," in *IEEE Radar Conference*, pp. 844–849, 2000.

[58] E. M. Miller, D. J. Andresh, and A. J. Terzuoli, "The effect of target model facetization on rcs prediction," in *International Symposium of IEEE Antenna and Propagation Society*, pp. 1404–1407, 1993.

[59] *http://www.saic.com/products/software/rcssig.*

[60] *http://www.roke.co.uk/sensors/epsilon/default.asp.*

[61] S. H. W. Simpson, P. Galloway, and M. Harman, "Applications of epsilon: a radar signature prediction and analysis tool," in *International Radar Symposium (IRS)*, 1998.

[62] *http://www.lucernhammer.tripointindustries.com/.*

[63] *http://www.wipl-d.com.*

[64] *http://www.feko.co.za.*

[65] L. M. Novak, S. D. Halversen, G. J. Owirka, and M. Hiett, "Effects of polarization and resolution on sar atr," *IEEE Transaction on Aerospace and Electronics Systems*, vol. 33, no. 1, pp. 102–115, 1997.

[66] R. O. Duda, P. E. Hart, and D. G. Stork, *Pattern classification*. John Willy and sons, Inc., 2001.

[67] S. Theodoridis and K. Koutroumbas, *Pattern recognition*. Academic press, 2003.

[68] L. M. Novak, M. C. Burl, and W. W. Irving, "Optimal polarimetric processing for enhanced target detection," *IEEE Transaction on Aerospace and Electronics Systems*, vol. 29, no. 1, pp. 234–243, 1993.

[69] *https://www.sdms.afrl.af.mil/datasets/mstar/*.

[70] L. M. Novak, G. J. Owirka, and A. L. Weaver, "Automated target recognition using enhanced resolution sar data," *IEEE Transaction on Aerospace and Electronics Systems*, vol. 35, no. 1, pp. 157–174, 1999.

[71] L. M. Novak, "State of the art of sar atr," in *IEEE Radar Conference*, pp. 836–843, 2000.

[72] J. A. O'Sullivan, M. D. DeVore, V. Kedia, and M. I. Miller, "Sar atr performance using conditional gaussian model," *IEEE Transaction on Aerospace and Electronics Systems*, vol. 37, no. 1, pp. 91–106, 2001.

[73] M. D. DeVore and J. A. O'Sullivan, "Performance complexity study of several approaches to atr from sar images," *IEEE Transaction on Aerospace and Electronics Systems*, vol. 38, no. 2, pp. 632–648, 2002.

[74] E. Krogager, "Decomposition of the radar target scattering matrix with application to high resolution target imaging," in *Telesystem Conference 1991*, pp. 77–82, 1991.

[75] M. Loiselet and J. F. Gardin, "Sar images interpretation using data analysis techniques," in *IEE Colloquium on Polarisation in Radar*, vol. 3, pp. 3/1–3/11, March 1996.

[76] F. Sadjadi, "Improved target classification using optimum polarimetric sar signatures," *IEEE Transaction on Aerospace and Electronics Systems*, vol. 38, no. 1, pp. 38–49, 2002.

[77] F. Sadjadi, "Enhanced target recognition using optimum polarimetric sar signatures," in *Radar Conference 1998*, pp. 293–298, 1998.

[78] F. Sadjadi, "Image classification in complex spaces," in *IGARSS 2002*, pp. 2504–2506, 2002.

[79] R. Bhalla and H. Liang, "Three dimensional scattering centre extraction using shooting and bouncing ray technique," *IEEE Transaction on Antenna and Propagation*, vol. 44, no. 11, pp. 1445–1453, 1996.

[80] R. Bhalla, J. Moore, and H. Liang, "A global scattering centre representation of complex targets using the shooting and bouncing ray technique," *IEEE Transaction on Antenna and Propagation*, vol. 45, no. 12, pp. 1850–1856, 1997.

[81] H. C. Chiang, R. L. Moses, and L. C. Potter, "Model based classification of radar images," *IEEE Transaction on Information Theory*, vol. 46, no. 5, pp. 1842–1845, 2000.

[82] L. C. Potter and R. L. Moses, "Attributed scattering centers for sar atr," *IEEE Transaction on Image Processing*, vol. 6, no. 1, pp. 79–91, 1997.

[83] D. Gross, "A neural network atr for high range resolution radar signature recognition of moving ground targets," in *33rd Asilomar Conference on Signals, Systems and Computers*, pp. 1235–1239, October 1999.

[84] Q. Zhao and Z. Bao, "Radar target recognition using radial basis function neural network," *Neural Network*, vol. 9, no. 4, pp. 709–720, 1996.

[85] Q. Zhao and J. C. Principe, "Support vector machines for sat atr," *IEEE Transaction on Aerospace and Electronics Systems*, vol. 37, no. 2, pp. 643–654, 2001.

[86] Y. Yang, Y. Qiu, and C. Lu, "Automatic target classification: experiments on the mstar sar images," in *Software Engineering, Artificial Intelligence, Networking and Parallel Computing, 2005*, pp. 2–7, May 2005.

[87] A. Kim, J. Fisher, A. Willsky, and P. Viola, "Nonparametric estimation of aspect dependence for atr," in *Proceedings of SPIE Conference on Algorithms for SAR Imagery VI*, pp. 332–342, April 1999.

[88] P. Runkle, P. Bharadwaj, and L. Carin, "Hidden markov model multi-mspect target classification," *IEEE Transaction on Signal Processing*, vol. 47, no. 7, pp. 2035–2040, 1999.

[89] X. Liao, P. Runkle, and L. Carin, "Identification of ground targets from sequential hrr radar signatures," *IEEE Transaction on Aerospace and Electronics Systems*, vol. 38, no. 4, pp. 1230–1242, 2002.

[90] B. Bhanu and S. Fonder, "Functional template-based sar image segmentation," *Pattern Recognition*, vol. 38, no. 4, pp. 61–77, 2004.

[91] M. Hellmann and G. Jager, "Fuzzy rule based classification of polarimetric sar data," *Aerospace Science and Technology*, vol. 6, pp. 217–232, 2002.

[92] C. T. Chen, K. S. Chen, and J. S. Lee, "The use of fully polarimetric information for fuzzy neural classification of sar images," *IEEE Transaction on Geoscience and Remote Sensing*, vol. 41, no. 9, pp. 2089–2100, 2003.

[93] J. S. Lee, M. R. Grunes, and G. Grandi, "Polarimetric sar speckle filtering and its implication for classification," *IEEE Transaction on Geoscience and Remote Sensing*, vol. 37, no. 5, pp. 2363–2373, 1999.

[94] M. R. A. Sadjadi, S. Ghaloum, and R. Zoughi, "Terrain classification in sar images using principal component analysis and neural network," *IEEE Transaction on Geoscience and Remote Sensing*, vol. 31, no. 2, pp. 511–515, 1993.

[95] Y. Hara, R. G. Atkins, H. Yueh, R. T. Shin, and J. A. Kong, "Application of neural networks to radar image classification," *IEEE Transaction on Geoscience and Remote Sensing*, vol. 32, no. 1, pp. 100–109, 1994.

[96] L. E. Pierce, F. T. Ulaby, K. Sarabandi, and M. C. Dobson, "Knowledge based classification of polarimetric sar images," *IEEE Transaction on Geoscience and Remote Sensing*, vol. 32, no. 5, pp. 1081–1086, 1994.

[97] F. T. Ulaby, R. K. Moore, and A. K. Fung, *Microwave remotesensing: active and passive*, vol. I. Addison-Wesley, 1986.

[98] W. L. Stutzman, *Polarization in electromagnetic systems*. Artech House, 1993.

[99] H. A. Zebker and J. J. V. Zyl, "Imaging radar polarimetry: a review," *Proceedings of IEEE*, vol. 79, no. 11, pp. 60–71, 1991.

[100] A. B. Kostinski and W. M. Boerner, "On foundation of radar polarimetry," *IEEE Transaction on Antenna and Propagation*, vol. 34, no. 12, pp. 1395–1404, 1986.

[101] E. Krogager, "Decomposition of the radar target scattering matrix with application to high resolution target imaging," in *Telesystems Conference 1991*, vol. 1, pp. 77–82, March 1991.

[102] B. Rigling and R. L. Moses, "Gtd-based scattering models for bistatic sar," in *SPIE algorithms for SAR imagery XI*, April 2004.

[103] B. Bhanu and Y. Lin, "Stochastic models for recognition of occluded targets," *Pattern Recognition*, vol. 36, pp. 2855–2873, 2003.

[104] U. Batuhan, S. C. Ahalt, and R. A. Mitchell, "Efficient atr using compression," *IEEE Transaction on Aerospace and Electronics Systems*, vol. 33, no. 4, pp. 1199–1211, 1997.

[105] J. H. G. Ender, "The meaning of k-space for classical and advanced sar-techniques," in *PSIP 2001*, pp. 60–71, Jan. 2001.

[106] J. F. Shaeffr, B. A. Cooper, K. W. Hom, R. C. Baucke, and J. Talcott, "A review of bistatic k-space imaging for electromagnetic prediction codes for scattering and antenna," *IEEE Antenna and Propagation Magazine*, vol. 39, no. 5, pp. 21–29, 1997.

[107] J. H. G. Ender, "Signal theoretical aspects of bistatic sar," in *IGARSS 2003*, vol. 3, pp. 1147–1441, July 2003.

[108] J. H. G. Ender, I. Waterschied, and A. R. Banner, "New aspects of bistatic sar processing and experiments," in *IGARSS 2004*, vol. 3, pp. 1758–1761, Sept. 2004.

[109] B. D. Jersek, B. D. Kernek, and A. J. Blanchard, "Microwave measurements of simulated atmospheric particles," in *IGARSS 95*, pp. 2115–2117, July 1997.

[110] B. D. Jersek, B. D. Krenek, and A. J. Blanchard, "Generation of holographic synthetic aperture radar images from bistatic waterline measurements of complex metallic objects," in *IGARSS 95*, pp. 2255–2257, July 1995.

[111] R. L. E. Jr., P. J. Collins, A. J. T. Jr., G. Nesti, and J. Fortuny, "Bistatic scattering characteristics of complex objects," *IEEE Transaction on Geoscience and Remote Sensing*, vol. 38, no. 5, pp. 2078–2092, 2000.

[112] R. Erickson, "Images of some rcs targets in a number of bistatic angles," in *IEEE Radar 1994*, pp. 63–67, Aug. 1994.

[113] R. K. Raney and G. J. Wessels, "Spatial considerations in sar speckle simulation," *IEEE Transaction on Geoscience and Remote Sensing*, vol. 26, no. 5, pp. 666–672, 1988.

[114] Dunteman and H. George, *Brief description: principal component analysis*. London: Sage, 1989.

[115] P. M. Kroonenberg, *Three mode principal component analysis: theory and applications*. Leiden : The Netherlands: DWO Press, 1983.

[116] A. W. Rihaczek and S. J. Hershkowitz, "Man-made target backscattering behaviour: applicability of conventional radar resolution theory," *IEEE Transaction on Aerospace and Electronics Systems*, vol. 32, no. 2, pp. 809–824, 1996.

[117] Y. Akyildiz and R. L. Moses, "Structure selection in synthetic aperture radar scattering models," in *ICASSP-2000*, pp. 3021–3024, June 2000.

[118] S. C. Tien, T. L. Chia, and Y. Lu, "Using invariants to recognise airplanes in inverse synthetic aperture radar images," *SPIE Optical Engineering Journal*, vol. 42, no. 1, pp. 200–210, 2003.

[119] B. Bhanu and G. Jones, "Increasing the discrimination of syntehtic aperture radar recognition models," *SPIE Optical Engineering Journal*, vol. 41, no. 12, pp. 3298–3306, 2002.

[120] T. Shen-Chi, T. L. Chia, and L. Yibin, "Using invariants to recognize airplanes in isar images," *SPIE Journal of Optical Eng.*, vol. 42, no. 1, pp. 200–210, 2003.

[121] S. Haykin, *Adaptive filter theory*. Prentice-Hall International Editions, 1991.

[122] E. Radoi, A. Quinquis, F. Totir, and F. Pellen, "Automatic target recognition using superresolution music 2d images and self-organising neural network," in *EUSIPCO 2004*, pp. 2139–2142, Sep. 2004.

[123] J. W. Odendaal, E. Barnard, and C. W. I. Pistorus, "Two-dimensional superresolution radar imaging using the music algorithm," *IEEE Transaction on Antenna and Propagation*, vol. 42, no. 10, pp. 1386–1391, 1994.

[124] J. Cui, G. Jon, and M. Brookes, "Radar shadow and superresolution features for automatic recognition of mstar targets," in *IEEE Radar Conference*, May 2005.

[125] A. K. Mishra and B. Mulgrew, "Sar-atr using one and 2d pca," in *Proceedings of the International Radar Symposium (India) 2005*, December 2005.

[126] H. Murase and S. K. Nayar, "Visual learning and recognition of 3-d objects from appearance," *Int. Journal of Computer Vision*, vol. 14, no. 1, pp. 5–24, 1995.

[127] S. K. Nayar, S. A. Nene, and H. Murase, "Subspace methods for robot vision," *IEEE Trans. on Robotics and Automation*, vol. 12, no. 15, pp. 750–758, 1996.

[128] V. Vincet, T. Ross, J. Mossing, S. Worrell, and M. Bryant, "Standard sar atr evaluation experiments using the mstar public release dataset," *Research Reports, Wright State University*, 1998.

[129] F. T. Ulaby, M. W. Whitt, and K. Sarabandi, "Avna - based polarimetric scatterometers," *IEEE Antenna and Propagation Magazine*, pp. 6–17, 1990.

[130] M. B. Wolfgang, "Recent advances in polarimetric interoferometric sar theory and technology and its application," in *MIKON 2000*, vol. 3, pp. 212–229, May 2000.

[131] K. C. Chang and Y. C. Lu, "High resolution polarimetric sar target classification with neural network," in *Proceedings of forth IEEE conference on fuzzy systems*, vol. 3, pp. 1681–1688, March 1995.

[132] G. Gavriloaia and O.-G. Suciu, "Target discrimination in the s.a.r. systems by using radar polarimetry," in *Telecommunications in Modern Satellite, Cable and Broadcasting Service, 2003. TELSIKS 2003. 6th International Conference on*, vol. 2, pp. 711–720, 2003.

[133] S. R. Cloude, "Target decomposition theorems in radar scattering," *Electronics Letters*, vol. 21, no. 1, pp. 22–24, 1985.

[134] A. Hauter, K. C. Chang, and S. Karp, "Polarimetric fusion for synthetic aperture radar target classification," *Pattern Recognition*, vol. 30, no. 5, pp. 769–775, 1997.

[135] W. L. C. L. K. Leung, "Feature motivated polarization scattering matrix decomposition," in *IEEE International Radar Conference*, pp. 549–557, 1990.

[136] D. Corr and A. F. Rodrigues, "Alternative basis matrices for polarimetric decomposition," in *EUSAR 2002*, June 2002.

[137] D. Corr, D. Blacknell, C. Oliver, and A. F. Rodrigues, "Unification of techniques to measure polarimetric signatures through image segmentation," in *EUSAR 2004*, pp. 60–71, June 2004.

[138] H. J. Li and R. Y. Lane, "Utilization of multiple polarization data for aerospace target identification," *IEEE Transaction on Antenna and Propagation*, vol. 43, pp. 1436–1440, Dec 1995.

[139] A. J. bennett and A. Currie, "The use of high resolution polarimetric sar for automatic target recognition," in *SPIE proceedings of algorithms for SAR imagery IX*, vol. 4727, pp. 146–152, April 2002.

[140] K. Daniel, K. Schmitt, and W. Wiesbeck, "Calibration of bistatic polarimetric radar system," *IEEE Transaction on Geoscience and Remote Sensing*, vol. 30, no. 5, pp. 847–852, 1992.

[141] H. S. M. Coxeter, *Projective geometry*. Blaisdell publishing company, 1964.

[142] G. Lei, "Recognition of planar objects in 3-d space from single perspective views using cross ratio," *IEEE Trans. on Robotics and Automation*, vol. 6, no. 4, pp. 432–437, 1990.

[143] *https://www.sdms.afrl.af.mil/datasets/gtri/*.